Thesis for the Degree of Doctor of Philosophy

Phase-sensitive amplifiers for nonlinearity impairment mitigation in optical fiber transmission links

Kovendhan Vijayan

CHALMERS

Photonics Laboratory
Department of Microtechnology and Nanoscience
Chalmers University of Technology
Göteborg, Sweden, 2021

Phase-sensitive amplifiers for nonlinearity impairment mitigation in optical fiber transmission links
Kovendhan Vijayan

ISBN: 978-91-7905-481-6
Doktorsavhandlingar vid Chalmers tekniska högskola
Ny serie nr 4948
ISSN 0346-718X

Chalmers University of Technology
Department of Microtechnology and Nanoscience - MC2
Photonics Laboratory
SE–412 96 Göteborg
Sweden
Phone: +46–(0)31–772 10 00

Front cover illustration: Measured constellation diagrams showing XPM and SPM mitigation using PSAs.

Printed in Sweden by
Reproservice
Chalmers Tekniska Högskola
Göteborg, Sweden, 2021

Phase-sensitive amplifiers for nonlinearity impairment mitigation in optical fiber transmission links

Kovendhan Vijayan
Photonics Laboratory
Department of Microtechnology and Nanoscience
Chalmers University of Technology

Abstract

The fundamental limitations in fiber-optic communication are caused by optical amplifier noise and the nonlinear response of the optical fibers. The quantum-limited noise figure of erbium-doped fiber amplifiers (EDFAs) or any phase-insensitive amplifier is 3 dB. However, the noise added by the amplification can be reduced using phase-sensitive amplifiers (PSAs), whose quantum-limited noise figure is 0 dB. PSAs can also compensate for the nonlinear distortions from the optical transmission fiber in the copier-PSA implementation. At the transmitter, a copier which is nothing but a phase-insensitive amplifier, is used to create a conjugated copy of the signal. The signal and idler are then co-propagated in the fiber link, experiencing correlated nonlinear distortions. The nonlinear distortions are reduced by the all-optical coherent superposition of the signal and idler in the PSA.

In this work, an investigation is made for the nonlinearity mitigation using the PSAs, by calculating the residual nonlinear distortion after the coherent superposition in a copier-PSA link. The nonlinearity mitigation efficiency in PSA links is studied with respect to modulation formats, symbol rates and number of wavelength channels. The effectiveness of nonlinearity mitigation is found to increase with higher-order modulation formats. However, the efficiency of nonlinearity mitigation decreases with increasing number of wavelength channels and increasing symbol rate resulting in larger residual nonlinear distortions. A modified Volterra nonlinear equalizer (VNLE) is implemented to reduce the residual nonlinear distortions after PSAs in single- and multi-channel PSA links. Cross-phase modulation mitigation using PSAs is also demonstrated.

Keywords: optical transmission, nonlinearity mitigation, phase-sensitive amplifier, low-noise amplification, self-phase modulation mitigation, cross-phase modulation mitigation, copier-PSA, modulation formats

Publications

This thesis is based on the work contained in the following papers:

[A] B. Foo, M. Karlsson, **K. Vijayan**, M. Mazur, and P. A. Andrekson, "An Analysis of Nonlinearity Mitigation Using Phase-Sensitive Optical Parametric Amplifiers", *Optics Express*, vol. 27, no. 22, pp. 31926-31941, October 2019.

[B] **K. Vijayan**, H. Eliasson, B. Foo, S. L. I. Olsson, M. Karlsson, and P. A. Andrekson, "Optical Bandwidth Dependency of Nonlinearity Mitigation in Phase-Sensitive Amplifier Links", in *European Conference on Optical Communication (ECOC)*, Sept 2018. DOI: 10.1109/ECOC.2018.8535427

[C] **K. Vijayan**, B. Foo, M. Karlsson, and P. A. Andrekson, "Long-haul Transmission of WDM Signals With In-Line Phase-Sensitive Amplifiers", in *European Conference on Optical Communication (ECOC)*, Sept 2019. DOI: 10.1049/cp.2019.1116

[D] **K. Vijayan**, B. Foo, M. Karlsson, and P. A. Andrekson, "Cross-Phase Modulation Mitigation in Phase-sensitive Amplifier Links", *IEEE Photonics Technology Letters*, vol. 31, no. 21, pp. 1733-1736, November 2019.

[E] **K. Vijayan**, Z. He, B. Foo, M. Karlsson, and P. A. Andrekson, "Modulation format dependence on transmission reach in phase-sensitively amplified fiber links", *Optics Express*, vol. 28, no. 23, pp. 34623-34638, November 2020.

[F] **K. Vijayan**, Z. He, B. Foo, J. Schröder, M. Karlsson, and P. A. Andrekson, "Phase-sensitively amplified wavelength-division multiplexed optical transmission systems", - **submitted** to **Optics Express**, March 2021.

Related work by the author (not included in this thesis):

[G] R. Kakarla, **K. Vijayan**, A. Lorences-Riesgo, and P. A. Andrekson "High Sensitivity Receiver Demonstration Using Phase Sensitive Amplifier for Free-Space Optical Communication", in *European Conference on Optical Communication (ECOC)*, Sept 2017. DOI: 10.1109/ECOC.2017.8346152

[H] R. Kakarla, **K. Vijayan**, J. Schröder, and P. A. Andrekson "Phase Noise Characteristics of Injection-Locked Lasers operated at Low Injection Powers", in *Optical Fiber Communication Conference (OFC)*, March 2018. DOI: /10.1364/OFC.2018.M4G.2

[I] H. Eliasson, **K. Vijayan**, B. Foo, S. L. I. Olsson, E. Astra, M. Karlsson, and P. A. Andrekson, "Phase-Sensitive Amplifier Link With Distributed Raman Amplification", *Optics Express*, vol. 26, no. 16, pp. 19854-19863, August 2018.

[J] **K. Vijayan**, B. Foo, H. Eliasson, and P. A. Andrekson "Cross-Phase Modulation Mitigation in WDM Transmission Systems Using Phase-Sensitive Amplifiers", in *European Conference on Optical Communication (ECOC)*, Sept 2018. DOI: 10.1109/ECOC.2018.8535265

[K] B. Foo, M. Karlsson, **K. Vijayan**, M. Mazur, P. A. Andrekson, "Combining phase-sensitive amplifiers with DSP for enhanced nonlinearity mitigation", in *European Conference on Optical Communication (ECOC)*, Sept 2019. DOI : 10.1049/cp.2019.0857

[L] P. Zhao, Z. Ye, **K. Vijayan**, C. Naveau, J. Schröder, M. Karlsson, P. A Andrekson "Waveguide tapering for improved parametric amplification in integrated nonlinear Si_3N_4 waveguides", *Optics Express*, vol. 28, no. 16, pp. 23467-23477, August 2020.

[M] **K. Vijayan**, Z. He, B. Foo, M. Karlsson, and P. A. Andrekson, "Nonlinearity mitigation dependence on modulation format in phase-sensitively amplified fiber links", in *Frontiers in Optics (FiO)*, September 2020. DOI: 10.1364/FIO.2020.FTh1E.1

Other work by the author (not included in this thesis):

[N] Z. He, **K. Vijayan**, M. Mazur, M. Karlsson, J. Schroder, "Look-up Table based Pre-distortion for Transmitters Employing High-Spectral-Efficiency Modulation Formats", in *European Conference on Optical Communication (ECOC)*, December 2020. DOI: 10.1109/ECOC48923.2020.9333231

In this thesis, we will refer to above publications with the alphabets.

Contents

Acknowledgement

First and foremost, I like to thank my supervisors Prof. Peter Andrekson and Prof. Magnus Karlsson for providing me an opportunity to pursue my doctoral studies at the Photonics lab. Certainly, their guidance and support have been the pillar of this work. I like to thank Prof. Andrew Ellis for accepting me as a visiting student, though the visit got cancelled due to covid-19. Dr. Jochen Schröder deserves a special mention for always being there to help me out with my writings and presentations.

I like to thank Dr. Ravikiran Kakarla and Dr. Samuel Olsson for helping me to understand the basics of PSAs and for the collaborations. Dr. Abel Lorences-Riesgo deserves a special thanks for teaching me how to implement the PSAs experimentally for the first time. I like to thank Dr. Henrik Eliasson for introducing me to the PSA-loop experiments, teaching me about Raman amplification and introducing me to the cluster simulations. Dr. Ben Foo with whom I had the privilege to work in the lab deserves a special thanks for all the help, fruitful discussions and his contribution to this work. I like to thank Dr. Mikael Mazur for all the help and discussions. I like to thank Dr. Vitor Ribeiro, Dr. Elham Nazemosadat, Dr. Ping Zhao, Dr. Corentin Naveau, Dr. Mehdi Jamshidifar, Dr. Zhichao Ye and Rasmus Larsson for all the discussions on parametric amplifiers and PSAs. I also like to thank Zonglong He for all his collaborations and contributions to this work. Ali Mirani deserves a special thanks for the exciting discussions on communication theory. I like to thank Krishna Sundar Twayana, Israel Rebolledo and Ekaterina Deriushkina for all the discussions on interferometry. Filip Hjort, Marcello Girardi, Michael Alexander Bergmann and Mehdi Jahed requires a special thanks for all the interesting talks out of research. Jeanette Träff and Debora Perlheden deserves a special thanks for helping with all the administrative stuff. I also like to thank all the other Photonics laboratory members for the nice discussions and work environment.

I like to thank all my friends who made my life outside research in Sweden. A special thanks to Dr. Shreyas Muralidhar, Dr. Sujeetha Selvakkumaran, Karthikeyan Muthusamy Sivanandham, Dinesh Kumar for their support and care. I also like to thank all the Photonics lab members for the ping-pong games and kitchen talks.

Last but not least, I would like to express my deepest gratitude to my wife

Nisha, whose support has been vital. Thanks a lot for taking care of our new born, Jishnu Dev for the last few months without my presence. My niece also needs a special mention whose questions are always difficult to answer. I also like to thank my parents and sister for all their support and care.

I also like to thank the Swedish Research Council for the financial support.

Kovendhan Vijayan

Göteborg
April 2021

Acronyms

IP	internet protocol
PSA	phase-sensitive amplifier
WDM	wavelength-division multiplexing
EDFA	erbium-doped fiber amplifier
DCF	dispersion compensating fiber
FBG	fiber Bragg grating
DCM	dispersion compensating module
OPC	optical phase conjugation
PCTW	phase-conjugated twin wave
DBP	digital back-propagation
VNLE	Volterra nonlinear equalizer
NFT	nonlinear Fourier transform
PIA	phase-insensitive amplifier
HNLF	highly nonlinear fiber
SNR	signal-to-noise ratio
XPM	cross-phase modulation
SPM	self-phase modulation
SE	spectral efficiency
SSMF	standard single-mode fiber
NLSE	nonlinear Schrödinger equation
DRA	distributed Raman amplification
SSFM	split-step Fourier method
GVD	group-velocity dispersion
ZDW	zero-dispersion wavelength
PMF	polarization-maintaining fiber
PMD	polarization-mode dispersion
PSP	principal states of polarization
FWM	four-wave mixing
EVM	error vector magnitude
NPSD	normalized power spectral density
QPSK	quadrature phase-shift keying
XpolM	cross-polarization modulation
FOPA	fiber-optic parametric amplifier

SRS	stimulated Raman scattering
SBS	stimulated Brillouin scattering
CW	continuous wave
SOA	semiconductor optical amplifier
ASE	amplified spontaneous emission
NF	noise figure
PDM	polarization-division multiplexing
AQN	amplified quantum noise
PS	phase-sensitive
PI	phase-insensitive
PTN	pump-transferred noise
OSNR	Optical signal-to-noise ratio
NLPN	nonlinear phase noise
DFB	distributed feedback laser
OIL	optical-injection locking
PLL	phase-locked loop
ISI	inter-symbol interference
FOM	figure of merit
EDC	electronic dispersion compensation
DAC	digital-to-analog converter
VSTF	Volterra series transfer function

Chapter 1

Introduction

Almost everything in this world is connected to the internet. The internet has revolutionized the way we learn, work, shop and more. The internet has made it easy, convenient and comfortable for people to accomplish anything from anywhere and anytime. People use the internet to gather needed information to keep them up to date on the news and trends in the world, to socialize with society, to communicate with their friends and relatives, to entertain themselves by watching movies, playing games, reading books and listening to music, and for business purposes including video conferencing and online trading.

The number of internet users, internet-based applications and devices using the internet are increasing every day. According to Cisco, the monthly global internet protocol (IP) traffic in 2017 was 122.4 Exabytes and is predicted to reach 396 Exabytes by 2022 [1], as shown in Fig. 1.1 (black dashed line with circle markers). Moreover, the global internet users will make up to 60% of the world's population, the number of connected devices will reach 28.5 billion and augmented reality and gaming will make up for 85% of the total traffic by 2022.

At the time of writing this thesis, the global pandemic caused by Covid-19 [2] has vastly changed our lifestyles [3]. There have been many restrictions on the movement of the people within the continents and countries, and even within buildings. However, most people were still able to carry out their work [4] or study [5] comfortably sitting at home, thanks to the internet. Apart from this, the internet is still playing a significant role in controlling this pandemic's spread by keeping people engaged and in developing the vaccines by sharing various test and diagnostics information through the cloud. This has also put an extra burden on the internet traffic [6].

The vast majority of the internet traffic passes through optical fiber networks. The various inventions in the field of fiber-optic communication have paved the way to meet these data traffic demands.

In this chapter, we will go through the evolution of fiber-optic communications, pointing out the important breakthroughs, which helped to meet the

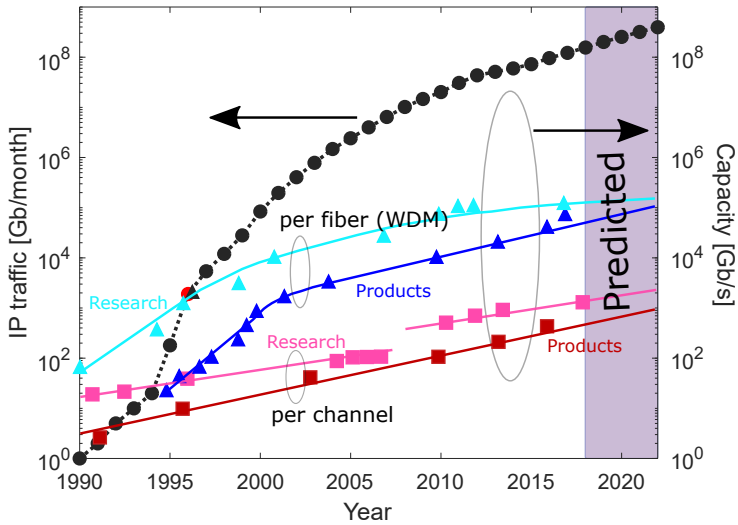

Figure 1.1: Evolution of the internet protocol (IP) data traffic (adopted from [1]) and fiber capacity [7] over the years. The IP traffic is shown by the dotted black line with circle markers. The red and magenta solid lines with square markers correspond to the capacity of a single-channel in terms of products and research, respectively. The capacity of wavelength-division multiplexed (WDM) links is shown in blue and cyan solid lines with triangle markers for products and research, respectively.

ever-increasing demands of internet traffic. We will then discuss the fundamental limitations of fiber links and how phase-sensitive amplifiers (PSAs) can be used to push these limits further. After that, other techniques to compensate for the detrimental nonlinear effects in the optical fiber are briefly reviewed. Finally, we will focus on what this thesis is about, summarizing the content of this thesis

1.1 Evolution of fiber-optic communication

The first historic event in the field of optical communication dates back to 1880. Alexander Graham Bell transmitted sound signals over 200 m with sunlight as the optical carrier known as the 'photophone' [8]. However, this did not create a significant impact in the field of communication due to the lack of a reliable intense light source and confined low-loss medium for light propagation. The first major breakthrough in fiber-optic communication was the realization of a coherent and monochromatic light source called the laser in 1960 [9], emitting light at 694.3 nm. This break-through not only sped up the research in optical communication but also in other fields of optics. Followed

by that, in 1962 came the demonstration of a semiconductor laser diode with gallium arsenide (GaAs) lasing around 850 nm [10, 11]. The first proposal to use clad glass fiber for transmitting information in the telecommunication industry came in 1966 [12]. The single-mode silica fibre losses were reduced to 0.2 dB/km in 1979 at 1550 nm [13] making it the best medium for long-distance communication. This major breakthrough made fiber-optic communication a viable solution. The first commercial optical transmission happened in 1977 at 44.736 Mb/s [14]. Due to the increasing data traffic demand and the inventions to meet the demand, the transmission window shifted to 1300 nm due to lower dispersion [15] and then to 1550 nm due to lower losses. The next major breakthrough in optical communication is the invention of the erbium-doped fiber amplifier (EDFA) in 1987 [16]. The introduction of EDFAs removed the need for repeaters in the fiber-optic communication links. Moreover, the capability of EDFAs to amplify multiple wavelength channels simultaneously made it possible to use wavelength-division multiplexed (WDM) signals. This was the beginning of the WDM era [17]. Another bottleneck was the dispersion in the single-mode fiber. The dispersion was compensated using dispersion compensating fibers (DCFs) [18, 19]. One other way to compensate for the dispersion is to use fiber-Bragg grating (FBG)-based dispersion compensating modules (DCMs) [20, 21]. The ever-increasing demand for data traffic led to the introduction of coherent communication [22, 23]. The information was encoded in both the amplitude and phase of the optical waves. The introduction of coherent communication enabled the usage of higher-order modulation formats [24], dual-polarization (DP) signals and compensation of fiber impairments in the digital domain [25]. This was one of the important breakthroughs in the field of optical communication. One of the latest transmission record achieved a data rate of 71.65 Tb/s over 6970 km with C- and L-band [26]. Comparing the first data transmission and this one, one can imagine the importance of the technological breakthroughs that have revolutionized fiber-optic communication. The evolution of fiber capacity in terms of products and research over the years is shown in Figure 1.1 [7]. The capacity of the WDM link is predicted to get saturated in both products and research. To increase the data rate further, space-division multiplexing (SDM) [27] was proposed. The data rate can be increased spatially, either be multiple cores [28] or multiple modes [29].

1.2 Fundamental limits

To increase the capacity of fiber-optic links, we need to understand the fundamental limitations and try to push the boundaries set by these limits. The signal when propagating in fiber is attenuated due to a small loss of 0.2 dB/km. Optical amplifiers are used to compensate for the fiber loss. The optical amplifiers apart from amplifying the signal also adds noise. At low signal powers, the noise added by the amplifiers limit the received signal quality as shown in Figure 1.2 (top). The noise cloud for the constellation point at low signal

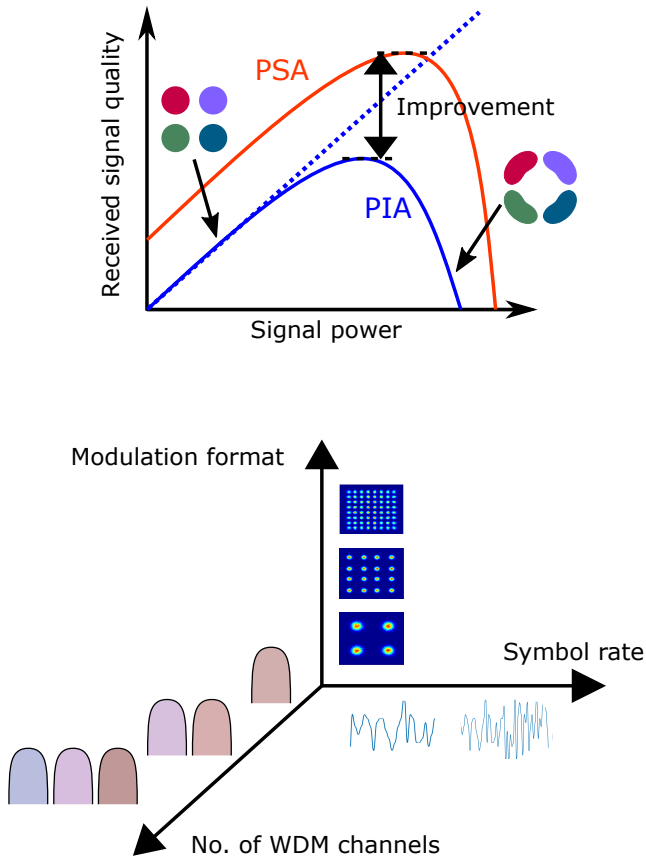

Figure 1.2: Top: Received signal quality after a fiber span and an EDFA is plotted against the signal (launch) power for PIA-linear medium (dotted blue line), PIA-fiber (solid blue line) and PSA-fiber (solid red line). The constellation points are shown for low and high signal powers.
Bottom: Illustration of the central idea of this thesis. This thesis studies the nonlinearity mitigation using copier-PSA in three different aspects - Modulation format, symbol rate and number of WDM channels.

power have a circularly symmetric Gaussian probability density function. To overcome the limit imposed by the amplifier loss, one can increase the signal power. Increasing the signal power improves the signal quality in a linear link (blue dotted lines), e.g. free space. At higher signal power, the Kerr nonlinearity in the optical fiber limits the signal quality, as shown by the solid blue lines. This is known as the nonlinear Shannon limit [30–32] which is still not well defined. Banana-shaped constellation points are obtained in the nonlinear regime due to the Kerr effect. Also, there exists an optimum between the limit imposed by noise and nonlinearity. Some techniques to push this nonlinear limit are optical solitons [33], optical phase conjugation (OPC) [34], phase-conjugated twin waves (PCTWs) [35], copier-PSA [36], digital-back propagation (DBP) [37,38], Volterra nonlinear equalizer (VNLE) [39,40], nonlinear Fourier transform (NFT) [41] and constellation shaping [42,43]. The optimum shifts to lower signal power if the system can accommodate more noise and to higher signal power if more nonlinearity can be tolerated.

1.2.1 Phase-sensitive optical amplifiers

One solution to address the limits on noise and nonlinearity is to use phase-sensitive amplifiers (PSAs) which forms the core of this thesis. The most common amplifier used in optical communications is the erbium-doped fiber amplifier (EDFA) [16,44], which is a phase-insensitive amplifier (PIA) as the gain is independent of the signal phase. PIA has a quantum-limited noise figure of 3 dB at high gain [45], considering the input signal is shot-noise limited. There is a special kind of amplifier known as phase-sensitive amplifiers (PSAs) whose gain depends on the signal phase. PSAs could have a NF of 0 dB, i.e., PSA can amplify signals without adding any excess noise.

One way to implement PSAs is to use the copier-PSA scheme [46,47]. The copier is used to create the idler, which is a conjugated copy of the signal. Both the signal and idler are co-propagated in the transmission span, experiencing correlated nonlinear distortions. The signal and idler are coherently superimposed at the PSA, enabling low-noise amplification [48,49] and nonlinearity mitigation [50]. In this case, the received signal quality is given by the solid red curve in Figure 1.2. PSA has improved the signal performance with regards to noise and nonlinear distortion. Copier-PSAs have been realized in $\chi^{(2)}$ [51] and $\chi^{(3)}$ [48] media based on parametric amplification. In this thesis, highly nonlinear fibers (HNLFs) based on $\chi^{(3)}$ nonlinearity are used for copier and PSA. The copier-PSA implementation is WDM compatible, and modulation format independent [49]. Though copier-PSA improves the transmission reach or the received signal-to-noise ratio (SNR), the main disadvantage of the copier-PSA implementation is the loss in spectral efficiency [52] due to the need of two waves, i.e, the signal and the idler.

1.3 This thesis

This work is focused on studying the nonlinearity mitigation efficiency using copier-PSAs against signal characteristics as shown in Figure 1.2 (bottom) i.e., modulation formats, symbol rates and number of WDM channels. Although a lot of experiments have been performed to verify the nonlinearity mitigation using PSAs [36, 50, 53], no complete analytic analysis has been presented. In [A], it is analytically shown that the nonlinearity mitigation in PSAs leads to residual distortions which depends on the involved optical bandwidth, dispersion map and power map. Also, a modified VNLE with less computational effort is proposed to compensate for the residual nonlinear distortion. The nonlinearity mitigation dependence on optical signal bandwidth is experimentally studied in [B] and [C] with different symbol rates and number of WDM channels, respectively. We verify in [D] that PSAs can mitigate both self-phase modulation (SPM) and cross-phase modulation (XPM). In [E], the nonlinearity mitigation dependence on modulation formats is studied. The enhancement in nonlinearity mitigation using the modified VNLE for the WDM PSA link is studied in [F].

This thesis is outlined as follows, the various impairments when an optical wave travels in the optical fibers are explained in chapter 2. The optical amplification and dispersion compensation used to overcome the linear impairments are discussed in chapter 3. Here. focus is given to fiber-based parametric amplifiers and their implementations in phase-sensitive mode. In chapter 4, the various optical and digital methods to compensate for nonlinear impairments are briefly discussed. Also, a detailed analysis on nonlinearity mitigation using copier-PSAs is outlined. The possible future works are listed in chapter 5. Finally, the papers are summarized in chapter 6.

Chapter 2

Wave Propagation in Optical fibers

The relationship between the induced dielectric polarization of the material and applied field depends on the field's strength. When the field is strong, the material response becomes nonlinear and at lower field strength it is linear. Therefore, if the propagating optical field is weak, only the linear effects are present and at high powers both linear and nonlinear effects affect the propagating field. Nonlinear effects can cause exchange of energy between frequencies or even create new frequency components. The linear effects that affect the optical field on propagation are fiber loss, chromatic dispersion and polarization-mode dispersion. The nonlinear effects are the Kerr effect and inelastic scattering effects, which includes the stimulated Raman and the stimulated Brillouin scattering. In this chapter, we start with modelling the propagation of optical fields in the fiber and then the linear and nonlinear effects are discussed with respect to the standard single-mode fiber (SSMF) used as transmission span and the highly nonlinear fiber (HNLF) used as the nonlinear medium to realize parametric amplifiers.

2.1 Numerical modelling

The propagation of electric field ignoring polarizaton in an optical fiber can be modelled using the scalar nonlinear Schrödinger equation (NLSE) as [54]

$$\frac{\partial \tilde{E}(z,t)}{\partial z} = \underbrace{-j\frac{\beta_2}{2}\frac{\partial^2 \tilde{E}(z,t)}{\partial t^2} + \frac{\beta_3}{6}\frac{\partial^3 \tilde{E}(z,t)}{\partial t^3}}_{\text{dispersion}} + \underbrace{\frac{g(z)-\alpha(z)}{2}\tilde{E}(z,t)}_{\text{power evolution}} + \underbrace{j\gamma|\tilde{E}(z,t)|^2\tilde{E}(z,t)}_{\text{Kerr effect}}, \tag{2.1}$$

The terms have been labelled according to the different effects. The envelope of the electric field, $\tilde{E}(z,t)$ is assumed to be slowly varying compared to the carrier wave, where the field is propagating in the z direction and t is co-moving time frame. For dispersion, up to third-order Taylor expansion coefficients are included. In the above mentioned effects, polarization-mode dispersion, Raman and Brillouin scattering have been neglected. The term g(z) in the power evolution can be used to model the distributed Raman amplification (DRA) in the transmission link and $\alpha(z)$ is the attenuation corresponding to fiber loss.

2.1.1 Split-step Fourier method

The split-step Fourier method (SSFM) is the most widely used numerical method for solving the NLSE. The method performs numerical operations in steps and involves moving back and forth between time and frequency domain which leads to the name, SSFM. First, the fiber is divided into small sections whose length corresponds to the step size (Δz). Although the linear and nonlinear effects act simultaneously in the fiber, an approximate solution can be obtained by dividing each step in equation (2.1) into two parts. One part to consider the linear effects in the frequency domain and the other for the nonlinear effects in the time domain. The linear effects in equation (2.1) are the dispersion, fiber loss (assuming $g(z) = 0$ - no DRA) whereas the nonlinear one is the Kerr effect. The linear part is

$$\hat{D} = -\frac{j\beta_2}{2}\frac{\partial^2}{\partial t^2} + \frac{\beta_3}{6}\frac{\partial^3}{\partial t^3} - \frac{\alpha}{2}, \tag{2.2}$$

while the nonlinear part is given by the nonlinear operator,

$$\hat{N} = j\gamma|\tilde{E}|^2. \tag{2.3}$$

The propagation is then done in steps with size Δz as

$$\tilde{E}(z+\Delta z,t) \approx \exp(\Delta z\hat{D})\exp(\Delta z\hat{N})\tilde{E}(z,t), \tag{2.4}$$

To increase the accuracy of the SSFM, symmetrized SSFM was suggested [54]. Here the nonlinear part is sandwiched by half of linear part on either side as,

$$\tilde{E}(z+\Delta z,t) \approx \exp(\frac{\Delta z\hat{D}}{2})\exp(\Delta z\hat{N})\exp(\frac{\Delta z\hat{D}}{2})\tilde{E}(z,t), \tag{2.5}$$

In this work, symmetrized SSFM was used to model the propagation of single- and multi-channel signals for single- and multi-span transmission links.

2.2 Fiber loss

The optical fibers made from silica are used as the medium for long-haul communications due to the low loss in the C-band (1530-1570nm). The loss is due

to material absorption and Rayleigh scattering. Material absorption can be reduced by increasing the purity of the fused silica. Then, the Rayleigh scattering dominates the fiber loss. The Rayleigh scattering is inversely proportional to the fourth power of wavelength. The power evolution of the optical field in the fiber is dictated by the Beer-Lambert law [54],

$$P(z) = P(0)\exp(-\alpha z), \tag{2.6}$$

where α is the attenuation constant in linear units corresponding to the one in the NLSE (equation (2.1)). It is common to represent α in units of dB/km known as the fiber-loss parameter (α [dB/km]). For an SSMF and an HNLF, the typical fiber-loss parameters are 0.2 dB/km and 0.9 dB/km, respectively. The fiber-loss parameter is wavelength-dependent and can be as high as a few dB/km in shorter wavelength regimes. However, it is almost constant over the C-band. The current lowest reported single-mode fiber loss is 0.14 dB/km [55].

2.3 Dispersion

The frequency-dependent effective index of the optical fiber leads to chromatic dispersion. Dispersion is due to material properties and waveguide design. The contribution from material properties is due to the dispersive behaviour of silica itself. The use of core and cladding for guiding the optical field in the fiber leads to dispersion from waveguide design. One can model the linear propagation of an optical field in the frequency domain neglecting losses as,

$$\tilde{E}(z,\omega) = \tilde{E}(0,\omega)\exp[j\beta(\omega)z], \tag{2.7}$$

where $\beta(\omega)$ is the propagation constant:

$$\beta(\omega) = \frac{n(\omega)\omega}{c}, \tag{2.8}$$

where $n(\omega)$ is the refractive index and c is the velocity of light in vacuum. To account for the frequency dependence of the propagation constant, the propagation constant can be expanded using a Taylor series around the carrier frequency (ω_0) as

$$\beta(\omega) = \beta_0 + \beta_1(\omega-\omega_0) + \frac{\beta_2}{2}(\omega-\omega_0)^2 + \frac{\beta_3}{6}(\omega-\omega_0)^3 + \ldots, \tag{2.9}$$

where $\beta_i \equiv \left.\frac{d^i\beta}{d\omega^i}\right|_{\omega=\omega_0}$ is the Taylor expansion coefficients. β_0 corresponds to the phase velocity of the carrier wave by $v_p = \frac{\omega_0}{\beta_0}$ and the group velocity at the carrier frequency (v_g) is related to β_1 as $v_g = \frac{1}{\beta_1}$. β_2 describes the frequency dependence of group velocity and is known as the group velocity dispersion (GVD) parameter given in units of [ps^2/km]. The GVD changes the shape of the optical pulse during propagation. The frequency dependence of the GVD

is given by the third-order Taylor expansion coefficient (β_3). The third-order Taylor expansion coefficient can distort ultra-short pulses and its effect is significant at lower values of GVD parameter. These Taylor expansion coefficients are used to include the dispersion in the NLSE (equation (2.1)). However, the more commonly used are the dispersion parameter (D) in [ps/(nm km)] and the dispersion slope (S) in [ps/(nm^2 km)], which are related to the Taylor expansion coefficients as

$$D = \frac{-2\pi c}{\lambda^2}\beta_2, \tag{2.10}$$

$$S = \left(\frac{2\pi c}{\lambda^2}\right)^2 \beta_3 + \frac{4\pi c}{\lambda^3}\beta_2, \tag{2.11}$$

where λ is the wavelength of the light. The wavelength at which the dispersion parameter changes sign is called the zero-dispersion wavelength (λ_{ZDW}). In general, terms only up to the dispersion parameter are often considered, but higher-order terms should be taken into account for wide bandwidth operation and operation near λ_{ZDW}. For the SSMF, the dispersion parameter, $D = 16$ ps/(nm km) at 1550 nm and the λ_{ZDW} is 1310 nm. The dispersion parameter for the HNLF at 1550 nm is usually between ± 2 ps/(nm km).

2.4 Fiber birefringence

A single-mode optical fiber supports two orthogonal polarizations of the electric field oscillating at the same frequency. The two orthogonal polarization modes can have different phase velocities due to fiber birefringence. When the effective index is different for different polarizations in the optical fiber, then fiber is said to birefringent. Fiber birefringence can be random or deterministic. Polarization maintaining fibers (PMFs) are designed to have a deterministic birefringence. The PMF may use longitudinal stress rods along the fiber that induces strong linear birefringence leading to a slow and a fast axis. The group velocity for the fast axis is higher compared to that of the slow axis. If an input field is launched along either of the two axes, the polarization state of the input field does not change during propagation. The group velocity difference between the fast and slow axis leads to differential group delay (DGD) between the polarizations also known as polarization mode dispersion (PMD). In the case of fibers with random birefringence, the orientation of the slow and fast axis is constant only for short distances and will vary across the fiber length. Also, the polarization coupling between change of fast and slow axis is random, leading to DGD variation with respect to frequency. Neglecting polarization-dependent losses, there exist two polarization states where the polarization of the output wave is independent of the optical wave frequency over a narrow frequency range (first-order approximation) known as the principal states of polarizations (PSPs) [56, 57]. Also, these correspond to the fast and slow axis locally. For the ideal SSMF, the PMD is zero due to the circular symmetry

of the fiber. However, fiber asymmetries due to non-uniformities in manufacturing, any stress or bending, environmental fluctuations in temperature, vibrations and any stress can lead to differences in the group velocities because of randomly varying birefringence. The PMD induced differential group delay in the SSMF can be calculated as [54]

$$\Delta t_{gp} = D_p \sqrt{L}, \tag{2.12}$$

where D_p is the PMD parameter. The typical value of (D_p) is 0.1 ps/$\sqrt{\text{km}}$. HNLFs can also be PMFs. However, obtaining homogeneous HNLFs with required dispersion and nonlinearity is difficult.

2.5 Kerr effect

The nonlinear response of a medium depends on the relationship between electric field and induced dielectric polarization. The total polarization of the medium $(\tilde{P})$ induced by a strong electric field is [54]

$$\tilde{P} = \epsilon_0(\chi^{(1)} \cdot \tilde{E} + \chi^{(2)} : \tilde{E}\tilde{E} + \chi^{(3)} \vdots \tilde{E}\tilde{E}\tilde{E}), \tag{2.13}$$

where, $\chi^{(N)}$ is the susceptibility of N^{th} order and a tensor of rank $N+1$. ϵ_0 is the vacuum permittivity. The first order susceptibility term corresponds to the linear polarization. The dispersion and fiber loss are related to the real and imaginary part of the first order susceptibility. The second-order susceptibility gives rise to second-order nonlinear effects like second harmonic generation, sum- and difference-frequency generation, which are present only in medium without inversion symmetry. The third-order susceptibility leads to the third-order nonlinear effects like third-harmonic generation and the Kerr effect. Silica fiber exhibits inversion symmetry due to the amorphous nature of the material. Then, the third-order nonlinear effects become dominant. Assuming that the electric field is linearly polarized and neglecting the third harmonic term (attenuated in the fiber), the total polarization induced in the optical fiber can be written as

$$P = \epsilon_0(\chi^{(1)} + \frac{3|\tilde{E}|^2}{4}\chi^{(3)})E = \epsilon_0 \chi_{\text{eff}} E, \tag{2.14}$$

where χ_{eff} is the effective susceptibility. The refractive index of the medium is related to the effective susceptibility as

$$n^2 = 1 + \chi_{\text{eff}}, \tag{2.15}$$

Then, the refractive index taking into account the nonlinear effects is [54]

$$n(\omega, I) = n(\omega) + n_2 I = n(\omega) + \tilde{n}_2 |E|^2, \tag{2.16}$$

where $n(\omega)$ is the linear refractive index, $\tilde{n}_2$ is the nonlinear-index coefficient, n_2 is the nonlinear Kerr parameter and I is the instantaneous intensity given by $I = \frac{1}{2} n \epsilon_0 c |\tilde{E}|^2$. The nonlinear-index coefficient is

$$\tilde{n}_2 = \frac{3}{8n} Re(\chi^{(3)}). \tag{2.17}$$

The nonlinear Kerr parameter and the nonlinear-index coefficient are related as

$$n_2 = \frac{2\tilde{n}_2}{\epsilon_0 n c}. \tag{2.18}$$

The refractive index is not only wavelength-dependent but also depends on the instantaneous intensity of the field. The Scottish physicist and mathematical lecturer John Kerr discovered the Kerr effect in 1875 [58, 59]. The Kerr effect can be defined as the change in the refractive index of the medium due to the intensity of the propagating field. The nonlinear coefficient (γ) expresses the strength of the nonlinear effects taking into account the transverse field distribution in an optical fiber.

$$\gamma = \frac{2\pi n_2}{\lambda A_{\text{eff}}}, \tag{2.19}$$

where A_{eff} is the effective mode area which depends on the fiber core radius and the core-cladding index difference [54]. For the SSMF, the nonlinear coefficient (γ) is about 1.3 (W km)$^{-1}$. In the case of the HNLFs used in our experiments, γ is around 10 (W km)$^{-1}$. HNLFs with γ as high as 30 (W km)$^{-1}$ have also been demonstrated [60, 61]. The Kerr effect induces a nonlinear phase shift on the propagating signal. The accumulated nonlinear phase shift during propagation in the optical fiber can be calculated as

$$\phi_{NL}(z) = \gamma \int_0^z P(z')dz', \tag{2.20}$$

where, P(z') represents the evolution of power along propagation. The accumulated nonlinear phase shift over a physical length (L) can also be calculated using the effective length (L_{eff}) as

$$\phi_{NL}(L) = \gamma L_{\text{eff}} P(0), \tag{2.21}$$

where

$$L_{\text{eff}} = \frac{1}{\alpha}[1 - \exp(-\alpha L)], \tag{2.22}$$

where α is the attenuation constant in m^{-1} and L is the physical length of the fiber. The effective length can be defined as the length over which a constant power can give the same nonlinear phase shift (ϕ_{NL}) as the total accumulated phase shift over the actual physical length. For a very long SSMF with $\alpha =$ 0.2 dB/km, the effective length is approximately 21 km. The different Kerr

nonlinear effects such as self-phase modulation (SPM), cross-phase modulation (XPM) and four-wave mixing (FWM) are discussed in this section. The SPM and XPM are phase-matched and causes phase modulation on the signals. The FWM involves transfer of energy between different frequency and needs to be phase matched to be efficient.

2.5.1 Self-phase modulation

The propagating optical signal field is phase modulated due to the variation in the refractive index of the optical fiber caused by its own intensity distribution. This is known as self-phase modulation (SPM). By neglecting dispersion and taking into account the fiber loss with the effective length, the nonlinear phase shift induced on the propagating field due to SPM is given by

$$\phi_{NL}^{SPM}(L) = \frac{2\pi}{\lambda}\tilde{n}_2|E|^2 L_{eff} = \gamma P L_{eff}, \tag{2.23}$$

where P is the power of the propagating wave. However, it is important to include dispersion especially for data signals and in this case, the NLSE has to be solved numerically. SPM causes a frequency chirp in the propagating optical pulses which changes the pulse shape and broadens the optical spectrum. The spectral broadening due to SPM was first observed with silica fibers in 1978 [62]. To illustrate the detrimental effect of SPM in fiber-optic communication system, the NLSE was solved with a 10 GBaud quadrature phase shift keying (QPSK). As the signal launch power in to the optical fiber was increased, penalties were observed in the error-vector magnitudes (EVMs) as shown in Figure 2.1 (top). At the bottom, the normalized power spectral density (NPSD) is plotted for different signal launch powers. One can observe that the spectral broadening increases with the launch powers. Mostly, SPM causes symmetric spectral broadening. SPM acts as one of the major limitations in single-channel fiber-optic transmission systems. The interaction between SPM and dispersion can also lead to an interesting phenomenon known as optical solitons [33, 63, 64]. The dispersive phase shift in the anomalous dispersion regime ($\beta_2 < 0$) and the nonlinear phase shift cancels each other, leading to pulse propagation without any change in shape. In fact, this was one of the first techniques used to compensate transmission span nonlinearity.

2.5.2 Cross-phase modulation

The propagating optical signal field is phase modulated due to the variation in the refractive index of the optical fiber caused by another field with different wavelength, direction or state of polarization. This is known as cross-phase modulation. Similar to SPM, neglecting dispersion, the nonlinear phase shift in one wavelength field due to cross phase-modulation caused by N other wavelength fields which are co-polarized and co-propagating is

$$\phi_{NL,1}^{XPM}(L) = 2\gamma P_2 L_{eff} + 2\gamma P_3 L_{eff} + .. + 2\gamma P_N L_{eff} + ..., \tag{2.24}$$

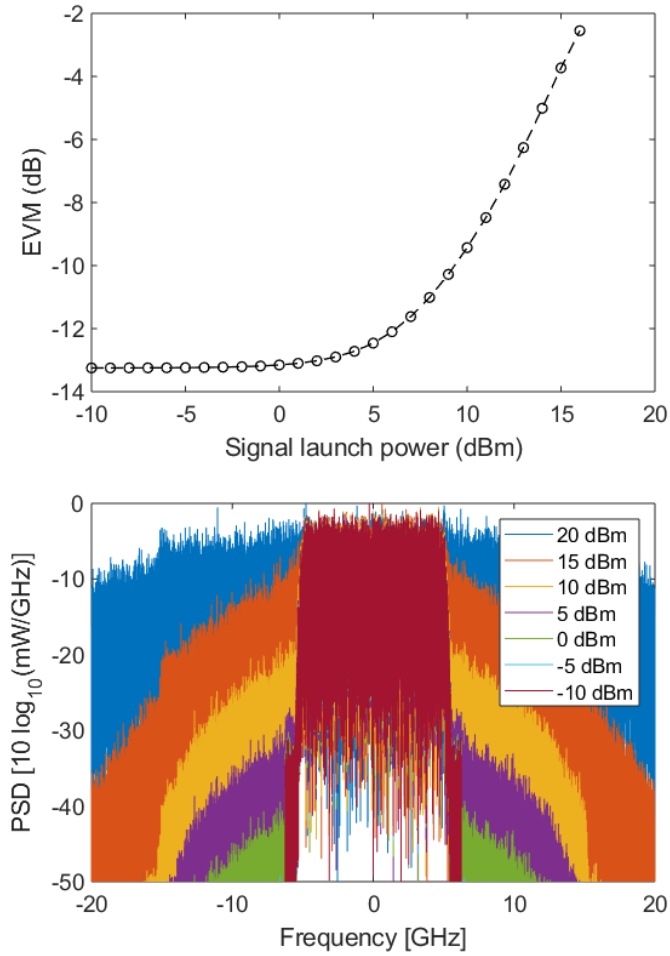

Figure 2.1: Numerical simulations illustrating self-phase modulation (SPM). Top: Error-vector magnitude (EVM) in decibels after propagation in an optical fiber plotted against the signal launch power, bottom: Normalised power spectral density (NPSD) of the signal spectrum after propagation for different launch powers. A 10 GBaud, 10%-root raised cosine, quadrature phase shift keying (QPSK) was propagated numerically in a fiber solving NLSE with $\alpha = 0.2$ dB/km, $D = 16$ ps/(nm km), $\gamma = 1.3$ (W km)$^{-}1$ and $L = 80$ km. The signal SNR at the input of the fiber was set to be 30 dB and no amplifier noise was added after propagation. As the launch power increases, the SPM becomes stronger resulting in EVM penalties and higher spectral broadening.

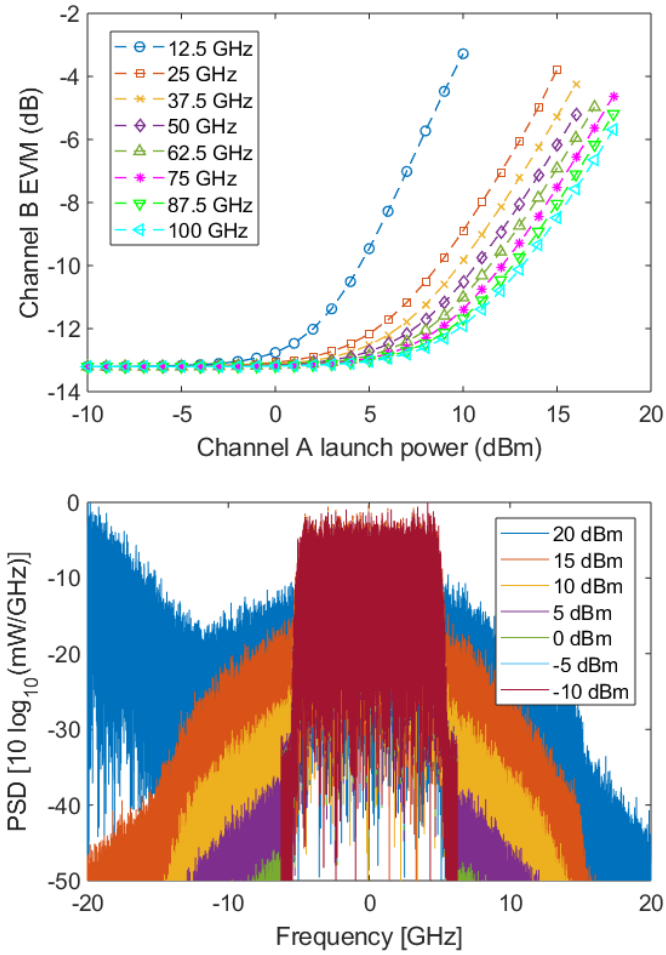

Figure 2.2: Numerical simulations illustrating cross-phase modulation (XPM). Top: EVM of channel B in decibels after propagation in an optical fiber plotted against the channel A launch power for different channel spacings, bottom: Normalised power spectral density (NPSD) of the channel B spectrum after propagation for different channel A launch powers spaced 50 GHz apart. Two 10 GBaud, 10%-root raised cosine, quadrature phase shift keying (QPSK) was propagated numerically in a fiber solving NLSE with $\alpha = 0.2$ dB/km, $D = 16$ ps/(nm km), $\gamma = 1.3$ (W km)$^{-}1$ and $L = 80$ km. The channel A and B SNR at the input of the fiber was set to be 30 dB and no amplifier noise was added after propagation. As the channel A launch power increases, the XPM becomes stronger resulting in EVM penalties and higher spectral broadening for channel B.

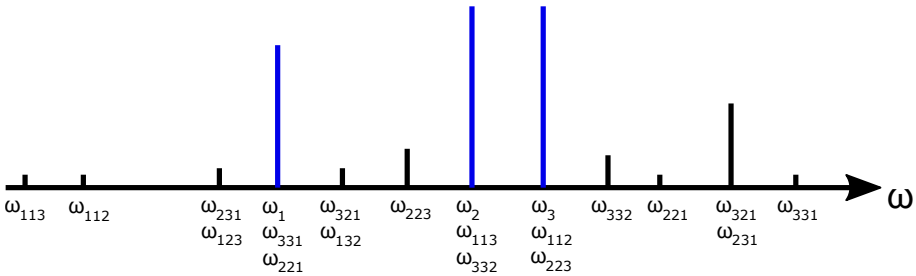

Figure 2.3: Possible FWM components from degenerate and non-degenerate FWM processes. The blue lines correspond to the input fields. [68]

where P_N is the power of N^{th} field. The first experimental verification of XPM was reported in 1985 [65]. For co-polarized different wavelength signals, the phase shift induced by XPM by a wavelength signal is two times stronger than that of SPM on itself. The strength of XPM depends on the degree of relative polarization between involved fields. XpolM can be defined as polarization modulation of an optical field caused by another field in different wavelength [66], which is a major limitation in polarization multiplexed optical transmission systems [67]. However, concerning this work, only single-polarization signals are used making XPM the dominating nonlinear effect limiting the performance. For XPM, the walk-off due to dispersion also plays a major role when the interacting fields are data signals. Numerical simulations were performed to study the impact of XPM with respect to channel spacing (walk-off) and power of the adjacent channel using a two channel system. Two channels A and B were co-propagated together in the same polarization with the scalar NLSE. Both channels contained 10 GBaud QPSK signals. The launch power of channel A and the spacing between channel A and B was swept. The launch power of channel B was kept constant at -10 dBm where there was no SPM. The EVM of channel B is plotted against the channel A launch power as shown in Figure 2.2 (top). As the channel A launch power was increased, the EVM increased for channel B due to XPM for all channel spacings. Also, as the channel spacing was increased, the XPM penalties reduce for the same channel A launch power due to higher walk-off. The NPSD of channel B after propagation is shown in Figure 2.2 (bottom) for a channel spacing of 50 GHz. The spectral broadening increases with the channel A launch power.

2.5.3 Four-wave mixing

As the name implies, four-wave mixing (FWM) involves nonlinear interaction between four fields. The nonlinear interaction leads to exchange of energy between them. FWM was first observed in 1974 in silica fibers [69] when compensating for dispersion. Two co-polarised co-propagating fields, E_1 and E_2 with frequencies ω_1 and ω_2 and propagation constants β_1 and β_2 in the optical

fiber produces an intensity beating at frequencies $\omega_2 - \omega_1$ which leads to variation in the refractive index due to the Kerr effect. The induced refractive index variations acts as a moving grating with propagation constant, $\beta_2 - \beta_1$. Now, if a third co-polarized field, E_3 is added at the frequency ω_3 with propagation constant β_3, then it will be phase modulated by the moving grating, generating side bands at $\omega_4 = \omega_3 \pm (\omega_2 - \omega_1)$ on co-propagation in the optical fiber. The efficiency of this process depends on the phase matching, also known as the Bragg condition, $\beta_4 - \beta_3 = \pm(\beta_2 - \beta_1)$ [52, 68, 70]. Similarly, E_2 beats with E_3 and phase modulates E_1, and E_2 is phase modulated by the beat of E_3 and E_1. If the FWM process involves optical fields oscillating at different frequencies, it is said to be non-degenerate and degenerate process involves two fields of the same frequency. In general, N frequency fields interaction creates a total of $\frac{N^2(N-1)}{2}$ frequency fields [71]. Starting with three waves and only considering first order FWM processes as shown in Figure 2.3, new fields are generated at frequencies,

$$\omega_{jkl} = \omega_j + \omega_k - \omega_l \tag{2.25}$$

The non-degenerate FWM processes, $j, k, l \in \{1, 2, 3\},\ j \neq k,\ j \neq l,\ k \neq l$ and the degenerate FWM processes, $j, k, l \in \{1, 2, 3\},\ j = k \neq l$, create three unique new frequency fields each. Some of the created frequencies may overlap with the original optical waves providing gain. Since only single-polarization signals are considered in this work and all the interacting fields are co-polarized, we will only consider scalar FWM.

In quantum-mechanical interpretation, two photons at frequencies of ω_1 and ω_2 are annihilated to produce two photons at frequencies of ω_3 and ω_4 fulfilling energy $(\omega_1 + \omega_2 = \omega_3 + \omega_4)$ and momentum conservation. In SSMF, operating in the C-band reduces the effect of FWM due to large dispersion. However in HNLFs with low dispersion, FWM processes can be used to realize parametric amplifiers. These parametric amplifiers are known as fiber-optic parametric amplifiers (FOPA). In this work, FOPAs based on scalar FWM processes are used for amplification. A more complete description of phase matching in FWM and how it affects the parametric amplification will be given in section 3.2.

2.6 Stimulated inelastic scattering

The nonlinear effects discussed so far are elastic meaning that there is no loss of energy to the medium. There exist certain effects where a part of the energy is given to the medium through the excitation of the vibrational modes. These are known as stimulated inelastic scattering. There are two important nonlinear effects that fall under this category known as stimulated Brillouin scattering and stimulated Raman scattering.

2.6.1 Stimulated Raman scattering

An optical field excites the vibrational modes of the material which emits another optical field of lower frequency or higher frequency. This is known as spontaneous Raman scattering. The lower frequency field is called the Stokes wave whereas the higher frequency is called the anti-Stokes wave. Raman scattering was observed first by C.V. Raman in 1928 [72] for which he was awarded the Nobel prize in Physics in 1930. In a simple-quantum mechanical picture, a photon is annihilated to give a photon of lower energy (Stokes) and a phonon conserving energy and momentum. Since the phonon energy corresponds to optical frequency, it is known as optical phonon. If an optical phonon of right energy and momentum is available, a photon of higher energy (anti-Stokes) can be obtained, which can happen at higher temperatures. The Raman scattering can be spontaneous or stimulated depending on the strength of the input optical field. Stimulated Raman scattering (SRS) was first observed with a ruby laser in 1962 [73]. SRS is observed at higher optical field strengths above a threshold. In optical fibers, the Raman gain bandwidth is broad due to the amorphous nature of silica. The peak gain is downshifted from the pump frequency by 13.2 THz. SRS also corresponds to the delayed Kerr response. The Raman scattering can produce the Stokes field in both forward and backward direction relative to the direction of pump propagation. SRS can be exploited to obtain amplification. Distributed Raman amplification (DRA) in the transmission span not only improves the span noise figure but also enhances the nonlinearity mitigation for copier-PSA systems. DRA has be used in [B] to study the optical bandwidth dependence on nonlinearity mitigation in copier-PSA systems. The implementation of DRA is discussed in section 3.1.3.1. For the HNLFs used for FOPAs, Raman scattering affects the noise figure, which will be discussed in section 3.2.5

2.6.2 Stimulated Brillouin scattering

Brillouin scattering is similar to Raman scattering except that it involves an acoustic phonon instead of an optical phonon. The involved phonon's energy is much lower compared to the Raman scattering. An optical field is absorbed by the medium, emitting a lower frequency field and an acoustic phonon. This phenomenon can also be spontaneous or stimulated, depending on the strength of the optical field. Stimulated Brillouin scattering (SBS) was first observed in 1964 [74] when exciting crystals with a maser. When the pump exceeds a certain threshold, the stokes field grows rapidly only in the backward direction relative to the pump. The peak gain is downshifted from the pump frequency by approximately 10 GHz with a frequency bandwidth less than 100 MHz in silica fibers.

The maximum continuous wave (CW) power that can be launched into the optical fiber is limited by SBS. With respect to the transmission span, there are no problems with SBS as only modulated signals are launched at higher

powers where the power is distributed over a frequency band. In the case of FOPAs, a high power CW pump is required for the nonlinear interaction. Any increase in power pump after a certain threshold reflects the pump back due to SBS. This limits the maximum power that can be launched into the FOPA. Several methods have been used to increase the SBS threshold.

As SBS depends on the acoustic phonons in the medium, one way to increase the threshold is to change the material properties. This can be done by doping the core with Al instead of Ge [75–77]. The down side is the increase in the fiber loss.

One other method is to phase modulate the pump with a number of RF tones [78] so that the pump power is spread over a frequency band. The frequency of the RF tone should be larger than the SBS gain bandwidth and each tone gives approximately three times increase in the SBS threshold. For a copier-PSA implementation with single-pump FOPAs, the phase modulation is transferred to the idler in the copier and due to dispersion in the transmission link, phase modulation is converted into intensity modulation distorting the idler. This affects the phase-sensitive operation at the PSA. However, in dual-pump FOPAs, the two pumps can be counter-phase modulated resulting in no broadening of the idler spectrum [79].

Another way to suppress the SBS is to apply temperature gradient [80, 81] or strain gradient [82–85] along the FOPA so that the reflected SBS peak from each point ends in different frequencies. However, the temperature or strain gradient will also affect the dispersion along the fiber. The dispersion variations in turn will affect the FOPA's gain bandwidth and noise properties which will be discussed in section 3.2.4. Significant improvement to fiber design lead to the fibers whose dispersion properties remain almost unchanged even with straining [86].

As the SBS gain is exponentially dependent on the Stokes field, using isolators [87–89] in between the HNLFs and dividing them into many sections can increase the SBS threshold. The disadvantage is that the FOPAs cannot be used bidirectionally and the insertion loss increases due to the isolator and extra splicings.

Some of these methods can be used together to obtain higher SBS threshold. In our work, the HNLF used for FOPAs are the special fibers strained having minimum dispersion variations along the length. The 600 m FOPA is separated into four sections with isolators in between them to further suppress the SBS.

Chapter 3

Overcoming linear impairments

The linear impairments that limit the performance of optical fiber transmission systems are fiber loss and dispersion. As this thesis involves only single-polarization signals, fiber birefringence is not considered. Though the losses in the SSMF are as low as 0.2 dB/km, the data signals are attenuated considerably at longer distances. Dispersion limits the transmission distance through pulse-broadening. In this chapter, we will discuss the various techniques to overcome fiber loss and dispersion. Fiber loss can be compensated by amplifying the signal with optical amplifiers, and dispersion can be undone by using dispersion compensating modules (DCMs) or filtering in the digital domain.

3.1 Optical amplification

In a fiber-optic communication systems, the signal gets attenuated on propagation. Repeaters were used to recover the signal before the advent of optical amplifiers, one for each wavelength channel. Repeaters are nothing but transceivers where the optical signals are converted to electrical domain and back to the optical domain. However, with increasing propagation distance and number of wavelength-division multiplexed (WDM) channels, the cost and complexity of optical networks would have increased drastically. The major breakthrough that helped to overcome these limitations were the introduction of optical amplifiers (EDFAs). The repeaters were replaced with EDFAs amplifying WDM channels simultaneously. There are also other amplifiers apart from EDFAs such as semiconductor optical amplifiers (SOAs), Raman amplifiers and parametric amplifiers. These amplifiers have different working principles but all fall under the category of phase-insensitive amplifiers (PIAs) as the gain is independent of the signal phase. However, parametric amplifiers on the other hand can be implemented in phase-sensitive mode which will be discussed in

section 3.2.7. During the process of amplification, noise is also added to the signal which degrades the signal quality in the form of the amplified spontaneous emission (ASE). Assuming that the gain, G is required to compensate for the loss in the fiber, the power spectral density of the ASE noise is [90, 91]

$$S_{ASE} = n_{sp} h \nu_0 (G - 1), \tag{3.1}$$

per polarization, where n_{sp} is the spontaneous emission factor, h is the Planck's constant and ν_0 is the frequency of light. The parameter that determines the performance of an amplifier in terms of added noise is known as the noise figure (NF). The NF is defined as the ratio of the electrical signal-to-noise ratio (SNR) at the input to the electrical SNR at the output of the amplifier when the input is shot-noise limited [92],

$$NF = \frac{SNR_{in}}{SNR_{out}}. \tag{3.2}$$

In the high gain regime, NF = $2n_{sp}$. In general, an ideal amplifier needs the following characteristics to support modern fiber-optic communication links with WDM and polarization-division multiplexed (PDM) signals, 1) low NF - to add as little noise as possible 2) broad gain bandwidth range - to amplify over the entire transmission window 3) polarization insensitive - to support PDM signals 4) low cross gain modulation on bit-level - no nonlinear distortions at saturation and 5) power-efficiency - low power consumption per unit gain.

Optical amplifiers are used in different configurations as shown in Figure 3.1. An optical amplifier can be used to obtain the high signal powers before launching into the transmission link as the power after the laser and modulators might be low. These amplifiers are known as boosters as shown in Figure 3.1 (a). The important requirement for the booster amplifier is to have high output saturation power. To increase the sensitivity of the receiver, optical amplifiers can be used before the detectors, called the preamplifier as shown in Figure 3.1 (b). The NF of the preamplifier determines the sensitivity of the receiver and should be as low as possible. In long-haul links, optical amplifiers are used periodically spanwise to compensate for the loss in that section of fiber known as the inline amplifiers.

The amplifier can be used before the span to pre-compensate for the span loss falling under type-A inline amplifier as shown in Figure 3.1 (c). The amplifier can also be used after the transmission span to compensate for the span loss known as type-B inline amplifier as shown in Figure 3.1 (d). Assuming linear transmission, amplifiers operating in the linear regime, identical losses and amplifiers in each span and high signal input power, the link NF for type-A and -B inline amplifiers are given as [52, 93]

$$NF^{A}_{PIA-PIA} = 1 + 2N(1 - \frac{1}{G}), \tag{3.3}$$

$$NF^{B}_{PIA-PIA} = 1 + 2NG(1 - \frac{1}{G}), \tag{3.4}$$

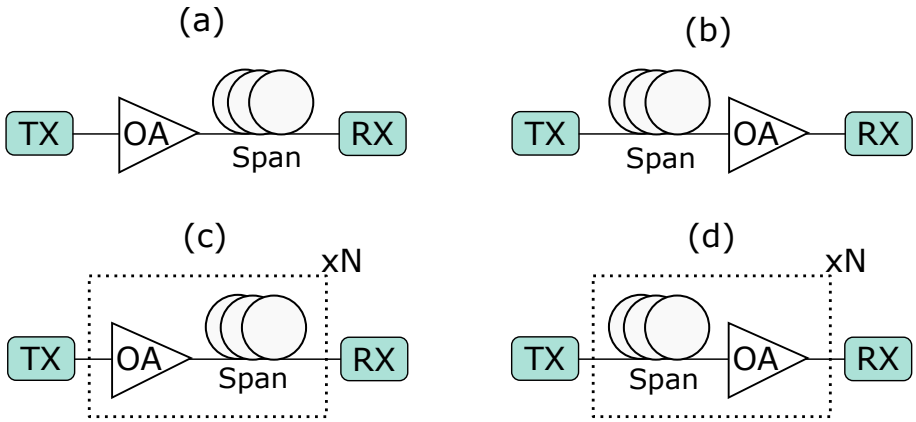

Figure 3.1: Different configurations in which optical amplifiers (OA) can be used in a fiber-optic communication link, a) booster amplifier, b) pre-amplifier, c) inline - type A amplifier, d) inline - type B amplifier. TX - transmitter and Rx- receiver.

where G is the gain in each span and N is the number of spans. The spontaneous emission factor is always greater than 1. Therefore, the quantum-limited NF is 3 dB [45]. In practice, the NF usually varies between 4-10 dB in commercial amplifiers. In this section, the various properties and applications of the above-mentioned amplifiers are discussed.

3.1.1 Erbium-doped fiber amplifiers

EDFAs are the most commercially used optical amplifiers. After its invention in 1986 [94], the EDFAs replaced the repeaters in the fiber links. The gain medium is the erbium-doped fiber which is pumped optically. The two different pumping wavelengths used to achieve population inversion are 980 nm and 1480 nm. The excited erbium ions would relax to the ground state through stimulated or spontaneous emission. Stimulated emission gives a photon of the same frequency, phase and polarization as the incoming photon. This amplifies the input signal. Spontaneous emission produces noise photons of random polarization, direction and frequency over the entire gain bandwidth. However, the spontaneous emission noise is amplified in the gain medium leading to amplified spontaneous emission (ASE). The ASE is added to the signal and acts as an optical noise source. Commercially available EDFAs have gain bandwidth that extends over the C- (1535 to 1565 nm) and L-band (1565 to 1610 nm). The EDFAs are polarization insensitive [95], can have high gains [96] and saturation powers, and low NFs [96]. Moreover, since the gain response time is in the order of milliseconds, they can amplify the signal without nonlinear distortions even when saturated [97]. EDFAs have been used in every possible configuration as listed above - booster, preamplifier and inline amplifier by optimizing the

design parameters. Though n_{sp} close to 1 have been demonstrated for EDFAs, the usual values lie between 2 and 3.

3.1.2 Semiconductor optical amplifiers

A semiconductor optical amplifier (SOAs) can be seen as a semiconductor laser without feedback. The SOAs were designed to work at 850 nm in the 1980s and in the late 1980s were operated at 1300 and 1550 nm. Population inversion is achieved through electrical pumping, the electrons and holes recombine producing stimulated and spontaneous emission. The stimulated and spontaneous emission leads to the gain and noise in the SOA, respectively. The main advantage of the SOAs is the electrical pumping which makes them more power-efficient and compact. The gain bandwidth of the SOAs can be 30-50 nm anywhere between 850 nm and 1600 nm. The n_{sp} is typically 2 [98]. The main issue with SOA is coupling loss between the device and the fiber which affects both the black-box gain and NF. The SOAs have a gain response time in the range of nanoseconds, which induces nonlinear distortions with multiple input channels especially when saturated [99, 100]. Also, the amplification in SOA is usually polarization-dependent. All these shortcomings make SOAs unpopular for amplification in fiber-optic communication systems. However, SOAs has attracted interest in terms of high-speed optical nonlinear processing [101, 102].

3.1.3 Raman amplifiers

Raman amplification is based on the stimulated Raman scattering discussed in section 2.6.1. A strong pump and a weak signal of lower energy than the pump is injected into the silica fiber. The pump photons are inelastically scattered resulting in lower energy photons corresponding to the energy of the weak signal and optical phonons. In this way, the weak signal is amplified. The optical phonon's energy is equal to the difference between the pump and signal photon energy. As the pump power is increased above a certain threshold, the signal gain increases exponentially. Raman gain was first observed in fibers in 1972 [103]. In silica fiber, the Raman gain bandwidth is 40 THz and the peak gain is around 13 THz downshifted from the pump frequency [54]. Thus, to amplify the signal at 1550 nm, the fiber needs to be pumped at 1450 nm. The broader gain bandwidth is due to the amorphous nature of silica. The gain in Raman amplification is also polarization-dependent, but can be made polarization independent by randomly scrambling the Raman pump polarization or by using backward pumping. The power efficiency of the Raman amplifier is low. The main advantage of Raman amplification is that the broad gain bandwidth can be tuned by just changing the pump frequency which makes it a strong contender for WDM amplification outside C- and L-band. In Raman amplification, the noise is caused by spontaneous Raman scattering which depends on temperature. The n_{sp} is atleast 1.3 at room temperature which is close to the quantum limit. The Raman gain response time is in the order of

tens of femtosecond and can cause nonlinear distortions in a WDM system at saturation. Raman amplifiers can be used as a lumped or distributed amplifier. The distributed Raman amplification (DRA) is attractive due to an increase in the transmission reach as a result of decreased link NF [104–106].

3.1.3.1 Distributed Raman amplification

Distributed Raman amplification (DRA) is where the transmission span itself acts as the gain medium. The distributed amplification can be visualized as many small amplifiers placed very close to each other compensating for the loss at every point in the transmission span leading to transparency. Such transparency can be obtained using ideal DRA. Since the signal power across the transmission span is constant, it said to be a flat power map. For an ideal DRA, where the local gain counterbalances the loss at each point along the span, assuming there are infinite amplifiers in the transmission link, the NF in decibels converges to [104],

$$NF_{DRA,ideal}(dB) \approx 10\log(2\alpha_s L + 1) \tag{3.5}$$

where $\exp(\alpha_s L)$ is the net gain needed to compensate the entire span loss and α_s is the attenuation constant at the signal wavelength. The link NF for a span of length 100 km with attenuation constant 0.2 dB/km followed by an EDFA of NF 4 dB is 24 dB. If the same span is amplified with ideal DRA, the link NF would be 10 dB. In this way, DRAs can reduce the link NF and improve the transmission reach. DRAs also enhance the nonlinearity mitigation in links utilizing copier-PSAs [107]. A symmetric power map is required to ideally compensate for transmission span nonlinearity. The easiest and simple method to increase the power map symmetry is to use a single-backward pumped Raman. In this configuration, the signal is initially attenuated but gets amplified in the latter part of the span such that the total net gain is equal to the span loss. However, the degree of flatness is not high in this DRA configuration. To further improve the flatness in the transmission span, one can divide the total transmission span into different segments and pump each of this segment backwards individually with a Raman pump. This was done in the [B] to obtain a flat power map to study the efficiency of nonlinearity mitigation with different symbol rates. The normalized power map for the three-segmented backward pumped DRA used in [B] is shown in Figure 3.2. There are also other ways to achieve similar or better flatness such as using bidirectional pumping with higher-order Raman amplification and fiber-Bragg gratings [108, 109] or by using fibers with different Raman gain parameters in cascade [110].

3.2 Parametric amplifiers

Parametric amplifiers are based on the process of four-wave mixing (FWM) in optical fibers. FWM leads to the exchange of energy between the four interact-

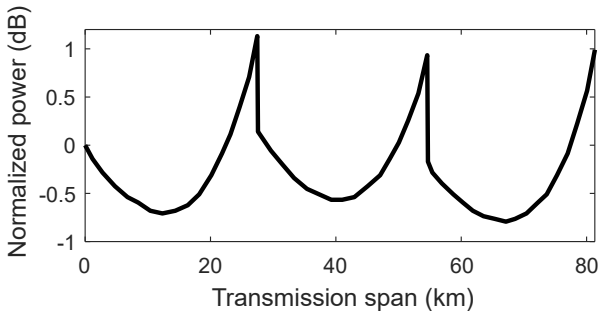

Figure 3.2: Normalized transmission span power map for the DRA used in [B]. The 81 km transmission span was divided into three sections of length 27 km and each section was individually backward pumped with the Raman pump. The glitches in the power map corresponds to the WDM coupler used to add the Raman pump into the transmission span.

ing fields at high powers in the optical fiber. Only scalar FWM is considered here and so all fields are assumed to be co-polarized. When two strong pumps at ω_{P1} and ω_{P2} are launched into the optical fiber with a weak signal at ω_S, one photon of each pump is annihilated to create one photon of the signal and one other photon of energy corresponding to ω_I called the idler. The newly generated idler frequency will be $\omega_I = 2\omega_P - \omega_S$. This process is known as non-degenerate or dual-pumped FWM. During the above process, the weak signal is amplified and the idler is produced. This can happen also with a single pump at ω_P. Two pump photon of same energy gives one signal photon and idler photon such as $\omega_I = 2\omega_P - \omega_S$. This is known as degenerate or single-pumped FWM. The degenerate and non-degenerate FWM processes that are used to achieve parametric amplification in optical fibers known as the fiber-optic parametric amplifiers (FOPAs). The gain in FOPAs are polarization-dependent. However, polarization-independent FOPAs have been demonstrated with orthogonal pumps [111, 112] or using the polarization diversity technique [113]. The gain bandwidth depends on the fiber design which will be discussed in detail in section 3.2.4. The gain response time is in the order of femtoseconds and therefore can cause nonlinear distortions to WDM signals under saturation [114]. However, the fast response time makes them interesting in high-speed signal processing [115, 116]. The main noise source is the amplified quantum noise (AQN) which is similar to the ASE. In this work, parametric amplifiers have been used as pre-amplifiers or inline amplifiers either in phase-insensitive (PI) or phase-sensitive (PS) mode. In this section, we will solve the coupled equations for the non-degenerate (dual-pumped) and degenerate (single-pumped) FWM processes in optical fibers to obtain the corresponding transfer functions. Then, the phase-matching conditions are explained describing the FOPA gain bandwidth. The phase-(in)sensitive operation of FOPAs are analysed. Finally,

the implementation of the copier-PSA is presented.

3.2.1 Dual-pumped or non-degenerate FWM

For a dual-pumped scalar FWM process, two pumps at ω_{P1} and ω_{P2}, a signal at ω_S and an idler at ω_I are launched in the fiber. Assuming the all the interacting fields have the same transverse field distribution, $f(x,y)$ and are co-polarized, the total electric field can be written as [54, 117]

$$\begin{aligned}\tilde{E}_{tol}(x,y,z) = \frac{f(x,y)}{2}[&\tilde{E}_{P1}(z)\exp(-i(\omega_{P1}t-\beta(\omega_{P1})z))\\ &+\tilde{E}_{P2}(z)\exp(-i(\omega_{P2}t-\beta(\omega_{P2})z))\\ &+\tilde{E}_{S}(z)\exp(-i(\omega_{S}t-\beta(\omega_{S})z))\\ &+\tilde{E}_{I}(z)\exp(-i(\omega_{I}t-\beta(\omega_{I})z))] + c.c.,\end{aligned} \tag{3.6}$$

where c.c. denotes the complex conjugate. Using equation (2.1), the above expression can be written as four-coupled equations for propagation along z, ignoring fiber loss, wavelength dependence on γ, the c.c. terms and other weak newly generated nonlinear frequency terms and considering the pumps, signal and idler are CWs [54, 117],

$$\begin{aligned}\frac{d\tilde{E}_{P1}}{dz} = j\gamma(&|\tilde{E}_{P1}|^2+2|\tilde{E}_{P2}|^2+2|\tilde{E}_{S}|^2+2|\tilde{E}_{I}|^2)\tilde{E}_{P1}\\ &+j2\gamma\tilde{E}_{S}\tilde{E}_{I}\tilde{E}^{*}_{P2}\exp(i\Delta\beta z),\end{aligned} \tag{3.7}$$

$$\begin{aligned}\frac{d\tilde{E}_{P2}}{dz} = j\gamma(&|\tilde{E}_{P2}|^2+2|\tilde{E}_{P1}|^2+2|\tilde{E}_{S}|^2+2|\tilde{E}_{I}|^2)\tilde{E}_{P2}\\ &+j2\gamma\tilde{E}_{S}\tilde{E}_{I}\tilde{E}^{*}_{P1}\exp(i\Delta\beta z),\end{aligned} \tag{3.8}$$

$$\begin{aligned}\frac{d\tilde{E}_{S}}{dz} = j\gamma(&|\tilde{E}_{S}|^2+2|\tilde{E}_{P1}|^2+2|\tilde{E}_{P2}|^2+2|\tilde{E}_{I}|^2)\tilde{E}_{S}\\ &+j2\gamma\tilde{E}_{P1}\tilde{E}_{P2}\tilde{E}^{*}_{I}\exp(-i\Delta\beta z),\end{aligned} \tag{3.9}$$

$$\begin{aligned}\frac{d\tilde{E}_{I}}{dz} = j\gamma(&\underbrace{|\tilde{E}_{I}|^2}_{\text{SPM}}+\underbrace{2|\tilde{E}_{P1}|^2+2|\tilde{E}_{P2}|^2+2|\tilde{E}_{S}|^2}_{\text{XPM}})\tilde{E}_{S}\\ &+j2\gamma\underbrace{\tilde{E}_{P1}\tilde{E}_{P2}\tilde{E}^{*}_{S}\exp(-i\Delta\beta z)}_{\text{FWM}},\end{aligned} \tag{3.10}$$

where

$$\Delta\beta = \beta(\omega_S)+\beta(\omega_I)-\beta(\omega_{P1})-\beta(\omega_{P2}), \tag{3.11}$$

is the linear phase mismatch. On the right-hand side of equations (3.7) to (3.10), the first term corresponds to the SPM-induced nonlinear phase shift,

the second group of terms correspond to the XPM-induced nonlinear phase-shift, and the last term corresponds to the FWM. The XPM-induced phase shift is twice that of the SPM-induced phase shift as all the interacting fields are co-polarized. It is also clear that the FWM depends on $\Delta\beta$ which causes the energy transfer between the fields. Assuming $\tilde{E}(z) = \sqrt{P(z)}\exp(j\phi(z))$, where P is the power and ϕ is the phase of the wave, then (3.7) to (3.10) can be written as [117]

$$\frac{dP_{P1}}{dz} = \frac{dP_{P2}}{dz} = -4\gamma\sqrt{P_{P1}P_{P2}P_SP_I}\sin(\theta), \tag{3.12}$$

$$\frac{dP_S}{dz} = \frac{dP_I}{dz} = 4\gamma\sqrt{P_{P1}P_{P2}P_SP_I}\sin(\theta), \tag{3.13}$$

where

$$\begin{aligned}\frac{d\theta}{dz} &= \Delta\beta + \gamma(P_{P1} + P_{P2} - P_S - P_I)\\ &+2\gamma(\sqrt{\frac{P_{P1}P_{P2}P_S}{P_I}} + \sqrt{\frac{P_{P1}P_{P2}P_I}{P_S}}\\ &-\sqrt{\frac{P_{P1}P_SP_I}{P_{P2}}} - \sqrt{\frac{P_{P2}P_SP_I}{P_{P1}}})\cos(\theta),\end{aligned} \tag{3.14}$$

where $\theta(z) = \Delta\beta z - \phi_{P1}(z) - \phi_{P2}(z) + \phi_S(z) + \phi_I(z)$ describes the relative phase between the interacting fields. The first term in equation (3.14) on the right hand side represents the linear phase shift and the second and third term correspond to the nonlinear phase shift. From equations (3.12) to (3.14), by controlling the relative phase, we can dictate the direction of power transfer either from the pump to the signal and idler waves or from signal and idler to the pump waves. For $\theta = \pi/2$, the power transfer is from the pump to signal and idler waves resulting in parametric amplification whereas $\theta = -\pi/2$ makes the power to flow from the signal and idler waves to the pump giving rise to parametric attenuation. Keeping the relative phase, $\theta(z) = \pi/2$ all along the fiber, phase matches the parametric amplification and is discussed in detail in section 3.2.3. Also, it is evident that the change in power is the same in the signal and idler and corresponds to change in the two pump powers such that the total power is conserved which leads us to the Manley-Rowe relation [117]. If we initially have strong pumps, a weak signal and no idler, the idler will be generated at an infinitesimal propagation distance [118] with $\theta = \pi/2$. Considering the phase-matched FWM process that amplifies the signal, $\theta = \pi/2$, the last term on the right-hand side of (3.14) becomes zero. Then (3.14) becomes

$$\frac{d\theta}{dz} = \Delta\beta + \gamma(P_{P1} + P_{P2} - P_S - P_I). \tag{3.15}$$

Introducing the phase mismatch parameter, $\kappa = \Delta\beta + \gamma(P_{P1} + P_{P2})$ and assuming the power of pumps are much higher than the signal and idler waves,

we can write the condition to remain phase-matched as

$$\frac{d\theta}{dz} = 0 = \Delta\beta + \gamma(P_{P1} + P_{P2}) \equiv \kappa. \tag{3.16}$$

Assuming the pumps are not depleted and the signal and idler powers are low compared to that of the pumps, the solutions to the coupled equations (3.9) to (3.10), neglecting a common phase term is [52]

$$\tilde{E}_S(z) = \mu(z)\tilde{E}_S(0) + \nu(z)\tilde{E}_I^*(0), \tag{3.17}$$

$$\tilde{E}_I(z) = \mu(z)\tilde{E}_I(0) + \nu(z)\tilde{E}_S^*(0), \tag{3.18}$$

where μ and ν are the transfer functions for the fiber given by

$$\mu(z) = \cosh(gz) + j\frac{\kappa}{2g}\sinh(gz), \tag{3.19}$$

$$\nu(z) = 2j\gamma\frac{\tilde{E}_{P1}(0)\tilde{E}_{P2}(0)}{g}\sinh(gz). \tag{3.20}$$

Also, $|\mu(z)|^2 - |\nu(z)|^2$ always equal to 1 which comes from the Manley-Rowe relation addressed above. The parametric gain coefficient is

$$g = \sqrt{4\gamma^2 P_{P1}P_{P2} - (\frac{\kappa}{2})^2}. \tag{3.21}$$

3.2.2 Single-pumped or degenerate FWM

For single pump degenerate FWM where the pump fields cannot be distinguished in frequency, the analysis should be carried out with just three waves. Assuming $\omega_{P1} = \omega_{P2} = \omega_P$ and $\Delta\beta = \beta(\omega_S) + \beta(\omega_I) - 2\beta(\omega_P)$, similar to equations (3.12) (3.13) and (3.14) for the dual-pump FWM, the equations for the single-pumped FWM processes are derived as [68, 119, 120]

$$\frac{dP_P}{dz} = -4\gamma\sqrt{P_P^2 P_S P_I}sin(\theta), \tag{3.22}$$

$$\frac{dP_S}{dz} = \frac{dP_I}{dz} = 2\gamma\sqrt{P_P^2 P_S P_I}sin(\theta), \tag{3.23}$$

$$\begin{aligned}\frac{d\theta}{dz} &= \Delta\beta + \gamma(2P_P - P_S - P_I) \\ &+\gamma(\sqrt{\frac{P_P^2 P_S}{P_I}} + \sqrt{\frac{P_P^2 P_I}{P_S}} - 4\sqrt{P_S P_I})cos(\theta),\end{aligned} \tag{3.24}$$

where the relative phase difference, $\theta(z) = \Delta\beta z - 2\phi_P(z) + \phi_S(z) + \phi_I(z)$, and the phase-matching condition can be written as

$$\kappa \equiv \Delta\beta + 2\gamma P_P = 0. \tag{3.25}$$

The transfer functions are [121]

$$\mu(z) = \cosh(gz) + j\frac{\kappa}{2g}\sinh(gz), \tag{3.26}$$

$$\nu(z) = j\gamma\frac{\tilde{E}_P^2(0)}{g}\sinh(gz). \tag{3.27}$$

The parametric gain coefficient,

$$g = \sqrt{\gamma^2 P_P^2 - (\frac{\kappa}{2})^2}. \tag{3.28}$$

3.2.3 Phase-matching

Phase-matching refers to the process of maintaining the relative phase (θ) between the different interacting waves constant during propagation. During propagation, the interacting optical fields experience relative phase shifts due to the linear phase mismatch caused by the difference in their propagation constants and the nonlinear phase shift due to SPM and XPM. The $\Delta\beta$ in equations (3.16) and (3.25), corresponds to the linear phase mismatch and the next term describes the nonlinear phase-shift. If the linear and the nonlinear phase shift cancel out each other, perfect phase matching is achieved where $\kappa = 0$. In the nearly phase-matched condition, the relative phase changes by a small amount during propagation still providing a good gain. For the single-pumped FOPAs operating at high gain, the maximum gain obtained with perfect phase-matching, i.e., $\kappa = 0$, is

$$G_S^{max} = G_S^{exp} \approx \frac{\exp(2\gamma P_P z)}{4}, \tag{3.29}$$

where the phase-matching condition becomes

$$\Delta\beta = -2\gamma P_P. \tag{3.30}$$

In the case of the dual-pumped FOPAs, the maximum gain and the phase-matching condition is

$$G_S^{max} = G_S^{exp} \approx \frac{\exp(4\gamma\sqrt{P_{P1}P_{P2}}z)}{4}, \tag{3.31}$$

where the phase-matching condition becomes

$$\Delta\beta = -\gamma(P_{P1} + P_{P2}). \tag{3.32}$$

At maximum gain, the gain exponential depends on the nonlinear phase shift and is known as the exponential gain regime. The other special case is when the linear phase shift becomes zero, i.e., $\Delta\beta = 0$, then for a single-pumped

FOPAs with $\kappa = -2\gamma P_P$, a quadratic dependence on the nonlinear phase-shift is obtained as

$$G_S^{quad} \approx (2\gamma P_P z)^2, \tag{3.33}$$

whereas for the dual-pumped FOPAs, still an exponential gain can be obtained [54, 122].

3.2.4 Gain bandwidth

The gain bandwidth of the FOPA depends on the linear phase mismatch. Taylor series coefficients for dispersion above fourth-order (β_4) is neglected in this analysis as their effect is very minimal. Also, the third-order Taylor series coefficient does not affect the linear phase mismatch. The linear phase mismatch can be Taylor expanded around the pump frequency (ω_P) for the single-pump configuration and written as [54, 68]

$$\begin{aligned} \Delta\beta &= \beta(\omega_S) + \beta(\omega_I) - 2\beta(\omega_P) \\ &\approx \beta_2(\omega_S - \omega_P)^2 + \frac{\beta_4(\omega_S - \omega_P)^4}{12}. \end{aligned} \tag{3.34}$$

The gain bandwidth of the single-pumped FOPA can be plotted with equation (3.34). Figure 3.3 shows the gain bandwidth for a single-pumped PIA with different λ_{ZDW} which is similar to sweeping the pump wavelength with fixed λ_{ZDW}. By pumping in the normal dispersion regime ($D < 0$), we obtain a quadratic gain as seen for $\lambda_P = \lambda_{ZDW} - 1.0$ nm. When pumped at the λ_{ZDW}, we obtain a flat quadratic gain limited by β_4 as shown in $\lambda_P = \lambda_{ZDW}$. As we pump in the anomalous dispersion regime ($D > 0$), the gain increases more than the quadratic gain as seen for $\lambda_P = \lambda_{ZDW}$+0.2 nm, $\lambda_P = \lambda_{ZDW}$+0.35 nm, $\lambda_P = \lambda_{ZDW} + 1$ nm and $\lambda_P = \lambda_{ZDW} + 2$ nm. We obtain exponential gains for $\lambda_P = \lambda_{ZDW} + 0.35$ nm, $\lambda_P = \lambda_{ZDW} + 1$ nm and $\lambda_P = \lambda_{ZDW} + 2$ nm. The single-pumped PIA should be pumped in the anomalous dispersion regime to achieve perfect phase matching. For large values of $\lambda_p - \lambda_{ZDW}$, second-order Taylor series dispersion coefficient, β_2 dominates and the fourth-order Taylor series dispersion coefficient, β_4 is less important. However, when operating close to λ_{ZDW} where the Taylor series dispersion coefficient, β_2, is very small, β_4 becomes dominant as seen for $\lambda_{ZDW} + 0.35$ nm.

For the dual-pump configuration, the linear phase mismatch can be Taylor expanded around the center frequency $\omega_C = \frac{\omega_{P1}+\omega_{P2}}{2}$ with $\omega_D = \frac{\omega_{P1}-\omega_{P2}}{2}$ as [54, 122]

$$\begin{aligned} \Delta\beta &= \beta(\omega_S) + \beta(\omega_I) - \beta(\omega_{P1}) - \beta(\omega_{P2}) \\ &\approx \beta_2[(\omega_S - \omega_C)^2 - \omega_D^2] + \frac{\beta_4[(\omega_S - \omega_C)^4 - \omega_D^4]}{12}. \end{aligned} \tag{3.35}$$

By placing the two pumps far away on either side of the λ_{ZDW} such that

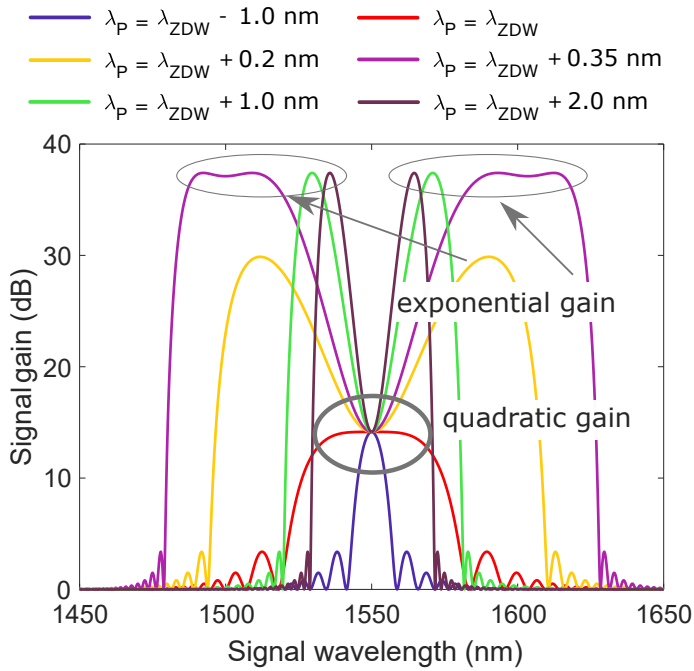

Figure 3.3: Analytically calculated gain bandwidth for a single-pumped FOPAs with $\lambda_P = 1550$ nm, $z = 500$ m, $\beta_3 = 0.1$ ps^3/km, $\beta_4 = 1$ x 10^{-4} ps^4/km, $\gamma = 10\ (W\ km)^{-1}$ and $P_P = 1$ W

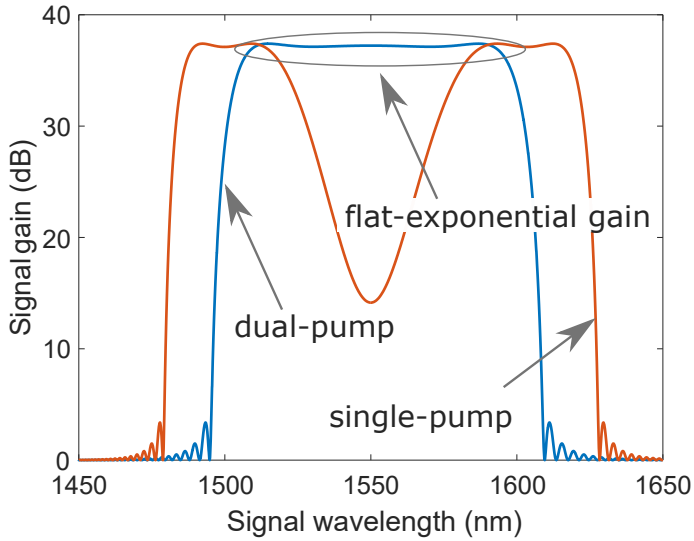

Figure 3.4: Comparison of the analytically calculated maximum gain bandwidth with single and dual-pump FOPAs with $\lambda_C = 1550$ nm, $z = 500$ m, $\beta_3 = 0.1$ ps^3/km, $\beta_4 = 1$ x 10^{-4} ps^4/km, $\gamma = 10$ W^{-1}km^{-1}. For single-pumped FOPA, $\lambda_C = \lambda_P = \lambda_{\text{ZDW}} + 0.35$ nm and $P_P = 1$ W. For dual-pumped FOPA, $\lambda_C = \frac{2}{\frac{1}{\lambda_{P1}}+\frac{1}{\lambda_{P2}}} = \lambda_{ZDW} + 0.05$ nm and $P_{P1} = P_{P2} = 0.5$ W. In both configurations, the pump wavelength were optimized with respect to the zero-dispersion wavelength (λ_{ZDW}) for maximum gain bandwidth.

ω_C is close to the zero-dispersion frequency, perfect phase matching can be achieved over the entire gain bandwidth. We also compare the gain bandwidth for the single-pumped and dual-pumped FOPAs in Figure 3.4. The pump frequencies are optimized in each case with respect to the λ_{ZDW} for flat gain bandwidths and we can find that the dual-pumped FOPAs can have exponential gain even in the center of the gain bandwidth which is not possible in the case of the single-pumped FOPAs. Dual-configuration FOPAs has certain advantages over the single-pump configuration. The gain depends on the total pump power and with dual-pump configuration, 3 dB higher total pump power can be obtained for the same SBS threshold providing higher gain. Moreover as mentioned in section 2.6.2, the two pumps can be counter phase-modulated to further increase the SBS threshold without broadening the idler spectrum. The main advantage is the flat broad gain bandwidth with exponential gain in a dual-pump configuration which is important for WDM systems. These gain bandwidths are obtained only considering four interacting fields but in reality, one might need to include more possible interactions. In case of the two pumps, a signal and three idlers might need to be considered [117,122,123]. Moreover, pump depletion should also be taken into account [117,124]. The AQN interaction with the pump also should be considered especially when modelling high gain FOPAs [52]. Solving the equation 2.1 numerically using SSFM is the most reliable way of modelling the gain bandwidth in FOPAs. In our experiments, the single-pumped FOPAs have been used as the signal bandwidths are not more than 35 GHz. However, it will be advantageous to move to dual-pumped FOPAs due to their flat gain bandwidth.

3.2.5 Noise in fiber-optic parametric amplifiers

In FOPAs, there are four different noise sources [125]. The fundamental noise is due to the amplification of vacuum fluctuations by the pump known as the amplified quantum noise [52, 126]. This leads to the quantum-limited NF of 3 dB in the case of phase-insensitive operation. The other three additive noise sources are Raman-scattering-induced noise, pump transferred noise (PTN) and pump residual noise [52, 125]. The Raman-scattering-induced noise is responsible for the asymmetric NF around the pump especially at high pump power and broader gain bandwidth [127, 128]. The fast gain response time of the FOPAs transfers the intensity noise from the pump to the signal and idler. This leads to significant PTN, especially at high signal power [129]. The intensity noise can be caused by the low optical signal-to-noise ratio (OSNR) of the pump [130]. Therefore, to reduce the detrimental effect of PTN, a high OSNR pump is required. The last one is the pump residual noise due to the imperfect filtering of the pump ASE after amplification. One can use cascaded filters to reduce the out of band ASE for the pump but the insertion loss also increases. Furthermore, the noise figure of the FOPAs can be affected by the variation of the fiber dispersion properties along the fiber length [131–133].

3.2.6 Phase-insensitive amplifier

In case of no idler at the input, i.e., $\tilde{E}_I(0) = 0$, from equations (3.17) and (3.18), the output signal and idler are given by

$$\tilde{E}_S(z) = \mu(z)\tilde{E}_S(0) \tag{3.36}$$

and

$$\tilde{E}_I(z) = \nu(z)\tilde{E}_S^*(0), \tag{3.37}$$

respectively. From the above equations, the output signal and idler do not depend upon the relative phase difference between the interacting waves. Therefore, they are said to be operating in PI mode, also know as phase-insensitive amplifiers (PIAs). The phase-insensitive operation is shown in figure 3.6(a). The signal gain for the PIAs can be calculated from equation (3.36) as

$$G_S = |\mu(z)|^2, \tag{3.38}$$

which in the case of dual-pumped PIAs can be written as

$$G_S = 1 + [\frac{2\gamma\sqrt{P_{P1}P_{P2}}}{g}\sinh(gz)]^2, \tag{3.39}$$

and for single-pumped PIAs is [68],

$$G_S = 1 + [\frac{\gamma P_P}{g}\sinh(gz)]^2. \tag{3.40}$$

The conversion efficiency for the generated idler which is the ratio of the output idler power to the input signal power, from equation (3.37) is

$$G_I = |\nu(z)|^2, \tag{3.41}$$

which for the dual-pumped PIAs is

$$G_I = [\frac{2\gamma\sqrt{P_{P1}P_{P2}}}{g}\sinh(gz)]^2. \tag{3.42}$$

and in the case of the single-pumped PIAs [68],

$$G_I = [\frac{\gamma P_P}{g}\sinh(gz)]^2. \tag{3.43}$$

At high gain, with the shot-noise limited input signal, the output signal and idler can have a quantum-limited NF of 3 dB [126, 134]. From equation 3.37, one can note that the generated idler is the conjugated copy of the signal. In this way, the PIA can act as the copier. Moreover, the noise in the idler will also be the conjugated copy of the signal noise. This enables the copier-PSA to mitigate nonlinear phase noise (NLPN) [135].

3.2.7 Phase-sensitive amplifiers

For the phase-insensitive (PI) operation, no idler was present at the FOPA input. If an idler is present at the input for the FWM process, coherent superposition of the signal and idler takes place. From equations (3.17) and (3.18), one can note that the output signal and idler depends on the relative phase between the interacting fields. This process is phase-sensitive and parametric amplifiers when implemented in phase-sensitive (PS) mode are known as phase-sensitive amplifiers (PSAs). One can categorize PSAs depending on the number of distinct signal and idler frequencies. If the signal and idler have the same frequency i.e., if only the signal is present which also satisfies the frequency condition to be an idler, it is known as one-mode PSA. If a signal and a idler with different frequencies are used, it is a two-mode PSA. Even four-mode PSAs have been analysed with one signal and three idlers occupying three different frequencies. However, four-mode PSAs cannot be described using equations (3.17) and (3.18), as three different FWM processes are involved. The one- and two-mode PSAs can be implemented using single-pump or dual-pump FOPAs whereas the four-mode PSAs can be implemented only using dual-pump FOPAs. The different PSA configurations [52,70] are shown in Figure 3.5 and will be briefly discussed in this section. The one-mode PSAs can be implemented with fully-degenerate FWM or signal-degenerate FWM process. In the fully-degenerate FWM process, the signal, the pump and the idler lie on the same frequency, $\omega_P = \omega_S = \omega_I$ as shown in Figure 3.5 (a). Therefore, implementing the fully-degenerate PSA requires interferometry techniques [136–138]. Moreover, the signal gain depends only quadratically on the nonlinear phase shift as the linear phase mismatch is zero whereas is other configurations exponentially dependence can be obtained. In general fully degenerate one-mode PSA is of no practical interest. The frequency relation between the interacting fields in case of the signal-degenerate FWM process is $\omega_{P1} + \omega_{P2} = 2\omega_S = 2\omega_I$ as shown in Figure 3.5 (b). The output signal for one-mode PSA implemented with signal degenerate FWM is given as

$$\tilde{E}_S(z) = \mu(z)\tilde{E}_S(0) + \nu(z)\tilde{E}_S^*(0). \tag{3.44}$$

Then, the PSA gain can be calculated as

$$G_S = \frac{|\tilde{E}_S(z)|^2}{|\tilde{E}_S(0)|^2} = |\mu(z)|^2 + |\nu(z)|^2 + 2|\mu(z)||\nu(z)|\cos(\phi(z)), \tag{3.45}$$

where the relative phase, $\phi(z) = 2\phi_S(z)$ assuming the pump phases are zero. The signal is amplified when $\phi_S(z) = 0$ and de-amplified at $\phi_S(z) = \frac{\pi}{2}$. Therefore, one signal quadrature will be amplified while attenuating the other quadrature, producing a squeezed output signal as shown in Figure 3.6 (b). In practice, one can choose which quadrature have to be squeezed by controlling the pump phase, $\phi_{P1}(z)$ or $\phi_{P2}(z)$. The one-mode PSAs has been used for optical phase regeneration [139]. However, one-mode PSAs cannot be used

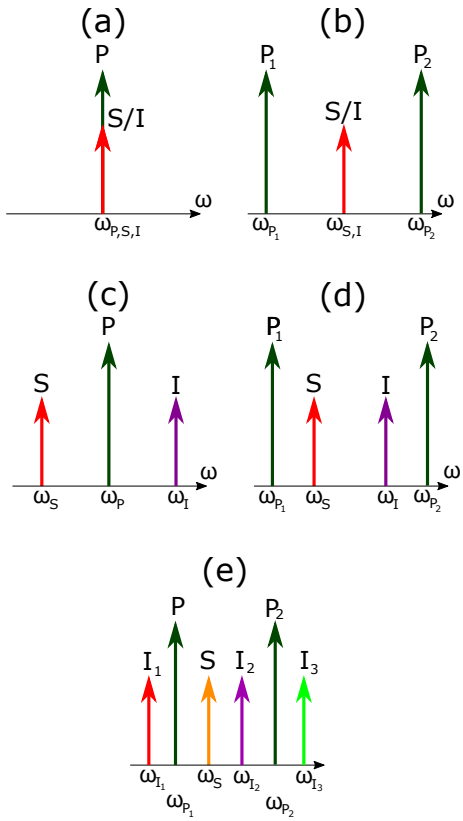

Figure 3.5: PSAs based on (a) fully-degenerate FWM, (b) signal-degenerate FWM, (c) pump-degenerate FWM, (d) non-degenerate FWM and (e) four-mode

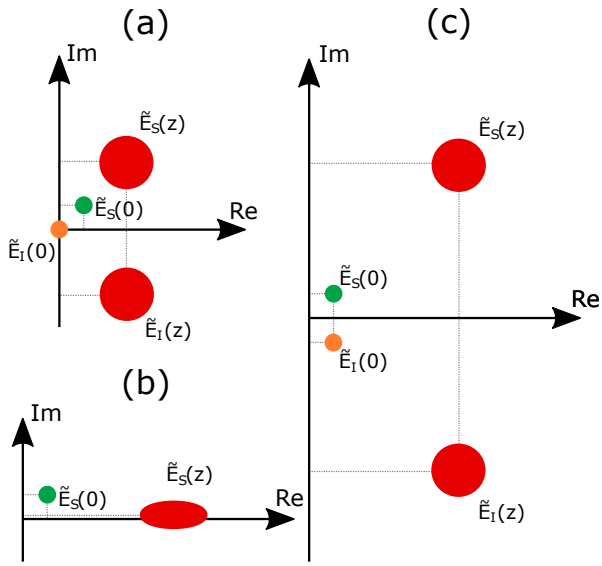

Figure 3.6: Amplification in the high-gain regime with (a) PIA (b) one-mode PSA (c) two-mode PSA, where $\tilde{E}_S(0)$ and $\tilde{E}_I(0)$ are the input signal and idler waves, respectively. The signal and idler output is given by $\tilde{E}_S(z)$ and $\tilde{E}_I(z)$, respectively. The gain in PSA is four times larger than the gain in PIA.

for amplifying signals modulated in both amplitude and phase like quadrature-amplitude modulation. Also, they are not compatible with wavelength-division multiplexed (WDM) signals.

The two mode PSAs can be realized using pump degenerate or non-degenerate FWM processes. In the pump-degenerate FWM, the signal and idler are located symmetrically around the pump with frequency relation, $2\omega_P = \omega_S + \omega_I$ as shown in Figure 3.5 (c). The non-degenerate FWM process for two-mode PSAs is shown in Figure 3.5 (d), the relation between the pump, signal and idler frequencies are given by $\omega_{P1} + \omega_{P2} = \omega_S + \omega_I$. The signal and idler at the output is given by equations (3.17) and (3.18), respectively. The PSA gain can be calculated assuming that the input signal and idler are balanced in power as

$$G_S = \frac{|\tilde{E}_S(z)|^2}{|\tilde{E}_S(0)|^2} = |\mu(z)|^2 + |\nu(z)|^2 + 2|\mu(z)||\nu(z)|\cos(\phi(z)), \tag{3.46}$$

where $\phi(z) = \phi_S(z) + \phi_I(z)$ when the pump phase(s) are zero. If the input idler is a conjugated copy of the signal as $\phi_S(z) = -\phi_I(z)$, then the signal will be amplified in both quadratures. Such an idler can be obtained from a PIA acting as a copier as discussed in section 3.2.6. The implementation is known as copier-PSA [46, 47]. The maximum PSA gain is

$$G_S^{max} = \frac{|\tilde{E}_S(z)|^2}{|\tilde{E}_S(0)|^2} = |\mu(z)|^2 + |\nu(z)|^2 + 2|\mu(z)||\nu(z)| = (|\mu(z)| + |\nu(z)|)^2. \tag{3.47}$$

In the high regime where $\mu(z) \approx \nu(z)$, the maximum phase-sensitive gain is equal to four times the gain of the phase-insensitive amplifier (equation (3.38)) with the same pump power as shown in Figure 3.6 (c). If the signal and idler are shot noise limited, considering only the signal, a quantum limited -3-dB NF can be obtained [70]. Considering both the signal and idler, the quantum-limited NF of two-mode PSA is 0 dB [45,123]. This can result in a transmission reach improvement of 6 dB. However, the major disadvantage is that the idler needs to be transmitted without carrying extra information. Therefore, the spectral efficiency is halved compared to the PIAs or the one-mode PSA at high SNRs. The two-mode PSA can be used for amplifying any modulation format and WDM signals.

A four-mode PSA can be implemented with a dual-pump FOPA. There are three FWM processes [52, 70, 123] involved between two pumps, one signal and three idlers as shown in Figure 3.5 (e). At high gain, the coherent superposition of the signal and idlers, increases the gain by 12 dB compared to PIAs [140]. With shot-noise limited input signals, a quantum limited NF of -6 dB can be achieved only considering the signal and 0 dB with signal and idlers. However, the spectral efficiency is reduced four times compared to a PIA and one-mode PSA and two times compared to two-mode PSA. Therefore it is not very interesting for fiber-optic communication. From now on we restrict our analysis and discussion to the two-mode PSAs using pump-degenerate and fully-degenerate FWM processes.

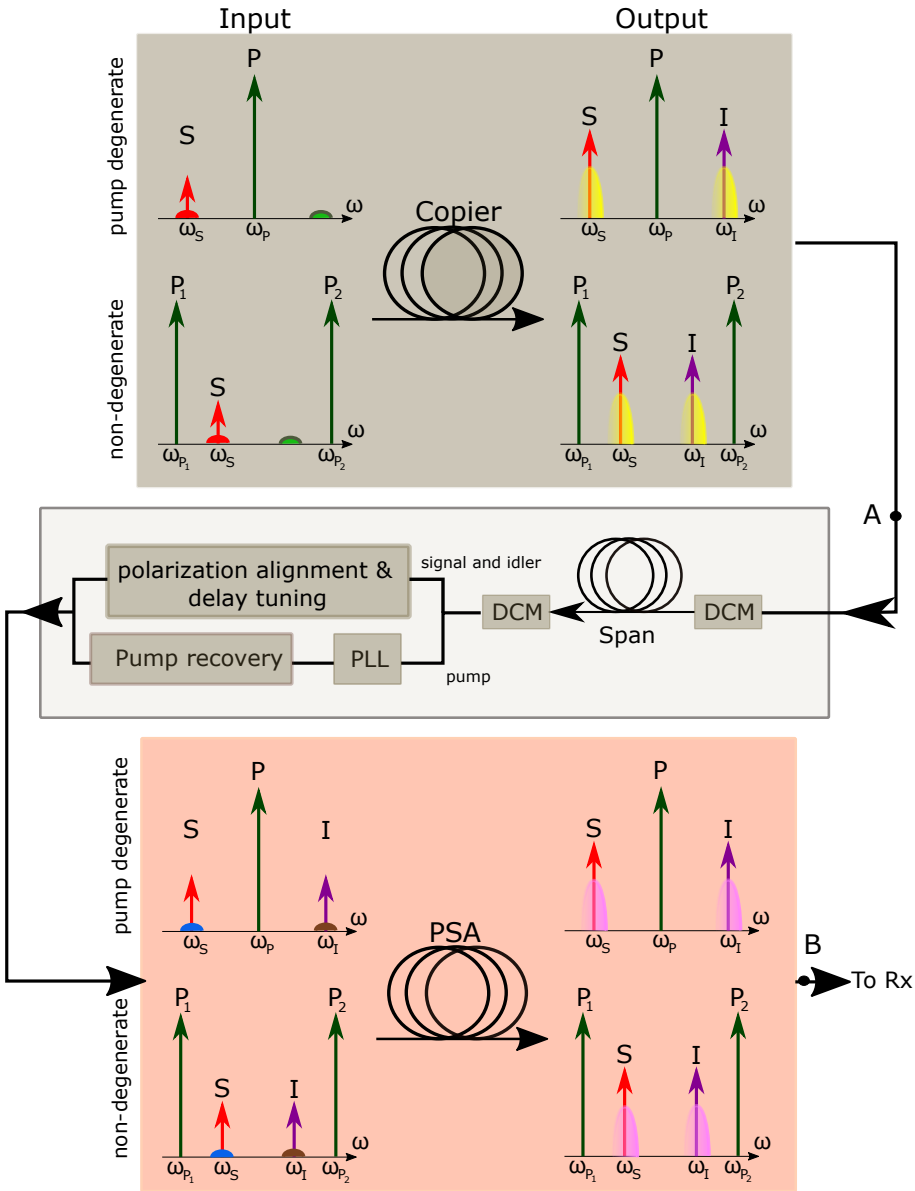

Figure 3.7: Copier-PSA implementation using pump-degenerate and non-degenerate FWM.

3.2.8 Copier-PSA implementation

The two-mode PSAs are mostly implemented using the copier-PSA scheme [53]. The copier-PSA implementation consists of two HNLFs which utilize pump-degenerate or non-degenerate FWM processes as shown in Figure 3.7. The signal in this section will correspond to the signal band which can be a single-channel [A,B,E] or a number of WDM channels [C,D,F]. The signal is combined with a high power pump(s) and launched into the first HNLF. The first HNLF acts as the copier. It generates the idler, a conjugated copy of the signal at $\omega_I = 2\omega_P - \omega_S$ for the pump-degenerate case and $\omega_I = \omega_{P1} + \omega_{P2} - \omega_S$ for the non-degenerate case. Assuming the signal is shot-noise limited, the uncorrelated noise at the signal and idler frequency add incoherently and produce correlated signal and idler noise at the output. After the copier, a set of three or four phase- and frequency locked waves are obtained. The second HNLF acts as the PSA. If the noise at the input of the PSA for the signal and idler is below the quantum-noise limit, which is the case if the loss between the copier and PSA is large enough, the frequency and phase-locked waves will provide a 6-dB higher SNR due to phase-sensitive operation at the linear transmission regime [49]. The loss attenuates the correlated noise and adds vacuum noise [93, 141, 142], leading to uncorrelated noise in the signal and idler. The transmission span is placed in between the copier and PSA which acts as the loss element in fiber links. However, if the noise at the PSA input is above the quantum-limit, depending upon the correlation between the signal and idler noise the SNR advantage of 6-dB decreases [135, 143].

The three or four frequency- and phase-locked waves at the output of the copier are ideal for phase-sensitive operation at the PSA. The transmission span is SSMF that distorts the waves due to dispersion and polarization-mode dispersion (PMD). The waves at the input of the PSA should be synchronized in time, aligned in polarization and stabilized in phase relative to each other for phase-sensitive operation. Let us assume that the signal and idler fields are given by $\tilde{E}_S(t,0)$ and $\tilde{E}_I(t,0) = \tilde{E}_S^*(t,0)$, respectively at the input of the transmission span. In the Fourier domain, the signal and idler are $\tilde{E}_S(\omega,0)$ and $\tilde{E}_I(\omega,0) = \tilde{E}_S^*(-\omega,0)$, respectively. After propagation in the fiber of length L with second-order Taylor series dispersion coefficient, β_2, the signal field is $\tilde{E}_S(\omega,0)\exp(j\frac{\beta_2}{2}\omega^2 L)$ whereas the idler field is $\tilde{E}_I(\omega,0)\exp(j\frac{\beta_2}{2}\omega^2 L) = \tilde{E}_S^*(-\omega,0)\exp(j\frac{\beta_2}{2}\omega^2 L)$. One can note that the idler is no more the conjugate of the signal because of the the extra phase terms due to dispersion. Therefore, the signal and idler need to be dispersion compensated in copier-PSA links. For dispersion compensation, two tunable channelized fiber-Bragg grating-based dispersion compensation modules slope-matched to SSMFs were used, sandwiching the transmission span. The two DCMs are used to set the required pre- and post-dispersion compensation in the transmission link. which plays an important role in nonlinearity mitigation with PSAs. Further, in order to temporally synchronize the signal and idler pulses, i.e., to compensate for the group delay difference, path length matching was done by separating

the signal and idler. Also, the polarization of the signal and idler are aligned in the polarization alignment and delay tuning stage. In order to avoid FWM between signal, idler and pump in the transmission span, the pump(s) is attenuated to lower powers. PSA requires a high OSNR, high power pump(s) to avoid pump transfer noise. The weak pump tone(s) is optically injection locked (OIL) in distributed feedback lasers (DFBs) to obtain the high quality pump(s). In OIL, the phase of the incoming light is seeded to the laser output within a bandwdith known as the locking bandwidth and the amplitude noise is suppressed [144, 145]. OIL at as low injected powers as -65 dBm has been demonstrated [146]. The generated pumps are then combined with the signal and idler launched into the PSA. As signal, idler and pump(s) are split, propagated in different fibers and then combined, the relative phase between the waves might fluctuate due to vibrations or thermal drifts. A phase-locked loop (PLL) fed with a fraction of the PSA output power is used to stabilize the relative phase along with the piezoelectric-transducer which is part of the pump recovery stage by maximising the PSA gain. A 40 kHz tone is phase-modulated on to the pump, which gets transferred from the pump to the signal through FWM is used as the reference for the PLL.

For a PSA-amplified multi-span link, the section between A and B in the Figure 3.7 has to be repeated for each transmission span. In our experiments, two-mode PSA was used utilizing pump-degenerate FWM for the copier and PSA. However, non-degenerate PSAs will be the better scheme for WDM applications due to the flatter gain bandwidth. For a single span transmission with the span in between the two HNLFs, PSA can act as a pre-amplifier. A copier-PSA implementation with PSA as a pre-amplifier was used in [D-F] to study cross-phase modulation mitigation, modulation format dependence and enhancement using Volterra nonlinear equalizer (VNLE) for multiple channels, respectively. The copier-PSA was also used in multi-span configurations using a circulating loop arrangement corresponding to type-A inline amplifiers in papers [A-C] to study nonlinearity mitigation dependence on dispersion map along with the VNLE, symbol rate and number of WDM channels, respectively.

3.2.8.1 Link noise figure

For the single-span link, in the linear transmission regime and linear region of operation for the amplifier, the noise figure for the copier-PSA is given as [49, 141]

$$NF_{copier-PSA} \approx \frac{G}{2}. \tag{3.48}$$

Similarly, for two cascaded PIAs, the link NF is [49]

$$NF_{PIA-PIA} \approx 2G. \tag{3.49}$$

In both the cases, the loss between the two stages is assumed to be large and also it is considered that the second amplifier compensates for the loss with the gain G. Comparing equations (3.48) and (3.49), a 6 dB advantage in SNR

can be seen for copier-PSA system compared to the PIA-PIA system. The principle 6-dB sensitivity improvement using copier-PSAs in single-span links is demonstrated with single [50, 147][E] and multiple [D] channels. For the multi-span link consisting of N spans, the PSA can be used as inline amplifier in two configurations namely type A and type B as shown in section 3.1 using copier-PSA. For multi-span links, in linear transmission regime and linear operation for the amplifier, the link NFs can be approximated as [52, 142],

$$NF^{A}_{copier-PSA} \approx \frac{5}{2} + \frac{N}{2}, \tag{3.50}$$

$$NF^{B}_{copier-PSA} \approx \frac{3G}{2} + \frac{NG}{2}. \tag{3.51}$$

where G is the inline amplifier gain which is equal to the transmission span losses. Also, identical power profiles are assumed for the signal and the idler. The copier is also considered to be operating with a high gain. From equations (3.50), (3.51), (3.3) and (3.4), in many number of spans, with high gain, a four times lower NF is obtained for both the types of inline amplification using copier-PSA compared to PIA-PIA. Therefore, in multi-span links, close to four times higher reach has been obtained for PSAs compared to PIAs in single-[53, 148][B] and multi-channel [C] systems.

3.3 Dispersion compensation

Unchirped pulses broaden during propagation in an optical fiber due to dispersion. This causes significant limitations in the fiber-optic communication systems in the form of inter-symbol interference (ISI). To overcome this, dispersion compensation is performed. Dispersion compensation can be done in either the optical or the digital domain. The optical compensation uses inline dispersion compensating fiber (DCFs) or dispersion-compensating modules (DCMs) made of chirped fiber-Bragg grating (FBG), whereas the digital compensation is performed at the transmitter or receiver.

3.3.1 Dispersion compensating fibers

In order to compensate for the accumulated dispersion and to undo the broadening in SSMF, fibers with negative dispersion ($D < 0$) called dispersion compensating fibers can be used. The dispersion parameter (D) can be as large as -300 ps/(nm km) in DCFs compared to the 16 ps/(nm km) for the SSMF. So, dispersion over very long SSMF can be compensated with short DCFs. To obtain high negative dispersion parameter and to stay in single mode regime, the core diameter is decreased and the refractive index difference is increased by doping. The addition of dopants increases the losses. The measure of dispersion compensation efficiency is given by a figure of merit (FOM). The FOM

is defined as the ratio of the dispersion parameter (D), and the loss per unit DCF length,

$$FOM = \frac{|D|}{\alpha/L_{DCF}}. \tag{3.52}$$

In DCFs, typically FOM is between 150 and 200 ps/(nm dB). But, DCFs with high FOM of 459 ps/(nm dB) have been demonstrated [149]. However, the DCFs also have high nonlinearities due to tighter confinement in the core which is another important limitation. Morover, to compensate dispersion for WDM systems, DCFs should also be slope-matched [150].

3.3.2 Fiber-Bragg grating based-dispersion compensating modules

A fiber-Bragg grating (FBG) is obtained by creating periodic gratings in the optical fiber. A photosensitive fiber is exposed to UV lasers in the presence of a grating which gets inscribed in the fiber. A chirped grating is fabricated by changing the period of grating along the length of the fiber which can used for dispersion compensation. These are known as the FBG based-dispersion compensating modules (DCMs) [21]. The absence of nonlinearities, lower loss, negligible latency have made the FBG-based DCMs attractive for dispersion compensation. They may be tunable and can be channelized or continuous in frequency. However, the group-delay ripple in FBG-based DCMs can limit the performance of the fiber-optic communication link [151].

In this work, the accumulated dispersion in the transmission span is compensated inline for every span using tunable channelized FBG-based DCMs. The tunability of the dispersion settings in the DCMs is useful when optimising the dispersion map for nonlinearity mitigation in PSA links. As DCMs are channelized, they have a limited bandwidth which also depends on the dispersion setting. The limited DCM bandwidth and the group-delay ripple can cause penalties in multi-span experiments. Moreover, to use more WDM channels and space them widely apart, moving from FBG based-DCMs to slope-matched DCF is required. However, the downside is that the dispersion map is no more easily tunable. This makes optimizing the dispersion map experimentally difficult.

3.3.3 Compensating dispersion in digital signal processing

In coherent systems, the dispersion compensation can be moved to the DSP at the receiver [152, 153]. By using electronic dispersion compensation (EDC), the dispersion compensation in the optical domain can be removed, reducing the loss in the transmission system and thus improve the overall link noise figure. EDC is performed by applying an inverse dispersion transfer function of the link. It can be implemented in both frequency and time domain. For

compensating smaller dispersion values, the time domain method is less complex and faster and vice versa. EDC is performed channel-wise and so is not energy efficient. As the modern transmitters also rely on the digital-to-analog converters (DACs), the EDC can also be performed in the transmitter.

Chapter 4

Overcoming nonlinear impairments

The Kerr nonlinearity is a major limiting factor in fiber-optic links giving rise to the nonlinear Shannon limit [30–32, 154–157]. These distortions can be caused due to intra-channel effects and inter-channel effects [30, 50]. The nonlinear beating within the frequencies of the same channel band causes the intra-channel effects which includes the signal-signal beating leading to SPM and signal-noise beating giving rise to the nonlinear phase noise (NLPN) [158, 159]. The intra-channel effect is a feature of single-channel transmission system. The inter-channel effects are caused by the interaction between the frequencies of neighbouring channel bands and the channel band of interest, where signal-signal beating leads to XPM and FWM and signal-noise beating results in NLPN. The WDM transmission systems are mainly affected by the inter-channel effects due to the Kerr nonlinearity. For SSMF, due to dispersion, the XPM becomes the dominant Kerr nonlinearity as pointed out in section 2.2. In this chapter, we first start with the analytical expressions for the Kerr nonlinear distortions in an optical fiber based on perturbation theory. Then, different techniques widely used to compensate the Kerr nonlinear distortions are discussed.

4.1 Nonlinear distortions in a weakly nonlinear regime

The NLSE is used to model the propagation of complex field envelope in the optical fiber as discussed in section 2.1. Assuming operation in a weakly nonlinear regime, i.e., the nonlinear distortions $\tilde{\delta}_{NL}(w, L)$ are small compared to the actual propagating field $\tilde{E}(0, w)$, the nonlinear distortions can be modelled as small perturbation to the linear solution using the perturbation theory [160].

This results in the power series expansion of the field as a function of γ. The field after propagating a distance L is given as

$$\tilde{E}(L,w) = \tilde{E}_0(L,w) + \underbrace{\gamma\tilde{E}_1(L,w) + \gamma^2\tilde{E}_2(L,w) + ...}_{\tilde{\delta}_{NL}(L,w)}, \tag{4.1}$$

where, $\tilde{E}_0(L,w)$ is the solution to the linear part of the NLSE and $\tilde{E}_1(L,w)$ and $\tilde{E}_2(L,w)$ are the higher order field contributions. Including only up to the first order expansion of γ, the nonlinear distortions is given by [161, 162]

$$\delta_{NL}(\omega,L) = j\gamma \iint \eta(\Delta\Omega,L)\tilde{E}(\omega_1,0)\tilde{E}^*(\omega_2,0) \tilde{E}(\omega-\omega_1+\omega_2,0)d\omega_1 d\omega_2, \tag{4.2}$$

where, $\eta(\Delta\Omega,L)$ is the nonlinear link transfer function and $\Delta\Omega = (\omega_1-\omega)(\omega_1-\omega_2)$. The nonlinear distortion (equation (4.2)) consists of two parts. The first part is the nonlinear link transfer function which is independent of the signal and the second part which is dependent on the interacting signals. The nonlinear distortions are calculated by summing the possible FWM products between spectral components at ω_1, ω_2 and $\omega_3 = \omega-\omega_1+\omega_2$ under the influence of the nonlinear link transfer function. Also, it is important to note that the influence of amplifier noise and NLPN is not taken into account in equation (4.2) when calculating the nonlinear distortions. The nonlinear link transfer function is given by [163]

$$\eta(\Delta\Omega,L) = \int_0^L \exp[G(z) + j\Delta\Omega D(z)]dz, \tag{4.3}$$

where, $G(z)$ describes the evolution of the signal amplitude on propagation also known as the power map and $D(z)$ corresponds to the accumulated dispersion. i.e., the dispersion map. The power map can be calculated from [162]

$$\frac{\partial G(z)}{\partial z} = g(z) - \alpha(z), \tag{4.4}$$

where, α is the fiber-loss parameter and $g(z)$ describes the evolution of signal power due to distributed Raman amplification (DRA). The dispersion map considering up to third-order dispersion is given as [163]

$$\frac{\partial D(z)}{\partial z} = \beta_2(z) + (\omega+\omega_2)\frac{\beta_3(z)}{2}, \tag{4.5}$$

where, $\beta_2(z)$ and $\beta_3(z)$ corresponds to the second-order and third-order dispersion along the link. With no DRA and assuming the loss and dispersion

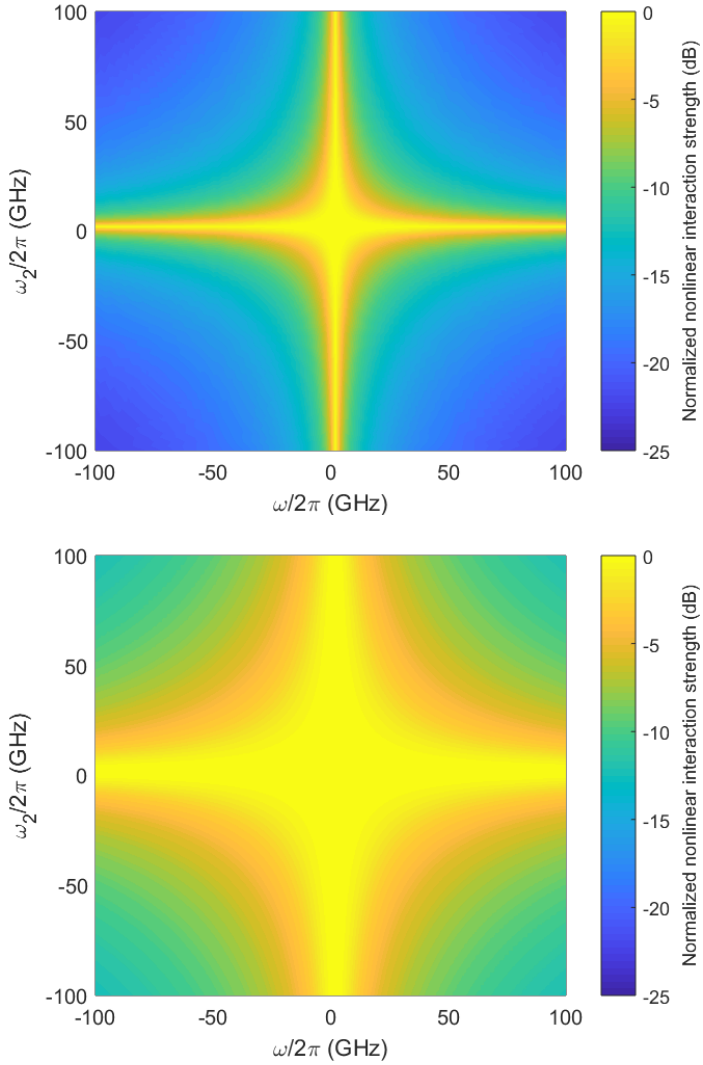

Figure 4.1: Normalized nonlinear interaction strength in decibels for $D = 16$ps/nm/km (top) and $D = 2$ps/nm/km (bottom). The nonlinear link transfer function is calculated with $\omega_1 = 0$, $D = 16$ps/nm/km, $\alpha = 0.2$ dB/km and $L = 80$ km and normalized. The nonlinear interaction is stronger for larger bandwidth in low dispersion fiber.

parameter are constant along the fiber, the nonlinear transfer function for a fiber length of L is given by

$$\eta(\Delta\Omega, L) = \frac{1 - \exp(-\alpha L + j\Delta\Omega[\beta_2 + (\omega + \omega_2)\frac{\beta_3}{2}]L)}{\alpha - j\Delta\Omega[\beta_2 + (\omega + \omega_2)\frac{\beta_3}{2}]}. \tag{4.6}$$

Moreover, the nonlinear link transfer function also corresponds to the strength of the nonlinear interaction between different frequencies, which is illustrated for different dispersion parameters in Figure 4.1. The normalized absolute value of the nonlinear link transfer function in decibels for $D = 16$ ps/nm/km is shown at the top which corresponds to SSMF and $D = 2$ ps/nm/km at the bottom. Stronger nonlinear interactions are observed for larger bandwidths for the low-dispersion fiber compared to the high dispersion one. It was also shown that for dispersion values corresponding to SSMF ($D = 16$ ps/nm/km), the third-order dispersion term can be neglected as it has a small impact on the nonlinear distortions [163]. Therefore, from now, we will not consider the third-order dispersion term in our work.

The main focus of this work is on PSA links which should be dispersion managed, i.e., the accumulated dispersion in each span is zero, as discussed in section 3.2.8. The nonlinear link transfer function for dispersion-managed links with pre- and post-dispersion compensation and $D(z) = \beta_2 z - D_0$ is [162]

$$\eta_{DM}(\Delta\Omega, L) = \frac{1 - \exp(-\alpha L + j\Delta\Omega\beta_2 L)}{\alpha - j\Delta\Omega\beta_2} \exp(-j\Delta\Omega D_0), \tag{4.7}$$

where D_0 is the dispersion pre-compensation which can vary from 0 to $\beta_2 L$. Assuming that the loss is also compensated in each span, the nonlinear link transfer function for the dispersion-managed links can be extended to N spans as [163]

$$\eta_{DM}^{N}(\Delta\Omega, L) = N\eta_{DM}(\Delta\Omega, L), \tag{4.8}$$

The nonlinear distortion after N spans is equal to the coherent addition of distortions from each span. The above analysis is valid only for the weakly nonlinear regime. One can extend the analysis to include higher-order terms in the power expansion of γ to make it valid at higher powers. Moreover, the inline-amplifier noise and NLPN were not taken into account. In order to analyse the nonlinear distortions at high powers, with inline-amplifier noise and NLPN, the NLSE should be solved numerically with the split-step Fourier method. Based on the above analysis, the nonlinearity compensation using Volterra nonlinear equalization and copier-PSAs is explained later in this chapter.

4.2 Nonlinearity compensation

The nonlinear distortions can be compensated using optical, digital and hybrid techniques. For digital techniques, the nonlinear compensation is carried out in the digital domain [25], which includes digital backpropagation (DBP) [164], Volterra nonlinear equalization (VNLE) [165], constellation shaping and nonlinear Fourier transformation (NFT). The idea behind using constellation shaping for nonlinearity mitigation is to reduce peak-to-average power. This is done in geometric shaping [42, 166] by restricting the higher energy symbols in the constellation and reducing the probability of the higher energy symbols in probabilistic shaping [43]. In NFT [41], the information is encoded into a nonlinear Fourier spectrum which is more robust to the Kerr nonlinear effects in the optical fiber. The major advantage of digital techniques is that implementing them does not require any change in the existing optical network infrastructure. The disadvantage of digital techniques, in general, is the increased complexity and energy consumption in processing especially when using a high bandwidth signal. When the nonlinear compensation is performed in the optical domain itself, it is referred to as an optical technique. The main advantage of the optical techniques is the ability to compensate nonlinearity with ease when using a wide bandwidth signal. However, this needs modification of the existing optical network. The different optical techniques to compensate nonlinear distortions are optical phase conjugation (OPC) [34] and copier-PSAs [36]. Phase-conjugated twin waves (PCTWs) [35] falls under the hybrid category since the nonlinearity is compensated in the digital domain whereas it involves the propagation of signal and conjugated copy of the signal in the optical domain. The spectral efficiency of copier-PSA and PCTWs is halved at high signal-to-noise ratios (SNRs) due to the requirement of the conjugated copy of the signal. The optical techniques can be used together with digital techniques to further enhance nonlinearity compensation as in [167], [A,F], which can also be called as hybrid techniques. In the section below, we will briefly discuss the most widely used nonlinearity compensation techniques.

4.2.1 Digital backpropagation

The most practised digital domain technique for nonlinearity compensation is digital backpropagation (DBP) [37, 38, 164, 168]. The DBP also acts as a benchmark for other nonlinearity compensation techniques. The transmission span nonlinearity and dispersion is simultaneously compensated by numerically backpropagating the signal field with inverted fiber parameters compared to the actual transmission fiber after detection. The major limitations in compensating nonlinear distortions using DBP are caused by the nonlinear phase noise (NLPN) [169, 170] and polarization-mode dispersion (PMD) [171, 172]. Moreover, DPB is computationally demanding [37] and to obtain effective nonlinearity mitigation in WDM systems, all the channels need to be simultaneously detected and backpropagated in the NLSE solver, increasing the complexity

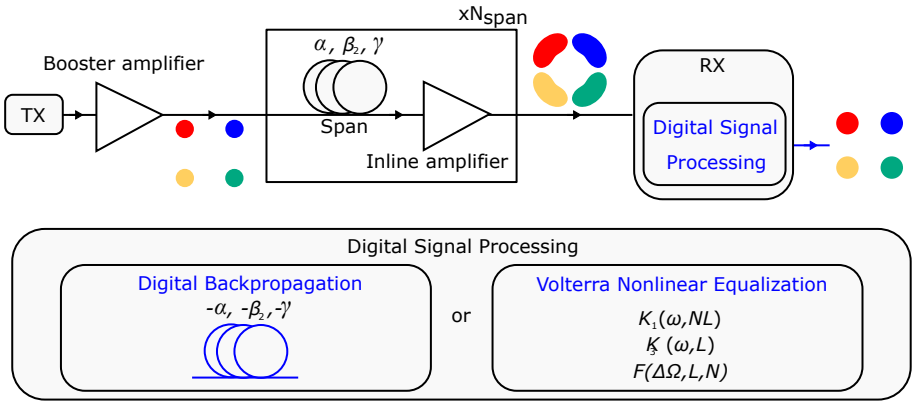

Figure 4.2: Schematic representation for digital backpropagation (DBP) and Volterra nonlinear equalization (VNLE). The Kerr nonlinearity in the transmission span are mitigated in the digital domian after detection either using DBP or VNLE. The constellation points are for illustration purpose.

drastically. The schematic representing the working principle of DBP is shown in Figure 4.2. A quadrature-phase shift keying (QPSK) signal is obtained from the transmitter. A booster amplifier is used to amplify the signal before propagation. The signal is propagated in an optical fiber with parameters $(\alpha, \beta_2, \gamma)$. After propagation, the signal is amplified to compensate for the link loss. The constellation representations with QPSK signals are also shown before and after propagation. The banana-shaped constellations after propagation in N spans clearly shows the nonlinear distortions. The constellation representations are only for the purpose of illustrating nonlinearity compensation and dispersion is neglected. Then, the signal is detected and propagated in a virtual optical fiber numerically with inverse parameters $(\text{-}\alpha, -\beta_2, -\gamma)$ compared to the actual transmission span. The numerical backpropagation is done by solving the NLSE using the split step Fourier method (SSFM). The constellation after DBP shows that the nonlinear distortions are compensated.

4.2.2 Volterra nonlinear equalization

Any nonlinear systems can be modelled using a Volterra series expansion [173, 174]. Volterra series can also be used to solve the NLSE to model the signal propagation in the optical fiber resulting in the Volterra series transfer function (VSTF) [165]. The VSTF gives the relationship between the input and output signals in the frequency domain with Volterra kernels. The signal after propagation in the optical fiber using the Volterra series transfer function is

given as [165],

$$\begin{aligned}\tilde{E}(\omega, L) = \sum_{n=1}^{\infty} \int ..... \int K_n(\omega_1, ., \omega_{n-1}, \omega - \omega_1 + \omega_2 - ..... \pm \omega_{n-1}, L) \\ \times \tilde{E}(\omega_1, 0)....\tilde{E}(\omega_{n-1}, 0) \\ \times \tilde{E}(\omega - \omega_1 + \omega_2 - ..... \pm \omega_{n-1}) d\omega_1 ....d\omega_{n-1}.\end{aligned} \tag{4.9}$$

The n^{th}-order Volterra kernel is given by K_n. The first order linear kernel corresponds to the linear response of the optical fiber, whereas the higher-order kernels are related to the nonlinear response. The even order kernels can be neglected as the second-order nonlinearities are absent in the NLSE. The VSTF is computationally efficient compared to solving the NLSE with recursive SSFM. One can also notice that the power expansion of the optical field as a function of γ in section 4.1 coincides with the VSTF. The N^{th} order perturbation term in power expansion corresponds to the $(2N+1)^{\text{th}}$ kernel term in VSTF [160]. Including the higher-order kernels increases the computational complexity as well as the accuracy at higher powers. The VSTF can be used to apply an inverse filter to compensate for the linear dispersion and fiber nonlinearity. This is known as Volterra nonlinear equalizer (VNLE). Less complex VNLE with just the first- and third-order kernels have been demonstrated to mitigate nonlinearity [175]. In general, a third-order VNLE for N spans with length, L, and considering only second-order dispersion is [39, 40]

$$\begin{aligned}\tilde{E}(\omega, 0) \approx K_1(\omega, NL)\tilde{E}(\omega, NL) \\ +\Gamma(\omega, NL) \iint F(\Delta\Omega, L, N) K_3(\Delta\Omega, L)\tilde{E}(\omega_1, NL)\tilde{E}^*(\omega_2, NL) \\ \times \tilde{E}(\omega - \omega_1 + \omega_2, NL) d\omega_1 d\omega_2,\end{aligned} \tag{4.10}$$

where K_1 is the first-order kernel that compensates for the fiber loss and dispersion and is given by,

$$K_1(\omega, NL) = \exp(\frac{\alpha L}{2} - i\frac{\beta_2 \omega^2}{2} NL], \tag{4.11}$$

K_3 is the third-order kernel that compensates for the nonlinear distortions:

$$K_3(\Delta\Omega, L) = \frac{1 - \exp[(\alpha - i\beta_2 \Delta\Omega)L]}{-\alpha + i\beta_2 \Delta\Omega}, \tag{4.12}$$

$F(\Delta\Omega)$ describes the phased-array effect which takes into account the coherent additions of nonlinearities over several spans.

$$F(\Delta\Omega, L, N) = \exp(i\frac{\beta_2 \Delta\Omega(N-1)L}{2}) \frac{\sin(\frac{\beta_2 \Delta\Omega NL}{2})}{\sin(\frac{\beta_2 \Delta\Omega L}{2})}, \tag{4.13}$$

Γ is the frequency-dependent nonlinear term:

$$\Gamma(\omega, NL) = -i\gamma K_1(\omega, NL). \tag{4.14}$$

Usually, the losses are compensated inline every span except for the last span. Therefore, the linear kernel, K_1, in the VNLE compensates for the whole dispersion in the transmission link and loss only for the last span. One can notice from equations (4.12)) and (4.6) that the nonlinear link transfer function is the same as the third-order nonlinear kernel of the VNLE. The nonlinear distortions in dispersion-managed links can be compensated by just replacing the third-order kernel and the phased-array effect corresponding to the link transfer function for N dispersion managed links. The required block size in the frequency domain for VNLE increases with the accumulated dispersion. In equation (4.10), a single step VNLE is demonstrated. However, to improve the performance of VNLE, multi-step implementation is required where the step size corresponds to an integer number of spans. The main limitation of VNLE is the complexity arising from the required block size and the step size. There have been substantial efforts to reduce the implementation complexity of the VNLE [175,176]. The working principle for the VNLE is similar to the DBP as shown in Figure 4.2, except that the VNLE is applied in the digital signal processing as in equation (4.10). A modified Volterra nonlinear equalizer can be used along with the PSA to enhance nonlinearity mitigation which is discussed in section 4.2.4

4.2.3 Optical phase conjugation

Optical phase conjugation [34,177,178] is the most studied optical nonlinearity compensation technique. The dispersion and nonlinearity accumulated in the first part of the transmission span is reversed in the second part after optical phase conjugation resulting in net zero dispersion and nonlinearity compensation. As discussed in section 2.1, the NLSE is given by,

$$\frac{\partial \tilde{E}}{\partial z} = -j\frac{\beta_2}{2}\frac{\partial^2 \tilde{E}}{\partial t^2} + \frac{\beta_3}{6}\frac{\partial^3 \tilde{E}}{\partial t^3} + \frac{g(z)-\alpha(z)}{2}\tilde{E} + j\gamma|\tilde{E}|^2\tilde{E}, \tag{4.15}$$

After phase conjugation, the propagation of the phase-conjugated signal is given by,

$$\frac{\partial \tilde{E}^*}{\partial z} = j\frac{\beta_2}{2}\frac{\partial^2 \tilde{E}^*}{\partial t^2} + \frac{\beta_3}{6}\frac{\partial^3 \tilde{E}^*}{\partial t^3} + \frac{g(z)-\alpha(z)}{2}\tilde{E}^* - j\gamma|\tilde{E}^*|^2\tilde{E}^*, \tag{4.16}$$

By comparing equations (4.15) and (4.16), one can understand the reversal of second-order dispersion and nonlinearity. However, to perfectly compensate for the nonlinearity, the third-order dispersion and the power map needs to be taken care of. The power map needs to be symmetric around the OPC unit for effective nonlinearity compensation. A flat power can be obtained with ideal DRA but is impossible in practice. However, DRA can be used to obtain

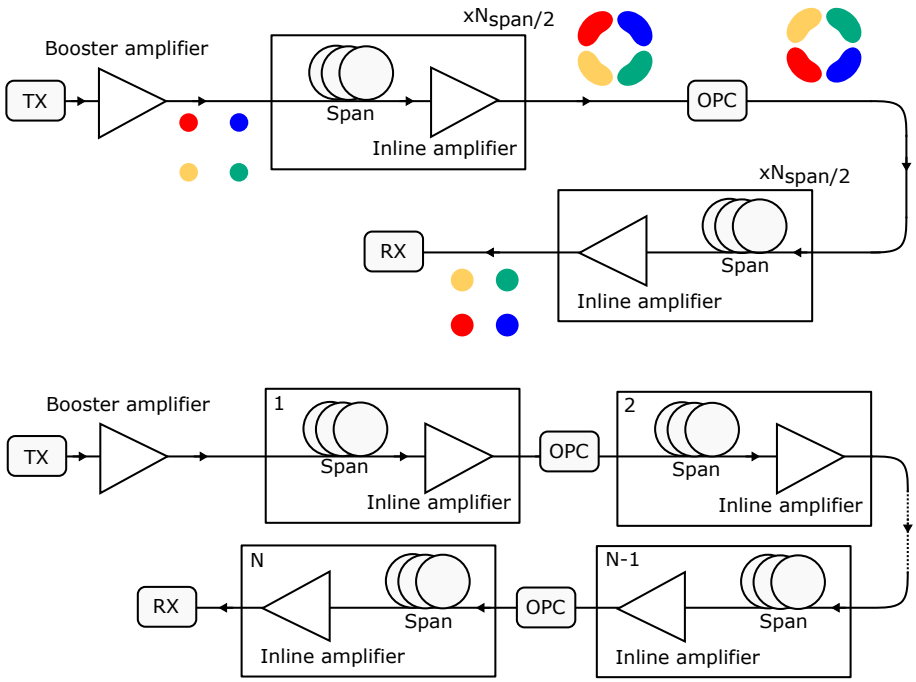

Figure 4.3: Schematic representation for optical phase conjugation. At the top is the mid-span spectral inversion (MSSI) and the inline OPCs is at the bottom. In the MSSI, the dispersion and nonlinearity in the first $N/2$ spans are compensated in the next $N/2$ spans by performing phase-conjugation in the mid-link. In the inline OPCs, the phase-conjugation is performed at the end of every span. The constellation points are for illustration purpose.

a high degree of symmetry in the power map [108]. An ideal OPC system to compensate for dispersion and nonlinearity was demonstrated in [179]. There, a specially designed fiber with required dispersion parameters was used with DRA to compensate nonlinearity and dispersion. OPC was first used for dispersion compensation in 1993 [180]. The nonlinearity mitigation using OPC was first experimentally demonstrated in 1994 [181]. The OPCs can be implemented in two ways as illustrated in Figure 4.3. One way is to use the OPC unit at the mid link, i.e., for N spans, an OPC unit is placed after $N/2$ spans, also known as mid-span spectral inversion (MSSI) [182, 183] as the spectrum is mirrored at the OPC unit. At the mid-span, OPC is performed, which inverts the constellation around the imaginary axis. In the representation of constellation points, dispersion is neglected. Then the signal is propagated in the second half to reverse dispersion and nonlinearity. The other way is to use many OPC units inline in the optical link [184–186] called as inline OPCs. Assuming a symmetric power map, the limiting factor in OPC links is the polarization-mode dispersion, whose detrimental effect can be reduced by decreasing the spacing between OPC units and employing more OPC units [184].

4.2.4 Copier-PSA

Another optical technique used to compensate for nonlinearity is the copier-PSA which is also the interest of this thesis. The implementation of the copier-PSA has already been discussed in section 3.2.8. The copier generates a conjugated copy of the signal called the idler. The signal and the idler propagate together in the transmission link. They experience correlated distortions due to the Kerr nonlinearity in the optical fiber. At the PSA, they are coherently combined, enabling nonlinearity mitigation [36, 50].

4.2.4.1 Analysis of nonlinearity mitigation

Let us start with a single span link of length L, the input signal to the transmission link is $\tilde{E}_S(t,0)$ and the idler is $\tilde{E}_I(t,0) = \tilde{E}_S^*(t,0)$. In the frequency domain, the input signal and idler are given as $\tilde{E}_S(w,0)$ and $\tilde{E}_I(w,0) = \tilde{E}_S^*(-\omega,0)$. Assuming the optical fiber as weakly nonlinear medium and the nonlinear distortions very small compared to the signal, the nonlinear distortions can be modelled as small perturbation to the linear solution using the perturbation theory [162]. In the time domain, considering nonlinear distortions up to first-order power expansion of γ (section 4.1), the signal and idler after propagation is given as

$$\tilde{E}_S(t,L) = \tilde{E}_s(t,0)[\exp(-\frac{\alpha}{2}L + j\frac{\beta_2\omega^2}{2}L)] + \delta_{NL,S}(t,L), \tag{4.17}$$

$$\tilde{E}_I(t,L) = \tilde{E}_I(t,0)[\exp(-\frac{\alpha}{2}L + j\frac{\beta_2\omega^2}{2}L)] + \delta_{NL,I}(t,L). \tag{4.18}$$

respectively. In copier-PSA links, the dispersion is compensated inline with optical dispersion compensation modules as explained in section 3.2.8. Moreover, assuming the link loss are compensated exactly by the PSA at high gain with $2|\mu| = 2|\nu| = \exp(\frac{\alpha}{2}L)$, where $G_{\text{PSA}} = |\mu + \nu|^2$, from equation (3.47), the signal at the PSA output is

$$\begin{aligned}\tilde{E}_{S,out}(t,L) = 0.5[\tilde{E}_S(t,0) + \delta_{NL,S}(t,L)] + 0.5[\tilde{E}_I(t,0) + \delta_{NL,I}(t,L)]^* \\ = \tilde{E}_S(t,0) + \delta_{NL,res}(t,L),\end{aligned} \tag{4.19}$$

PSA can mitigate some of the nonlinear distortions in the transmission span due to the coherent superposition of the signal and idler [35] but there remains the term given by $\delta_{NL,res}(t,L)$ known as the residual nonlinear distortion:

$$\delta_{NL,res}(t,L) = 0.5[\delta_{NL,S}(t,L) + \delta^*_{NL,I}(t,L)]. \tag{4.20}$$

By taking the Fourier transform of equation (4.20), we get

$$\delta_{NL,res}(\omega,L) = 0.5[\delta_{NL,S}(\omega,L) + \delta^*_{NL,I}(-\omega,L)], \tag{4.21}$$

which is similar as in [A]. There, the above analysis was carried out in the frequency domain assuming that the μ and ν are constant over the signal bandwidth. From equation (4.2), the nonlinear distortion in the signal and idler can be written as,

$$\begin{aligned}\delta_{NL,S}(\omega,L) = j\gamma \iint \eta_S(\Delta\Omega,L)\tilde{E}_S(\omega_1,0)\tilde{E}^*_S(\omega_2,0) \\ \tilde{E}_S(\omega-\omega_1+\omega_2,0)d\omega_1 d\omega_2,\end{aligned} \tag{4.22}$$

$$\begin{aligned}\delta_{NL,I}(\omega,L) = j\gamma \iint \eta_I(\Delta\Omega,L)\tilde{E}_I(\omega_1,0)\tilde{E}^*_I(\omega_2,0) \\ \tilde{E}_I(\omega-\omega_1+\omega_2,0)d\omega_1 d\omega_2,\end{aligned} \tag{4.23}$$

respectively. We can calculate $\delta^*_{NL,I}(-\omega,L)$ as follows,

$$\begin{aligned}\delta^*_{NL,I}(-\omega,L) = [j\gamma \iint \eta_I((\omega_1+\omega)(\omega_1-\omega_2),L)\tilde{E}_I(\omega_1,0) \\ \tilde{E}^*_I(\omega_2,0)\tilde{E}_I(-\omega-\omega_1+\omega_2,0)d\omega_1 d\omega_2]^*,\end{aligned} \tag{4.24}$$

$$\begin{aligned}\delta^*_{NL,I}(-\omega,L) = -j\gamma \iint \eta^*_I((\omega_1+\omega)(\omega_1-\omega_2),L)\tilde{E}^*_I(\omega_1,0) \\ \tilde{E}_I(\omega_2,0)\tilde{E}^*_I(-\omega-\omega_1+\omega_2,0)d\omega_1 d\omega_2.\end{aligned} \tag{4.25}$$

Substituting $\tilde{E}_I(\omega,0) = j\tilde{E}^*_S(-\omega,0)$ in the above equation,

$$\begin{aligned}\delta^*_{NL,I}(-\omega,L) = \gamma \iint \eta^*_I((\omega_1+\omega)(\omega_1-\omega_2),L)(j\tilde{E}^*_S(-\omega_1,0))^* \\ (j\tilde{E}^*_S(-\omega_2,0))(j\tilde{E}^*_S(\omega+\omega_1-\omega_2,0))^* d\omega_1 d\omega_2,\end{aligned} \tag{4.26}$$

$$i\delta^*_{NL,I}(-\omega, L) = -j\gamma \iint \eta^*_I((\omega_1+\omega)(\omega_1-\omega_2), L)\tilde{E}_S(-\omega_1, 0) \tilde{E}^*_S(-\omega_2, 0)\tilde{E}_S(\omega+\omega_1-\omega_2, 0)d\omega_1 d\omega_2, \tag{4.27}$$

Replacing $\omega_{1,2} \longleftrightarrow -\omega_{1,2}$,

$$j\delta^*_{NL,I}(-\omega, L) = -j\gamma \iint \eta^*_I(\Delta\Omega, L)\tilde{E}_S(\omega_1, 0)\tilde{E}^*_S(\omega_2, 0) \tilde{E}_S(\omega-\omega_1+\omega_2, 0)d\omega_1 d\omega_2. \tag{4.28}$$

Substituting equations (4.22) and (4.28) in equation (4.20),

$$\delta_{NL,res}(\omega, L) = j\gamma \iint \eta_{res}(\Delta\Omega, L)\tilde{E}_S(\omega_1, 0)\tilde{E}^*_S(\omega_2, 0) \tilde{E}_S(\omega-\omega_1+\omega_2, 0)d\omega_1 d\omega_2, \tag{4.29}$$

where $\eta_{res}(\Delta\Omega, L) = 0.5[\eta_S(\Delta\Omega, L) - \eta^*_I(\Delta\Omega, L)]$ is the effective link transfer function after the nonlinear compensation in the PSA. Assuming that the signal and idler are propagated in identical links, i.e., $\eta_S(\Delta\Omega, L) = \eta_I(\Delta\Omega, L)$,

$$\begin{aligned}\eta_{res}(\Delta\Omega, L) &= 0.5[\eta_S(\Delta\Omega, L) - \eta_S(\Delta\Omega, L)^*] \\ &= jIm(\eta_S(\Delta\Omega, L)).\end{aligned} \tag{4.30}$$

Expanding for the residual nonlinear distortions with equations (4.7), (4.30) and (4.29),

$$\delta_{NL,res}(\omega, L) = j\gamma \iint jIm\left(\frac{1-\exp(-\alpha L + j\Delta\Omega\beta_2 L)}{\alpha - j\Delta\Omega\beta_2}\exp(-j\Delta\Omega D_0)\right) \tilde{E}_S(\omega_1, 0)\tilde{E}^*_S(\omega_2, 0)\tilde{E}_S(\omega-\omega_1+\omega_2, 0)d\omega_1 d\omega_2. \tag{4.31}$$

The residual nonlinear distortion corresponds only to the imaginary part of the link transfer function as the nonlinear distortions corresponding to the real part is cancelled by the PSA. The residual nonlinear distortion shows the effectiveness of the nonlinearity mitigation in PSAs. The smaller the value of the residual nonlinear distortions, the more efficiently the nonlinearity is mitigated and vice versa. The effective link transfer function for the PIA and PSA links are shown in Figure 4.4. Also, it is worth noting that the residual nonlinear distortion depends on the dispersion map (D_0), power map (α or $g(z) - \alpha(z)$ considering DRA) and the optical signal bandwidth. For plotting the link transfer function, the optimum dispersion map for a 10 GBaud signal was assumed. This analysis can be extended easily to multi-span link, assuming the nonlinear distortion from each span is the same as there is no accumulated dispersion in each of the spans. Therefore, the nonlinear distortions add in-phase, and the electric field of a link with N spans is

$$\tilde{E}_S(\omega, NL) = \tilde{E}_S(\omega, 0) + N\delta_{NL,res}(\omega, L). \tag{4.32}$$

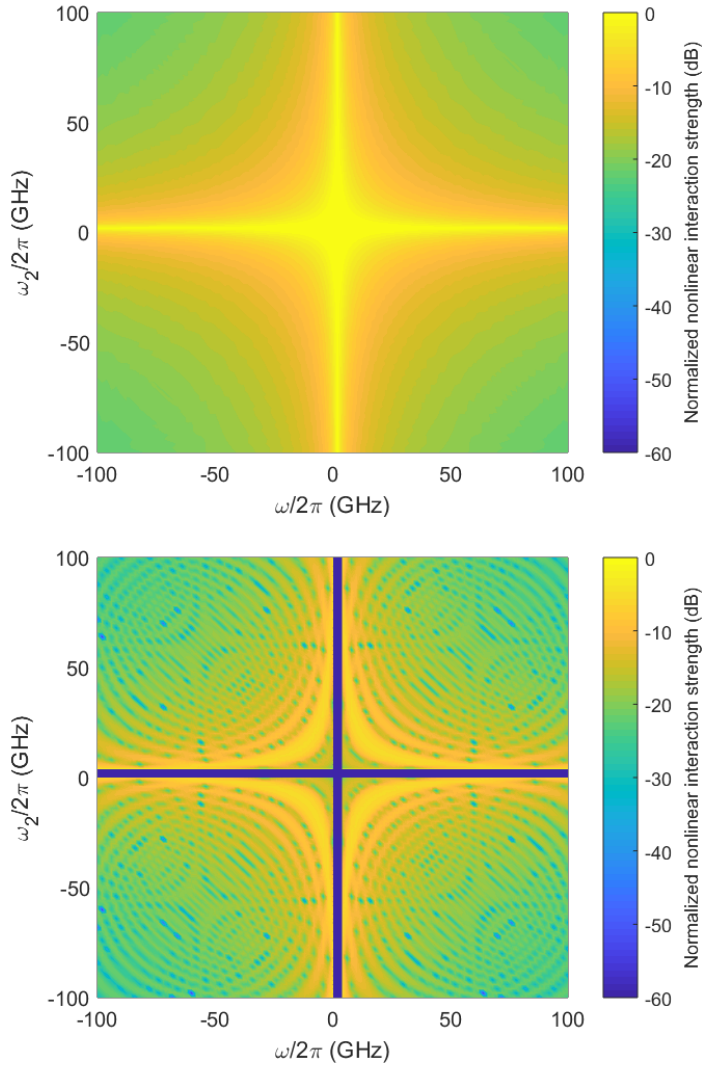

Figure 4.4: Normalized nonlinear interaction strength in decibels for PIA (top) and PSA (bottom) links. The nonlinear transfer function is calculated with $\omega_1 = 0$, $D = 16$ps/nm/km, $\alpha = 0.2$ dB/km and $L = 80$ km and normalized. The nonlinear distortions can be obtained by integrating the nonlinear transfer function over the required signal bandwidth. From, this one can understand that the nonlinear distortions are lower for PSA links compared to the PIA links.

The assumptions made in section 4.1 still holds for the above analysis. In addition to that, it is assumed that the signal and idler are propagated in the identical fiber parameters to have the same link transfer function, which is not the case in practice. The signal and idler are centered at different frequencies leading to differences in the dispersion and power maps.

4.2.4.2 Modified third-order VNLE

One way to compensate the residual nonlinear distortion is to use a modified VNLE as shown in [A] for single channel and [F] for WDM system. In the PSA link, with inline dispersion compensation and optical amplification, the first order kernel from equation (4.11) is reduced to

$$K_1(\omega, z) = 1, \tag{4.33}$$

The PSA would remove the nonlinear distortion due to the real part of the link transfer function and therefore, the third-order kernel, K_3 have to just compensate for the residual nonlinear distortion after the PSA. Therefore, equation (4.12) becomes

$$K_3(\Delta\Omega, z) = jIm\{\frac{1-\exp(-\alpha L + j\Delta\Omega\beta_2 L)}{\alpha - j\Delta\Omega\beta_2}\exp(-j\Delta\Omega D_0)\}. \tag{4.34}$$

With inline dispersion compensation, there is no accumulation of dispersion in each span and the nonlinear distortions in each span are the same. Therefore, $F(\Delta\Omega, N, L)$ becomes equal to the number of spans to account for the coherent addition of nonlinear distortions over all the spans.

4.2.4.3 Nonlinearity mitigation dependence on dispersion map

The dispersion map plays an important role in nonlinearity mitigation with PSAs. The dispersion pre-compensation and post-compensation are optimized numerically [36, 50, 107] or experimentally [53] in copier-PSA links for best link performance at high launch powers. Also, the optimum dispersion map depends on the optical signal bandwidth and power map. One can note that, from equation (4.31), the dispersion pre-compensation adds a phase shift to the link transfer function, by which one can reduce the residual nonlinear distortions. Moreover, different dispersion pre-compensation values might be required depending on other parameters (optical signal bandwidth and power map) to lower the residual distortions. This is why dispersion map optimization improves nonlinearity mitigation in PSA links. For all the experiments involved in this thesis (A- F), the dispersion map was optimized experimentally with the help of tunable fiber-Bragg grating-based dispersion compensating modules. It was also shown in [A] & [F] that the impact of the dispersion map on the residual nonlinearity can be reduced by using the modified VNLE.

For multi-span links, we considered that the same nonlinear distortions coherently add up in each span. One can reduce the total residual nonlinear

distortions for N spans by combining the nonlinear distortions from each span in a destructive way. However, the optimization space increases as D_{maps}^{N}, which is almost impossible to perform at a higher number of spans, where D_{maps} corresponds to the number of dispersion maps in one span. The dispersion map optimization has been performed with fewer spans in [187, 188]. To perform dispersion map optimization for a large number of spans, one can assign random dispersion maps with all possibilities to each of the span so that the coherent build-up of the nonlinear distortions is restricted.

4.2.4.4 Nonlinearity mitigation dependence on power map

The effectiveness of nonlinearity mitigation also depends on the power map. As the fiber loss is fixed, the power map can be altered with DRA. Assuming the input signal bandwidth is fixed, one has to optimize the dispersion and power map together to reduce the residual nonlinear distortions. One special case worth mentioning is to consider a symmetric power map ($G(z) = G(L - z)$) and an asymmetric dispersion map ($D(z) = -D(L - z)$). In equation (4.31), one can substitute $D_0 = \frac{\beta_2 L}{2}$ for antisymmetric dispersion map and $\alpha = 0$ for symmetric power map, which makes the residual nonlinear distortion zero. One way to achieve a symmetric power map is to use ideal DRA. Therefore, with ideal DRA and 50% dispersion pre-compensation, PSA can perfectly mitigate nonlinearity irrespective of the optical signal.

With ideal DRA a flat power map can be obtained, but it is not easy to achieve a flat power map in practice. However, using higher-order Raman pumps and bi-directional pumping, the highest degree of symmetry in the power map can be attained. In [B], for the experiments, though the symmetry in the power map was achieved to a certain extent, the net gain for the signal and idler was not the same. It is due to the Raman gain differences at the signal and idler frequencies. In this case, $\eta_S(\Delta\Omega, L) \neq \eta_I(\Delta\Omega, L)$, and PSA was not able to compensate perfectly for the nonlinearity.

4.2.4.5 Nonlinearity mitigation dependence on optical signal bandwidth

The optical signal bandwidth can be increased by increasing the symbol rate [A-B] or by including more WDM channels [C] & [F]. Moreover, the optical signal spectrum also changes with pulse-shaping which in turn changes the residual nonlinear distortions. The residual nonlinear distortion increases with optical signal bandwidth even with optimum dispersion pre-compensation. By using the modified VNLE over the entire signal bandwidth, the residual nonlinear distortions can be reduced [A] & [F].

4.2.4.6 Dependence on modulation format

The spectral efficiency of an optical link can be increased using higher-order modulation formats. The higher-order modulation formats are more suscep-

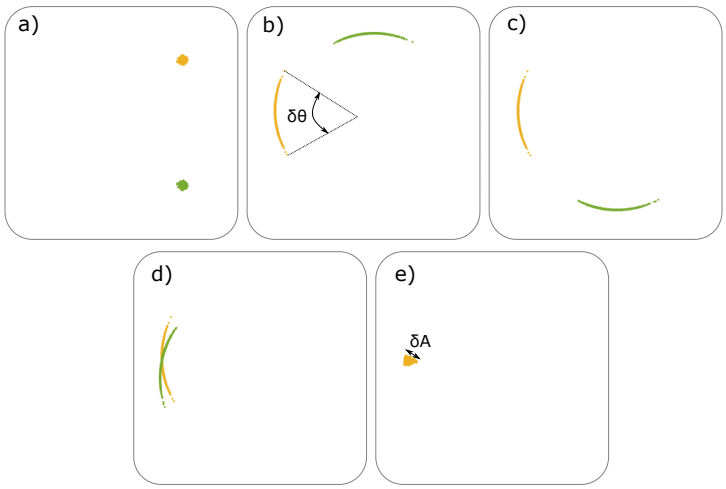

Figure 4.5: Schematic representation of coherent superposition in the copier-PSA: a) Constellation points of signal (orange) and idler (green), b) Constellation points with nonlinear distortions modelled as phase rotations ($\delta\theta$) neglecting dispersion, c) After conjugation of idler, d) Coherent addition of the signal and idler maximising the output signal power and e) The output signal after coherent superposition in the PSA with amplitude distortions (δA).

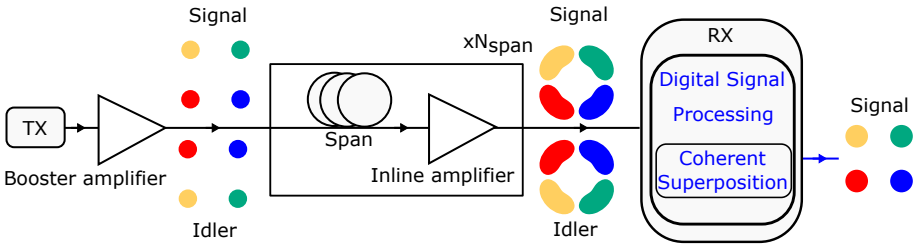

Figure 4.6: Schematic representation for phase-conjugated twin waves. The signal and the conjugated copy of the signal called the idler are co-propagated in the span to experience correlated distortions, which are then cancelled at the receiver digital signal processing with coherent superposition. The constellation points are for illustration purpose.

tible to noise as the constellation points are close to each other. Neglecting dispersion, one can model the nonlinear distortions in the transmission span as phase rotations ($\delta\theta$). The nonlinear compensation using coherent superposition with just phase rotations is explained step by step in Figure 4.5. PSAs mitigate these phase distortions converting them into amplitude distortions ($\delta A \approx (\delta\theta)^2$) [E]. Small phase distortions lead to small amplitude distortions and vice versa. Therefore, PSAs are better at mitigating smaller nonlinear distortions. Also, the amplitude distortions affect the gain, and noise figure of the PSA [50]. Therefore, the transmission improvement using PSAs compared to PIAs are enhanced for higher-order modulation formats [E]. However, the enhancement might decrease when operating at a higher bit-error rate.

4.2.5 Phase-conjugated twin waves

The Phase-conjugated twin waves (PCTWs) are very similar to the copier-PSAs. Figure 4.6 illustrates the principle behind PCTWs. The signal and phase-conjugated copy of the signal are propagated together in the transmission span either in orthogonal polarization [35], frequencies [189], time [190], or space [191]. The signal and phase-conjugated copy of the signal are detected synchronously, and then the coherent superposition is performed in the digital domain to mitigate span nonlinearity. A similar analysis as in the case of PSAs has been performed for PCTWs [192] and most of the analysis which is done above for the PSA still holds for PCTWs. Symmetric power map and asymmetric dispersion map leads to ideal cancellation of nonlinearity. The nonlinearity mitigation can be performed only once in PCTWs at the receiver, however, with the PSA, the compensation can be performed spanwise.

Chapter 5

Outlook

In this chapter, the possible future works with respect to parametric amplifiers and transmission nonlinearity mitigation are discussed.

5.1 Broadband parametric amplifiers

Fiber-optic parametric amplifiers (FOPAs) have gathered attention due to their high gain, broad gain bandwidth, and ability to work in phase-sensitive mode, performing almost noiseless amplification. The PSAs implemented in this work are based on the pump-degenerate FWM process. As discussed in section 3.2.4, this scheme can only provide exponential gain in two side lobes where perfect phase matching occurs. Near the pump frequency, only quadratic gain is obtained as the linear phase mismatch term becomes zero. If one want to extend our wavelength-division multiplexed (WDM) systems to occupy larger bandwidth, a flat broad gain bandwidth is required. This can be achieved in many ways. One technique uses phase-shifters in between the different spools of the HNLFs to change the pump phase improving phase-matching known as quasi-phase-matching [193]. Another technique already discussed is to use two pumps to utilize non-degenerate FWM for amplification. By choosing the proper pump frequency and power according to the dispersion properties of the fiber, broad flat gain bandwidth can be obtained with also exponential gain in the center as shown in Figure 3.4. This could be the first step to move closer to the implementation of PSAs that supports large signal bandwidths.

5.1.1 Integrated platform

A promising nonlinear platform for parametric amplifiers based on $\chi^{(3)}$ is Si_3N_4. Si_3N_4 waveguides can have ten times higher nonlinear-index coefficient (n_2) as well as confine light ten times more tight compared to the HNLFs used in FOPAs. Si_3N_4 waveguides can provide a hundred times larger non-

linear phase shift compared to HNLFs of the same length and pump power. Therefore, a few meters of Si_3N_4 waveguides can produce the same gain as a few hundred meters of HNLFs, making them compact. The SBS threshold is very high in Si_3N_4 waveguides and is not a limiting factor as it is for HNLFs. The dispersion properties can be engineered more precisely, and this leads to much broader gain bandwidth. Multiple waveguides can be fabricated on the same chip for amplifying signals in different polarization, wavelength bands and cores. Moreover, the Raman scattering, which fundamentally limits the noise performance in FOPAs, is small. Recently, parametric amplifiers operating in phase-sensitive mode with the on-chip gain of 9.5 dB and noise figure (NF) of approximately 1.2 dB have been demonstrated [194]. However, the coupling loss from the fiber to the waveguide is few dBs, affecting the black-box NF for the Si_3N_4 platform. If the coupling issue is solved, Si_3N_4 platform will be a viable contender for implementing PSAs.

5.2 PSA fiber links at low SNR

The need to co-propagate an idler, containing no additional information, along with the signal, normally leads to a reduction of the spectral efficiency (SE) in PSA links. However, PSA-based links can actually reach higher SE than PIA links when operating at low SNRs. PSAs with higher SE than PIAs have already been demonstrated for deep-space communication applications where the benefit of low-noise amplification was exploited [195]. This can be extended to fiber links. A preliminary numerical study is performed here with single-channel 10 GBaud QPSK data signal.

The SE is plotted against the SNR of the PIA (SNR_{PIA}) in terms of the Shannon limit and for the QPSK format in Fig. 5.1. The SE corresponding to the Shannon limit [52] is plotted for PIA (red-dotted curve) with $\log_2(1 + SNR_{\mathrm{PIA}})$ whereas for the PSA (red-solid curve) it is $\frac{1}{2}\log_2(1 + 4SNR_{\mathrm{PIA}})$. In case of the PSA, the factor of 4 comes from the SNR improvement due to the low-noise amplification and the factor of $\frac{1}{2}$ accounts for the extra bandwidth occupied by the idler. The PIA and PSA links are studied at low SNRs, where FECs are required to provide error free transmission (post-FEC BER $< 10^{-15}$). It has been shown that a better metric to predict the post-FEC BER of soft-decision (SD) FECs is generalized mutual information (GMI) [196]. In this study, the GMI provides the maximum number of information bits per transmitted symbol over a memoryless AWGN auxiliary channel with bit-wise decoder [197,198]. The GMI is obtained by Monte Carlo simulations [199]. The GMI is equal to the SE for PIAs. In case of the PSA, the SE curve is shifted to left by 6 dB due to the SNR improvement and divided by 2 as the PSA requires the signal and a copy. The PIA and PSA Shannon SE cross at $SNR_{\mathrm{PIA}} = 3$ dB. Therefore, the PSA links have higher SE than PIA links below 3 dB SNR. For the QPSK modulation format, since the upper bound SE in case of PSAs is 1 (bits/s/Hz), the PIA and PSA curves cross at $SNR_{\mathrm{PIA}} = -0.6$ dB. At high

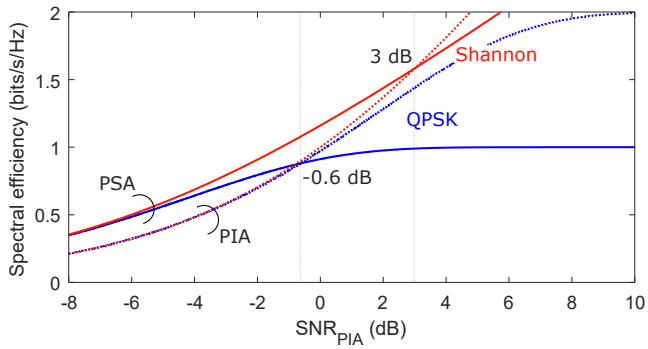

Figure 5.1: Spectral efficiency versus signal-to-noise ratio (SNR) of the PIA. The red curves correspond to Shannon and the blue curves correspond to quadrature phase shift keying (QPSK). The dotted and solid lines correspond to phase-insensitive amplifiers (PIAs) and phase-sensitive amplifiers (PSAs), respectively. For Shannon, the PIA and PSA curves cross at 3 dB whereas for QPSK it happens at -0.6 dB.

SNRs, the SE of PIAs are twice that of the PSAs. As the SNR decreases, the ratio of the SE_{PSA} to SE_{PIA} increases and becomes one at SNRs which correspond to the crossing point of PIA and PSA curves. The PSAs become more spectrally efficient than the PIAs for SNRs below the crossing point as the ratio of SE_{PSA} to SE_{PIA} starts to increase. Moving to still lower SNRs, the ratio of SE_{PSA} to SE_{PIA} reaches two.

Simulations were performed with single- and multi-span links utilizing PIAs and PSAs. A 80 km SSMF was used as the transmission span. The propagation was modelled by solving NLSE using SSFM. The transmission span was dispersion managed and optimized for both PIA and PSA links. Additional span losses were emulated using variable-optical attenuator assuming linear propagation. The NF for the PIA was 4 dB. The PSA was emulated as in [C] where the NF of the PSA was 1 dB. In the single-span links, the GMI was calculated at optimum launch powers (P_{IN}) for different span losses and the SE was obtained from the GMI. The SE for the PIA links is equal to the simulated GMI. However, we divide the GMI by two to take into account the extra bandwidth occupied by the idler for the PSA. The spectral efficiency is plotted for a single-span PIA and PSA links against the span loss in Figure 5.2. The SE of PIA starts to decrease at lower span losses and crosses the SE of PSA at approximately 70.4 dB span loss. This shows us that the SE of PSA links is larger than the PIA links at span losses above 70.4 dB.

The multi-span transmission links were simulated with PIA and PSA as inline amplifiers. For the PIA, dispersion unmanaged links are considered as they have less penalties from nonlinear distortions. For each span, the GMI was calculated for different P_{IN}. The GMI is obtained from the optimum P_{IN} from which the SE is calculated similar to single-span links. The SE is plotted

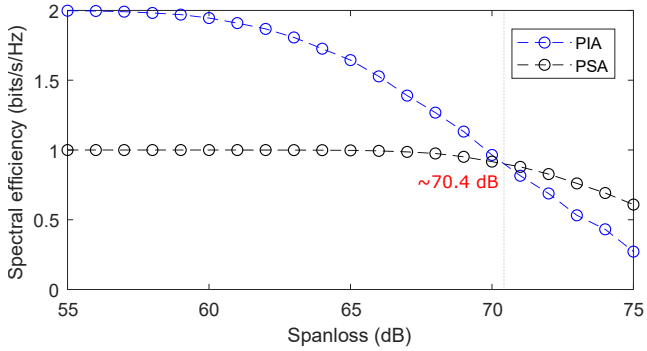

Figure 5.2: Spectral efficiency (SE) is against the span loss for single-span links for phase-insensitive amplifier (PIA) and phase-sensitive amplifier (PSA). The maximum spectral efficiency for the phase-insensitive amplifier utilizing single-polarization (SP) quadrature phase shift keying (QPSK) signal is two whereas for PSA it is one due to the need for the conjugated copy of the signal. The SE curves for PIA and PSA crosses at approximately 70.4-dB span loss. This also shows that the single-span links using PSAs as preamplifier has higher SE than PIA links when the span loss is greater than 70.4 dB.

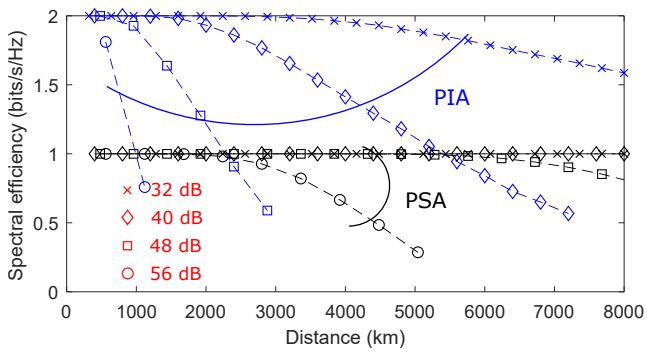

Figure 5.3: Spectral efficiency (SE) is against the distance for phase-insensitive amplifier (PIA) and phase-sensitive amplifier (PSA) used inline in multi-span links with different span losses. The maximum spectral efficiency for the phase-insensitive amplifier utilizing single-polarization (SP) quadrature phase shift keying (QPSK) signal is two whereas for PSA it is one due to the need for the conjugated copy of the signal. The SE decreases with distance for both PIA and PSA links. As the span loss increases, the SE curves of PIA and PSA crosses at shorter distances after which the PSA links are spectrally efficient than the PIA links.

against the distance for different span losses in Figure 5.3. The different span losses are 32, 40, 48 and 56 dB that correspond to spans of length 160, 200, 240 and 280 km assuming the fiber loss is 0.2 dB/km. For a span loss of 32 dB, the SE of PIA links are always higher than the PSA links considering a maximum distance of 8000 km as the curves for PIA and PSA do not cross. When the span loss is 56 dB, the SE curves for PIA and PSA cross at approximately 1000 km. Therefore, the PSA has higher spectral efficiency than that of the PIA beyond 1000 km.

In the multi-span links, the reach improvement using PSAs compared to PIAs are studied at the same SE. At SE of 0.95, the transmission reach for PIA with 48 dB span loss is approximately 2300 km whereas for PSA it is approximately 6500 km. So, the transmission reach improvement obtained when using PSA compared to PIA is approximately 2.8 times. At a distance of 5400 km, the PIA link with 40 dB span loss and PSA link with 48 dB span loss have a SE of 0.99. However, using PSA reduces the number of amplifiers from 27 to approximately 22.

Though only single-channel systems are discussed here, we expect the PSAs to be more spectrally efficient than the PIAs even for a WDM system as PSAs are capable of amplifying WDM channels and mitigating XPM. However, as reported in [C], the XPM mitigation is less effective than the SPM mitigation in PSAs. By combining digital techniques with PSAs, the efficiency of nonlinearity mitigation can likely be further enhanced especially in WDM systems.

5.3 Nonlinearity mitigation

There are different optical techniques for nonlinearity compensation, as addressed in this thesis. One possible work is to compare them assuming ideal conditions. With ideal distributed Raman amplification (DRA), optimized dispersion map, generalized mutual information (GMI) as the metric, the performance of inline optical-phase conjugation (OPC), phase-conjugated twin waves (PCTWs) and copier-PSAs can be compared at the same SE for multi-channel systems. One would expect that the copier-PSAs and PCTWs would perform very similar in terms of nonlinearity mitigation. However, the PSAs can also provide the benefits of low-noise amplification. The most interesting part will be the comparison between OPCs and PSAs, where the additional bandwidth occupied by the idler needs to be taken into account for PSAs as we do in the above section. One could also study the effect of the OPC unit or PSA spacing on system performance.

The fiber nonlinearity can be mitigated spanwise by inline PSAs. The effectiveness of nonlinearity mitigation in PSAs depends on the dispersion map. It was studied in [200] that by performing multi-span dispersion optimization, the residual nonlinearity can be further reduced. One other technique used in this thesis to reduce the residual nonlinearity is to apply the modified VNLE after the mitigation in the PSAs. The modified VNLE can be computationally

complex, especially with many wavelength channels. One possible work could be to compare the performance of these two techniques considering their pros and cons.

Chapter 6

Summary of papers

This thesis is about the nonlinearity mitigation in phase-sensitively amplified links and contains seven appended papers as summarized

PAPER A

B. Foo, M. Karlsson, **K. Vijayan**, M. Mazur, and P. A. Andrekson, "An Analysis of Nonlinearity Mitigation Using Phase-Sensitive Optical Parametric Amplifiers", *Optics Express*, vol. 27, no. 22, pp. 31926-31941, October 2019.

In this paper, a thorough investigation has been done analytically on the nonlinearity mitigation in PSAs, similar to section 4.2.4.1. Using perturbation theory, a residual nonlinear distortion has been established when the PSA mitigates nonlinearity using the copier-PSA implementation in single- or multi-span links. A modified Volterra nonlinear equalizer (VNLE) with low computational effort is proposed to compensate for the residual nonlinear distortion after nonlinear compensation in the PSA. The investigation was verified with numerical simulations using a 10 GBaud, 28 GBaud and 50 GBaud signals. As the symbol rate was increased, the residual nonlinear distortion after the PSA also increases, reducing the reach improvement when using a PSA compared to a PIA. Also, the VNLE was found to be more effective in mitigating the residual nonlinear distortions, especially at higher symbol rates.

My contribution: I assisted B. Foo in the experiments. I presented the corresponding conference paper [K] at the European Conference on Optical Communication (ECOC) 2019 in Dublin, Ireland.

PAPER B

K. Vijayan, H. Eliasson, B. Foo, S. L. I. Olsson, M. Karlsson, and P. A. Andrekson, "Optical Bandwidth Dependency of Nonlinearity Mitigation in Phase-Sensitive Amplifier Links", in *European Conference on Optical Communication (ECOC)*, Sept 2018. DOI: 10.1109/ECOC.2018.8535427

In this paper, the optical bandwidth dependence on nonlinearity mitigation in PSAs is studied by comparing a 10 GBaud signal and a 28 GBaud signal in a multi-span link. The reach improvement from using a PSA compared to a PIA was 5 times for the 10 GBaud signal and 3.4 times for the 28 GBaud signal, showing that the effectiveness of nonlinearity mitigation in PSAs decreases with increasing symbol rate. As per the analytical investigation, adding distributed Raman amplification should increase the efficiency of nonlinearity mitigation in PSAs. This was also demonstrated for the 10 GBaud signal, where the reach improvement for PSA compared to PIA increased to 5.3 times. However, for the 28 GBaud signal such an increase was not observed due to the experimental limitations, .

My contribution: I performed the experiments with H. Eliasson and B. Foo. I wrote the paper with assistance from the co-authors. I presented it at the European Conference on Optical Communication (ECOC) 2018 in Rome, Italy.

PAPER C

K. Vijayan, B. Foo, M. Karlsson, and P. A. Andrekson, "Long-haul Transmission of WDM Signals With In-Line Phase-Sensitive Amplifiers", in *European Conference on Optical Communication (ECOC)*, Sept 2019.
DOI: 10.1049/cp.2019.1116

In this paper, three wavelength-division multiplexed (WDM) channels were used to study the efficacy of nonlinear mitigation in a PSA link. In a multi-span link, one, two and three 10 GBaud channels with a 12.5 GHz spacing were used in both simulations and experiments. As the number of channels was increased, the reach and optimal launch power decreased for both PIA and PSA systems. It was also found that PSAs can mitigate SPM better than XPM.

My contribution: I performed the measurements and simulations with the support of B. Foo. I wrote the paper with assistance from the co-authors. I presented it at the European Conference on Optical Communication (ECOC) 2019 in Dublin, Ireland.

PAPER D

K. Vijayan, B. Foo, M. Karlsson, and P. A. Andrekson, "Cross-Phase Modulation Mitigation in Phase-sensitive Amplifier Links", *IEEE Photonics Technology Letters*, vol. 31, no. 21, pp. 1733-1736, November 2019.

In this paper, wavelength-division multiplexed (WDM) system was used to study the cross-phase modulation (XPM) mitigation in a single-span PSA link. Two 10 GBaud channels spaced 25 GHz apart was used to study the mitigation of SPM and XPM separately in a PSA link. This is to our knowledge, the first demonstration of XPM mitigation in a PSA amplified link. In the simulations, the PSA was found to mitigate SPM better compared to XPM. However, the SPM and XPM mitigation has similar performance in the experiments. Also, three 10 GBaud channels spaced 12.5 GHz apart were used to obtain a 9.5 dB allowable span loss increase using PSA compared to PIA for the center channel.

My contribution: I performed the measurements and simulations with the support of B. Foo. I wrote the paper with assistance from the co-authors.

PAPER E

K. Vijayan, Z. He, B. Foo, M. Karlsson, and P. A. Andrekson, "Modulation format dependence on transmission reach in phase-sensitively amplified fiber links", *Optics Express*, vol. 28, no. 23, pp. 34623-34638, November 2020.

In this paper, we show that the reach improvement when using PSAs compared to PIAs is enhanced for higher-order modulation formats. This is due to the fact that higher-order modulation formats are more susceptible to smaller phase noise and PSAs are better in mitigating smaller phase distortions. Numerical simulations were performed for single- and multi-span links with single- and multi-channel systems using 10 GBaud signals. For all the configurations, the transmission reach increase using PSAs with respect to PIAs was higher for higher-order modulation format signals. This was also experimentally verified with a single-span, single-channel experiment. A 13.3-dB transmission reach increase was obtained for PSAs compared to PIAs with 64-QAM signal.

My contribution: I performed the experiments and simulations. I wrote the paper with assistance from the co-authors.

PAPER F

K. Vijayan, Z. He, B. Foo, J. Schröder, M. Karlsson, and P. A. Andrekson, "Phase-sensitively amplified wavelength-division multiplexed optical transmission systems", - **submitted** to **Optics Express**, March 2021.

In this paper, the transmission reach improvement when using modified VNLE with PSAs for a WDM system is studied. The transmission reach was improved for ten 10 GBaud channels in PSA links by applying the modified VNLE to the entire signal band. The VNLE also reduced the dispersion map dependence on nonlinearity mitigation significantly. This was also verified in experiments with three 10 GBaud channels in a single-span link.

My contribution: I performed the experiments and simulations. I wrote the paper with assistance from the co-authors.

References

[1] Cisco White Paper, "Cisco VNI global IP traffic forecast, 2017-2022," 2018. [Online]. Available: https://newsroom.cisco.com/press-release-content?type=webcontent&articleId=1955935

[2] M. Ciotti, M. Ciccozzi, A. Terrinoni, W. Jiang, C. Wang, and S. Bernardini, "The COVID-19 pandemic," *Crit Rev Clin Lab Sci.*, vol. 57, no. 6, p. 365–388, 2020.

[3] M. Xiang, Z. Zhang, and K. Kuwahara, "Impact of covid-19 pandemic on children and adolescents' lifestyle behavior larger than expected," *Progress in cardiovascular diseases*, 2020.

[4] H. Holgersen, Z. Jia, and S. Svenkerud, "Who and how many can work from home? Evidence from task descriptions." *Journal for labour market research*, vol. 55, no. 1, 2021.

[5] B. Means and J. Neisler, "Teaching and Learning in the Time of COVID: The Student Perspective," *ONLINE LEARNING*, vol. 25, no. 1, pp. 8–27, 2021.

[6] A. Feldmann, O. Gasser, F. Lichtblau, E. Pujol, I. Poese, C. Dietzel, D. Wagner, M. Wichtlhuber, J. Tapiador, N. Vallina-Rodriguez, O. Hohlfeld, and G. Smaragdakis, "The lockdown effect: Implications of the covid-19 pandemic on internet traffic," in *Proceedings of the ACM Internet Measurement Conference*, ser. IMC '20. New York, NY, USA: Association for Computing Machinery, 2020, p. 1–18. [Online]. Available: https://doi.org/10.1145/3419394.3423658

[7] P. J. Winzer, D. T. Neilson, and A. R. Chraplyvy, "Fiber-optic transmission and networking: the previous 20 and the next 20 years," *Opt. Express*, vol. 26, no. 18, pp. 24 190–24 239, Sep 2018.

[8] A. G. Bell, "Apparatus for signalling and communicating, called photophone," Patent 235,199, 1880.

[9] T. H. Maiman, "Stimulated optical radiation in ruby," *Nature*, no. 4736, pp. 493–494, 1960.

[10] M. I. Nathan, W. P. Dumke, G. Burns, F. H. Dill, and G. Lasher, "Stimulated emission of radiation from GaAs p-n junctions," *Applied Physics Letters*, vol. 1, no. 3, pp. 62–64, 1962. [Online]. Available: https://doi.org/10.1063/1.1777371

[11] R. N. Hall, G. E. Fenner, J. D. Kingsley, T. J. Soltys, and R. O. Carlson, "Coherent light emission from GaAs junctions," *Phys. Rev. Lett.*, vol. 9, pp. 366–368, Nov 1962. [Online]. Available: https://link.aps.org/doi/10.1103/PhysRevLett.9.366

[12] K. C. Kao and G. A. Hockham, "Dielectric-fibre surface waveguides for optical frequencies," *Proceedings of the Institution of Electrical Engineers*, vol. 113, no. 7, pp. 1151–1158, 1966.

[13] T. Miya, Y. Terunuma, T. Hosaka, and T. Miyashita, "Ultimate low-loss single-mode fibre at 1.55 μm," *Electronics Letters*, vol. 15, no. 4, pp. 106–108, 1979.

[14] R. S. Kerdock and D. H. Wolaver, "Atlanta fiber system experiment: results of the atlanta experiment," *The Bell System Technical Journal*, vol. 57, no. 6, pp. 1857–1879, 1978.

[15] D. Payne and W. A. Gambling, "Zero material dispersion in optical fibres," *Electronics Letters*, vol. 11, pp. 176–178, 1975.

[16] R. J. Mears, L. Reekie, I. Jauncey, and D. N. Payne, "Low-noise erbium-doped fibre amplifier operating at 1.54 μm," *Electronics Letters*, vol. 23, no. 19, pp. 1026–1028, 1987.

[17] A. Gnauck, R. Tkach, A. Chraplyvy, and T. Li, "High-capacity optical transmission systems," *J. Lightwave Technol.*, vol. 26, no. 9, pp. 1032–1045, May 2008. [Online]. Available: http://jlt.osa.org/abstract.cfm?URI=jlt-26-9-1032

[18] A. M. Vengsarkar, A. E. Miller, and W. A. Reed, "Highly efficient single-mode fiber for broadband dispersion compensation," in *Conference on Optical Fiber Communication/International Conference on Integrated Optics and Optical Fiber Communication*. Optical Society of America, 1993, p. PD13. [Online]. Available: http://www.osapublishing.org/abstract.cfm?URI=OFC-1993-PD13

[19] L. Gruner-Nielsen, M. Wandel, P. Kristensen, C. Jorgensen, L. V. Jorgensen, B. Edvold, B. Palsdottir, and D. Jakobsen, "Dispersion-compensating fibers," *Journal of Lightwave Technology*, vol. 23, no. 11, pp. 3566–3579, 2005.

[20] F. Ouellette, "All-fiber filter for efficient dispersion compensation," *Opt. Lett.*, vol. 16, no. 5, pp. 303–305, Mar 1991. [Online]. Available: http://ol.osa.org/abstract.cfm?URI=ol-16-5-303

[21] K. O. Hill and G. Meltz, "Fiber Bragg grating technology fundamentals and overview," *Journal of Lightwave Technology*, vol. 15, no. 8, pp. 1263–1276, 1997.

[22] K. Kikuchi, "Fundamentals of coherent optical fiber communications," *J. Lightwave Technol.*, vol. 34, no. 1, pp. 157–179, Jan 2016. [Online]. Available: http://jlt.osa.org/abstract.cfm?URI=jlt-34-1-157

[23] C. Laperle and M. O'Sullivan, "Advances in high-speed DACs, ADCs, and DSP for optical coherent transceivers," *Journal of Lightwave Technology*, vol. 32, no. 4, pp. 629–643, 2014.

[24] S. L. Olsson, J. Cho, S. Chandrasekhar, X. Chen, P. J. Winzer, and S. Makovejs, "Probabilistically shapedPDM 4096-QAM transmission over up to 200 km of fiber using standard intradyne detection," *Opt. Express*, vol. 26, no. 4, pp. 4522–4530, Feb 2018. [Online]. Available: http://www.opticsexpress.org/abstract.cfm?URI=oe-26-4-4522

[25] J. C. Cartledge, F. P. Guiomar, F. R. Kschischang, G. Liga, and M. P. Yankov, "Digital signal processing for fiber nonlinearities [invited]," *Opt. Express*, vol. 25, no. 3, pp. 1916–1936, Feb 2017. [Online]. Available: http://www.opticsexpress.org/abstract.cfm?URI=oe-25-3-1916

[26] J.-X. Cai, H. G. Batshon, M. V. Mazurczyk, O. V. Sinkin, D. Wang, M. Paskov, W. W. Patterson, C. R. Davidson, P. C. Corbett, G. M. Wolter, T. E. Hammon, M. A. Bolshtyansky, D. G. Foursa, and A. N. Pilipetskii, "70.46 Tb/s over 7,600 km and 71.65 Tb/s over 6,970 km transmission in C+L band using coded modulation with hybrid constellation shaping and nonlinearity compensation," *J. Lightwave Technol.*, vol. 36, no. 1, pp. 114–121, Jan 2018. [Online]. Available: http://jlt.osa.org/abstract.cfm?URI=jlt-36-1-114

[27] D. J. Richardson, J. M. Fini, and L. E. Nelson, "Space-division multiplexing in optical fibres," *Nature Photonics*, vol. 7, no. 5, pp. 354–362, 2013.

[28] B. J. Puttnam, R. S. Luís, W. Klaus, J. Sakaguchi, J. . Delgado Mendinueta, Y. Awaji, N. Wada, Y. Tamura, T. Hayashi, M. Hirano, and J. Marciante, "2.15 Pb/s transmission using a 22 core homogeneous single-mode multi-core fiber and wideband optical comb," in *2015 European Conference on Optical Communication (ECOC)*, 2015, pp. 1–3.

[29] P. Sillard, M. Bigot-Astruc, and D. Molin, "Few-mode fibers for mode-division-multiplexed systems," *J. Lightwave Technol.*, vol. 32, no. 16, pp. 2824–2829, Aug 2014. [Online]. Available: http://jlt.osa.org/abstract.cfm?URI=jlt-32-16-2824

[30] R. Essiambre, G. Kramer, P. J. Winzer, G. J. Foschini, and B. Goebel, "Capacity limits of optical fiber networks," *Journal of Lightwave Technology*, vol. 28, no. 4, pp. 662–701, 2010.

[31] A. D. Ellis, J. Zhao, and D. Cotter, "Approaching the non-linear shannon limit," *Journal of Lightwave Technology*, vol. 28, no. 4, pp. 423–433, Feb 2010. [Online]. Available: http://jlt.osa.org/abstract.cfm?URI=jlt-28-4-423

[32] R. Essiambre and R. W. Tkach, "Capacity trends and limits of optical communication networks," *Proceedings of the IEEE*, vol. 100, no. 5, pp. 1035–1055, 2012.

[33] A. Hasegawa and F. Tappert, "Transmission of stationary nonlinear optical pulses in dispersive dielectric fibers. I. Anomalous dispersion," *Applied Physics Letters*, vol. 23, no. 3, pp. 142–144, 1973.

[34] R. A. Fisher, B. R. Suydam, and D. Yevick, "Optical phase conjugation for time-domain undoing of dispersive self-phase-modulation effects," *Opt. Lett.*, vol. 8, no. 12, pp. 611–613, Dec 1983. [Online]. Available: http://ol.osa.org/abstract.cfm?URI=ol-8-12-611

[35] X. Liu, A. Chraplyvy, P. Winzer, R. Tkach, and S. Chandrasekhar, "Phase-conjugated twin waves for communication beyond the Kerr nonlinearity limit," *Nature Photonics*, vol. 7, no. 7, pp. 560–568, 2013.

[36] B. Corcoran, S. L. I. Olsson, C. Lundström, M. Karlsson, and P. A. Andrekson, "Mitigation of nonlinear impairments on QPSK data in phase-sensitive amplified links," in *European Conference on Optical Communication*, 2013.

[37] E. Ip and J. M. Kahn, "Compensation of dispersion and nonlinear impairments using digital backpropagation," *Journal of Lightwave Technology*, vol. 26, no. 20, pp. 3416–3425, 2008. [Online]. Available: http://jlt.osa.org/abstract.cfm?URI=jlt-26-20-3416

[38] X. Li, X. Chen, G. Goldfarb, E. Mateo, I. Kim, F. Yaman, and G. Li, "Electronic post-compensation of WDM transmission impairments using coherent detection and digital signal processing," *Opt. Express*, vol. 16, no. 2, pp. 880–888, Jan 2008. [Online]. Available: http://www.opticsexpress.org/abstract.cfm?URI=oe-16-2-880

[39] F. P. Guiomar, J. D. Reis, A. L. Teixeira, and A. N. Pinto, "Mitigation of intra-channel nonlinearities using a frequency-domain Volterra series equalizer," *Opt. Express*, vol. 20, no. 2, pp. 1360–1369, Jan 2012. [Online]. Available: http://www.opticsexpress.org/abstract.cfm?URI=oe-20-2-1360

[40] L. Liu, L. Li, Y. Huang, K. Cui, Q. Xiong, F. N. Hauske, C. Xie, and Y. Cai, "Intrachannel nonlinearity compensation by inverse Volterra series transfer function," *Journal of Lightwave Technology*, vol. 30, no. 3, pp. 310–316, 2012.

[41] S. K. Turitsyn, J. E. Prilepsky, S. T. Le, S. Wahls, L. L. Frumin, M. Kamalian, and S. A. Derevyanko, "Nonlinear fourier transform for optical data processing and transmission: advances and perspectives," *Optica*, vol. 4, no. 3, pp. 307–322, Mar 2017. [Online]. Available: http://www.osapublishing.org/optica/abstract.cfm?URI=optica-4-3-307

[42] T. Freckmann, R. J. Essiambre, P. J. Winzer, G. J. Foschini, and G. Kramer, "Fiber capacity limits with optimized ring constellations," *IEEE Photonics Technology Letters*, vol. 21, no. 20, pp. 1496–1498, 2009.

[43] T. Fehenberger, G. Böcherer, A. Alvarado, and N. Hanik, "Ldpc coded modulation with probabilistic shaping for optical fiber systems," in *Optical Fiber Communication Conference*. Optical Society of America, 2015, p. Th2A.23. [Online]. Available: http://www.osapublishing.org/abstract.cfm?URI=OFC-2015-Th2A.23

[44] E. Desurvire, J. R. Simpson, and P. C. Becker, "High-gain erbium-doped traveling-wave fiber amplifier," *Opt. Lett.*, vol. 12, no. 11, pp. 888–890, Nov 1987. [Online]. Available: http://ol.osa.org/abstract.cfm?URI=ol-12-11-888

[45] C. M. Caves, "Quantum limits on noise in linear amplifiers," *Phys. Rev. D*, vol. 26, pp. 1817–1839, 1982. [Online]. Available: https://link.aps.org/doi/10.1103/PhysRevD.26.1817

[46] R. Tang, P. Devgan, J. Lasri, V. Grigoryan, and P. Kumar, "Experimental investigation of a frequency-nondegenerate phase-sensitive optical parametric amplifier," in *Optical Fiber Communication Conference and Exposition and The National Fiber Optic Engineers Conference*. Optical Society of America, 2005, p. OWN6. [Online]. Available: http://www.osapublishing.org/abstract.cfm?URI=OFC-2005-OWN6

[47] R. Tang, J. Lasri, P. S. Devgan, V. Grigoryan, P. Kumar, and M. Vasilyev, "Gain characteristics of a frequency nondegenerate phase-sensitive fiber-optic parametric amplifier with phase self-stabilized input," *Opt. Express*, vol. 13, no. 26, pp. 10 483–10 493, Dec 2005. [Online]. Available: http://www.opticsexpress.org/abstract.cfm?URI=oe-13-26-10483

[48] Z. Tong, C. Lundström, P. A. Andrekson, M. Karlsson, and A. Bogris, "Ultralow noise, broadband phase-sensitive optical amplifiers, and their applications," *IEEE Journal of Selected Topics in Quantum Electronics*, vol. 18, no. 2, pp. 1016–1032, 2012.

[49] Z. Tong, C. Lundström, P. Andrekson, C. McKinstrie, M. Karlsson, D. Blessing, E. Tipsuwannakul, B. Puttnam, H. Toda, and L. Grüner-Nielsen, "Towards ultrasensitive optical links enabled by low-noise phase-sensitive amplifiers," *Nature Photonics*, vol. 5, no. 7, pp. 430–436, 2011.

[50] S. L. I. Olsson, B. Corcoran, C. Lundström, T. A. Eriksson, M. Karlsson, and P. A. Andrekson, "Phase-sensitive amplified transmission links for improved sensitivity and nonlinearity tolerance," *Journal of Lightwave Technology*, vol. 33, no. 3, pp. 710–721, 2015.

[51] K. J. Lee, F. Parmigiani, S. Liu, J. Kakande, P. Petropoulos, K. Gallo, and D. Richardson, "Phase sensitive amplification based on quadratic cascading in a periodically poled lithium niobate waveguide," *Opt. Express*, vol. 17, no. 22, pp. 20 393–20 400, Oct 2009. [Online]. Available: http://www.opticsexpress.org/abstract.cfm?URI=oe-17-22-20393

[52] P. A. Andrekson and M. Karlsson, "Fiber-based phase-sensitive optical amplifiers and their applications," *Adv. Opt. Photon.*, vol. 12, no. 2, pp. 367–428, Jun 2020. [Online]. Available: http://aop.osa.org/abstract.cfm?URI=aop-12-2-367

[53] S. Olsson, H. Eliasson, E. Astra, M. Karlsson, and P. Andrekson, "Long-haul optical transmission link using low-noise phase-sensitive amplifiers." *Nature communications*, vol. 9, no. 1, pp. 2513–2513, 2018.

[54] G. P. Agrawal, *Nonlinear Fiber Optics*, 5th ed. Academic Press, 2013.

[55] Y. Tamura, H. Sakuma, K. Morita, M. Suzuki, Y. Yamamoto, K. Shimada, Y. Honma, K. Sohma, T. Fujii, and T. Hasegawa, "The first 0.14-dB/km loss optical fiber and its impact on submarine transmission," *Journal of Lightwave Technology*, vol. 36, no. 1, pp. 44–49, 2018.

[56] C. D. Poole and R. E. Wagner, "Phenomenological approach to polarisation dispersion in long single-mode fibres," *Electronics Letters*, vol. 22, no. 19, pp. 1029–1030, 1986.

[57] J. P. Gordon and H. Kogelnik, "PMD fundamentals: Polarization mode dispersion in optical fibers," *Proceedings of the National Academy of Sciences*, vol. 97, no. 9, pp. 4541–4550, 2000. [Online]. Available: https://www.pnas.org/content/97/9/4541

[58] J. Kerr, "XL. a new relation between electricity and light: Dielectrified media birefringent," *The London, Edinburgh, and Dublin Philosophical Magazine and Journal of Science*, vol. 50, no. 332, pp. 337–348, 1875.

[59] ——, "LIV. a new relation between electricity and light: Dielectrified media birefringent (second paper)," *The London, Edinburgh, and Dublin Philosophical Magazine and Journal of Science*, vol. 50, no. 333, pp. 446–458, 1875.

[60] T. Nakanishi, M. Hirano, T. Okuno, and M. Onishi, "Silica-based highly nonlinear fiber with $\gamma = 30$/W/km and its FWM-based conversion efficiency," in *Optical Fiber Communication Conference*, 2006.

[61] M. Hirano, T. Nakanishi, T. Okuno, and M. Onishi, "Silica-based highly nonlinear fibers and their application," *IEEE Journal of Selected Topics in Quantum Electronics*, vol. 15, no. 1, pp. 103–113, 2009.

[62] R. H. Stolen and C. Lin, "Self-phase-modulation in silica optical fibers," *Physical Review A*, vol. 17, pp. 1448–1453, 1978. [Online]. Available: https://link.aps.org/doi/10.1103/PhysRevA.17.1448

[63] L. F. Mollenauer, R. H. Stolen, and J. P. Gordon, "Experimental observation of picosecond pulse narrowing and solitons in optical fibers," *Physical Review Letters*, vol. 45, no. 13, pp. 1095–1098, 1980.

[64] A. Hasegawa and Y. Kodama, "Signal transmission by optical solitons in monomode fiber," *Proceedings of the IEEE*, vol. 69, no. 9, pp. 1145–1150, 1981.

[65] A. R. Ghraplyvy and J. Stone, "Measurement of cross-phase modulation in coherent wavelength-division multiplexing using injection lasers," in *Optical Fiber Communication*. Optical Society of America, 1985, p. TUO6. [Online]. Available: http://www.osapublishing.org/abstract.cfm?URI=OFC-1985-TUO6

[66] A. Bononi, P. Serena, N. Rossi, and D. Sperti, "Which is the dominant nonlinearity in long-haul PDM-QPSK coherent transmissions?" in *European Conference on Optical Communication*, 2010.

[67] N. Rossi, P. Serena, and A. Bononi, "Symbol-rate dependence of dominant nonlinearity and reach in coherent WDM links," *Journal of Lightwave Technology*, vol. 33, no. 14, pp. 3132–3143, 2015.

[68] J. Hansryd, P. A. Andrekson, M. Westlund, Jie Li, and P.-O. Hedekvist, "Fiber-based optical parametric amplifiers and their applications," *IEEE Journal of Selected Topics in Quantum Electronics*, vol. 8, no. 3, pp. 506–520, 2002.

[69] R. H. Stolen, J. E. Bjorkholm, and A. Ashkin, "Phase-matched three-wave mixing in silica fiber optical waveguides," *Applied Physics Letters*, vol. 24, no. 7, pp. 308–310, 1974. [Online]. Available: https://doi.org/10.1063/1.1655195

[70] M. Karlsson, "Transmission systems with low noise phase-sensitive parametric amplifiers," *Journal of Lightwave Technology*, vol. 34, no. 5, pp. 1411–1423, 2016.

[71] B. Goebel and N. Hanik, "Analytical calculation of the number of four-wave-mixing products in optical multichannel communication systems," 2008.

[72] C. V. Raman and K. S. Krishnan, "A new type of secondary radiation," *Nature*, vol. 121, no. 11, pp. 501–502, 1928.

[73] E. Woodbury and W. Ng, "Ruby laser operation in near IR," *Proceedings of the Institute of Radio Engineers*, vol. 50, no. 11, pp. 2347–2348, 1962.

[74] R. Y. Chiao, C. H. Townes, and B. P. Stoicheff, "Stimulated Brillouin scattering and coherent generation of intense hypersonic waves," *Physical Review Letters*, vol. 12, pp. 592–595, 1964. [Online]. Available: https://link.aps.org/doi/10.1103/PhysRevLett.12.592

[75] M. D. Mermelstein, "SBS threshold measurements and acoustic beam propagation modeling in guiding and anti-guiding single mode optical fibers," *Opt. Express*, vol. 17, no. 18, pp. 16 225–16 237, Aug 2009. [Online]. Available: http://www.opticsexpress.org/abstract.cfm?URI=oe-17-18-16225

[76] L. Grüner-Nielsen, S. Dasgupta, M. D. Mermelstein, D. Jakobsen, S. Herstrøm, M. E. V. Pedersen, E. L. Lim, S. u. Alam, F. Parmigiani, D. Richardson, and B. Pálsdóttir, "A silica based highly nonlinear fibre with improved threshold for stimulated brillouin scattering," in *36th European Conference and Exhibition on Optical Communication*, 2010, pp. 1–3.

[77] L. Grüner-Nielsen, D. Jakobsen, S. Herstrøm, B. Pálsdóttir, S. Dasgupta, D. Richardson, C. Lundström, S. Olsson, and P. Andrekson, "Brillouin suppressed highly nonlinear fibers," in *European Conference and Exhibition on Optical Communication*. Optical Society of America, 2012, p. We.1.F.1. [Online]. Available: http://www.osapublishing.org/abstract.cfm?URI=ECEOC-2012-We.1.F.1

[78] J. Hansryd and P. A. Andrekson, "Broadband CW Pumped Fiber Optical Parametric Amplifier with 49 dB Gain and Wavelength Conversion Efficiency," in *Optical Fiber Communication Conference*. Optical Society of America, 2000, p. PD3. [Online]. Available: http://www.osapublishing.org/abstract.cfm?URI=OFC-2000-PD3

[79] Min-Chen Ho, M. E. Marhic, K. Y. K. Wong, and L. G. Kazovsky, "Narrow-linewidth idler generation in fiber four-wave mixing and parametric amplification by dithering two pumps in opposition of phase," *Journal of Lightwave Technology*, vol. 20, no. 3, pp. 469–476, 2002.

[80] Y. Imai and N. Shimada, "Dependence of stimulated brillouin scattering on temperature distribution in polarization-maintaining fibers," *IEEE photonics technology letters*, vol. 5, no. 11, pp. 1335–1337, 1993.

[81] J. Hansryd, F. Dross, M. Westlund, P. A. Andrekson, and S. N. Knudsen, "Increase of the SBS threshold in a short highly nonlinear fiber by applying a temperature distribution," *Journal of Lightwave Technology*, vol. 19, no. 11, pp. 1691–1697, 2001.

[82] N. Yoshizawa and T. Imai, "Stimulated Brillouin scattering suppression by means of applying strain distribution to fiber with cabling," *Journal of Lightwave Technology*, vol. 11, no. 10, pp. 1518–1522, 1993.

[83] J. D. Marconi, J. M. Chavez Boggio, and H. L. Fragnito, "7.3 dB increase of the SBS threshold in an optical fiber by applying a strain distribution," in *Optical Fiber Communication Conference, 2004. OFC 2004*, vol. 1, 2004, pp. 35–.

[84] J. M. C. Boggio, J. D. Marconi, and H. L. Fragnito, "Experimental and numerical investigation of the SBS-threshold increase in an optical fiber by applying strain distributions," *J. Lightwave Technol.*, vol. 23, no. 11, p. 3808, Nov 2005. [Online]. Available: http://jlt.osa.org/abstract.cfm?URI=jlt-23-11-3808

[85] M. Takahashi, M. Tadakuma, and T. Yagi, "Dispersion and Brillouin managed HNLFs by strain control techniques," *J. Lightwave Technol.*, vol. 28, no. 1, pp. 59–64, Jan 2010. [Online]. Available: http://jlt.osa.org/abstract.cfm?URI=jlt-28-1-59

[86] B. P.-P. Kuo, J. M. Fini, L. Grüner-Nielsen, and S. Radic, "Dispersion-stabilized highly-nonlinear fiber for wideband parametric mixer synthesis," *Optics Express*, vol. 20, no. 17, pp. 18 611–18 619, 2012. [Online]. Available: http://www.opticsexpress.org/abstract.cfm?URI=oe-20-17-18611

[87] Y. Takushima and T. Okoshi, "Suppression of stimulated Brillouin scattering using optical isolators," *Electronics Letters*, vol. 28, no. 12, pp. 1155–1157, 1992.

[88] C. Lundström, R. Malik, L. Gruner-Nielsen, B. Corcoran, S. L. I. Olsson, M. Karlsson, and P. A. Andrekson, "Fiber optic parametric amplifier with 10-dB net gain without pump dithering," *IEEE Photonics Technology Letters*, vol. 25, no. 3, pp. 234–237, 2013.

[89] K. K. Y. Wong, K. Shimizu, K. Uesaka, G. Kalogerakis, M. E. Marhic, and L. G. Kazovsky, "Continuous-wave fiber optical parametric amplifier with 60 dB gain using a novel two-segment design," in *Conference on Lasers and Electro-Optics, 2003. CLEO '03.*, 2003, pp. 1112–1113.

[90] G. P. Agrawal, *Fiber-Optic Communication Systems*, 4th ed. John Wiley & Sons, 2010.

[91] S. Kumar and M. Deen, "Fiber optic communications: Fundamentals and applications," 2014.

[92] D. M. Baney, P. Gallion, and R. S. Tucker, "Theory and measurement techniques for the noise figure of optical amplifiers," *Optical Fiber Technology*, vol. 6, no. 2, pp. 122–154, 2000. [Online]. Available: https://www.sciencedirect.com/science/article/pii/S1068520000903274

[93] Z. Tong, C. J. McKinstrie, C. Lundström, M. Karlsson, and P. A. Andrekson, "Noise performance of optical fiber transmission links that use non-degenerate cascaded phase-sensitive amplifiers," *Optics Express*, vol. 18, no. 15, pp. 15 426–15 439, 2010. [Online]. Available: http://www.opticsexpress.org/abstract.cfm?URI=oe-18-15-15426

[94] S. Poole, D. Payne, R. Mears, M. Fermann, and R. Laming, "Fabrication and characterization of low-loss optical fibers containing rare-earth ions," *Journal of Lightwave Technology*, vol. 4, no. 7, pp. 870–876, July 1986.

[95] C. R. Giles, E. Desurvire, J. R. Talman, J. R. Simpson, and P. C. Becker, "2-Gbit/s signal amplification at lambda = 1.53 mu m in an erbium-doped single-mode fiber amplifier," *Journal of Lightwave Technology*, vol. 7, no. 4, pp. 651–656, 1989.

[96] R. I. Laming, M. N. Zervas, and D. N. Payne, "Erbium-doped fiber amplifier with 54 dB gain and 3.1 dB noise figures," *IEEE Photonics Technology Letters*, vol. 4, no. 12, pp. 1345–1347, 1992.

[97] E. Desurvire, C. R. Giles, and J. R. Simpson, "Gain saturation effects in high-speed, multichannel erbium-doped fiber amplifiers at lambda =1.53 mu m," *Journal of Lightwave Technology*, vol. 7, no. 12, pp. 2095–2104, 1989.

[98] P. M. Becker, A. A. Olsson, and J. R. Simpson, *Erbium-doped fiber amplifiers: fundamentals and technology*. Elsevier, 1999.

[99] A. A. M. Saleh and I. M. I. Habbab, "Effects of semiconductor-optical-amplifier nonlinearity on the performance of high-speed intensity-modulation lightwave systems," *IEEE Transactions on Communications*, vol. 38, no. 6, pp. 839–846, 1990.

[100] L. H. Spiekman, J. M. Wiesenfeld, A. H. Gnauck, L. D. Garrett, G. N. Van Den Hoven, T. Van Dongen, M. J. H. Sander-Jochem, and J. J. M. Binsma, "Transmission of 8 DWDM channels at 20 Gb/s over 160 km of standard fiber using a cascade of semiconductor optical amplifiers," *IEEE Photonics Technology Letters*, vol. 12, no. 6, pp. 717–719, 2000.

[101] K. E. Stubkjaer, "Semiconductor optical amplifier-based all-optical gates for high-speed optical processing," *IEEE journal of selected topics in quantum electronics*, vol. 6, no. 6, pp. 1428–1435, 2000.

[102] T. Durhuus, B. Mikkelsen, C. Joergensen, S. Lykke Danielsen, and K. E. Stubkjaer, "All-optical wavelength conversion by semiconductor optical amplifiers," *Journal of Lightwave Technology*, vol. 14, no. 6, pp. 942–954, 1996.

[103] R. H. Stolen and E. P. Ippen, "Raman gain in glass optical waveguides," *Applied Physics Letters*, vol. 22, no. 6, pp. 276–278, 1973. [Online]. Available: https://doi.org/10.1063/1.1654637

[104] C. Headley and G. Agrawal, *Raman amplification in fiber optical communication systems*. Academic press, 2005.

[105] L. Mollenauer, J. Gordon, and M. Islam, "Soliton propagation in long fibers with periodically compensated loss," *IEEE Journal of Quantum Electronics*, vol. 22, no. 1, pp. 157–173, 1986.

[106] P. Rosa, G. Rizzelli, X. Pang, O. Ozolins, A. Udalcovs, M. Tan, M. Jaworski, M. Marciniak, S. Sergeyev, R. Schatz, G. Jacobsen, S. Popov, and J. D. Ania-Castañón, "Unrepeatered 240-km 64-QAM transmission using distributed Raman amplification over smf fiber," *Applied Sciences*, vol. 10, no. 4, 2020. [Online]. Available: https://www.mdpi.com/2076-3417/10/4/1433

[107] H. Eliasson, S. L. I. Olsson, M. Karlsson, and P. A. Andrekson, "Mitigation of nonlinear distortion in hybrid Raman/phase-sensitive amplifier links," *Opt. Express*, vol. 24, no. 2, pp. 888–900, Jan 2016. [Online]. Available: http://www.opticsexpress.org/abstract.cfm?URI=oe-24-2-888

[108] J. D. Ania-Castañón, "Quasi-lossless transmission using second-order Raman amplification and fibre Bragg gratings," *Opt. Express*, vol. 12, no. 19, pp. 4372–4377, Sep 2004. [Online]. Available: http://www.opticsexpress.org/abstract.cfm?URI=oe-12-19-4372

[109] T. J. Ellingham, J. D. Ania-Castanon, R. Ibbotson, X. Chen, L. Zhang, and S. K. Turitsyn, "Quasi-lossless optical links for broad-band transmission and data processing," *IEEE Photonics Technology Letters*, vol. 18, no. 1, pp. 268–270, 2006.

[110] T. Okuno, T. Tsuzaki, and M. Nishimura, "Novel optical hybrid line configuration for quasi-lossless transmission by distributed Raman amplification," *IEEE Photonics Technology Letters*, vol. 13, no. 8, pp. 806–808, 2001.

[111] K. K. Y. Wong, M. E. Marhic, K. Uesaka, and L. G. Kazovsky, "Polarization-independent two-pump fiber optical parametric amplifier," *IEEE Photonics Technology Letters*, vol. 14, no. 7, pp. 911–913, 2002.

[112] T. Tanemura and K. Kikuchi, "Polarization-independent broad-band wavelength conversion using two-pump fiber optical parametric amplification without idler spectral broadening," *IEEE Photonics Technology Letters*, vol. 15, no. 11, pp. 1573–1575, 2003.

[113] K. K. Y. Wong, M. E. Marhic, K. Uesaka, and L. G. Kazovsky, "Polarization-independent one-pump fiber-optical parametric amplifier," *IEEE Photonics Technology Letters*, vol. 14, no. 11, pp. 1506–1508, 2002.

[114] T. Torounidis, H. Sunnerud, P. Hedekvist, and P. Andrekson, "Amplification of WDM signals in fiber-based optical parametric amplifiers," *IEEE Photonics Technology Letters*, vol. 15, no. 8, pp. 1061–1063, 2003.

[115] M. Westlund, M. Sköld, and P. A. Andrekson, "All-optical phase-sensitive waveform sampling at 40 GSymbol/s," in *Optical Fiber Communication Conference/National Fiber Optic Engineers Conference*. Optical Society of America, 2008, p. PDP12. [Online]. Available: http://www.osapublishing.org/abstract.cfm?URI=NFOEC-2008-PDP12

[116] M. Sköld, M. Westlund, H. Sunnerud, and P. A. Andrekson, "All-optical waveform sampling in high-speed optical communication systems using advanced modulation formats," *J. Lightwave Technol.*, vol. 27, no. 16, pp. 3662–3671, Aug 2009. [Online]. Available: http://jlt.osa.org/abstract.cfm?URI=jlt-27-16-3662

[117] M. E. Marhic, *Fiber Optical Parametric Amplifiers, Oscillators and Related Devices*. Cambridge University Press, 2007.

[118] K. Inoue and T. Mukai, "Signal wavelength dependence of gain saturation in a fiber optical parametric amplifier," *Optics Letters*, vol. 26, no. 1, pp. 10–12, 2001. [Online]. Available: http://ol.osa.org/abstract.cfm?URI=ol-26-1-10

[119] G. Cappellini and S. Trillo, "Third-order three-wave mixing in single-mode fibers: exact solutions and spatial instability effects," *J. Opt. Soc. Am. B*, vol. 8, no. 4, pp. 824–838, Apr 1991. [Online]. Available: http://josab.osa.org/abstract.cfm?URI=josab-8-4-824

[120] R. Stolen and J. Bjorkholm, "Parametric amplification and frequency conversion in optical fibers," *IEEE Journal of Quantum Electronics*, vol. 18, no. 7, pp. 1062–1072, 1982.

[121] C. J. McKinstrie and S. Radic, "Phase-sensitive amplification in a fiber," *Optics Express*, vol. 12, no. 20, pp. 4973–4979, 2004. [Online]. Available: http://www.opticsexpress.org/abstract.cfm?URI=oe-12-20-4973

[122] C. J. McKinstrie, S. Radic, and A. R. Chraplyvy, "Parametric amplifiers driven by two pump waves," *IEEE Journal of Selected Topics in Quantum Electronics*, vol. 8, no. 3, pp. 538–547, 2002.

[123] C. J. McKinstrie, S. Radic, and M. G. Raymer, "Quantum noise properties of parametric amplifiers driven by two pump waves," *Optics Express*, vol. 12, no. 21, pp. 5037–5066, 2004. [Online]. Available: http://www.opticsexpress.org/abstract.cfm?URI=oe-12-21-5037

[124] Y. Chen and A. W. Snyder, "Four-photon parametric mixing in optical fibers: effect of pump depletion," *Optics Letters*, vol. 14, no. 1, pp. 87–89, 1989. [Online]. Available: http://ol.osa.org/abstract.cfm?URI=ol-14-1-87

[125] Z. Tong, A. Bogris, M. Karlsson, and P. A. Andrekson, "Full characterization of the signal and idler noise figure spectra in single-pumped fiber optical parametric amplifiers," *Optics Express*, vol. 18, no. 3, pp. 2884–2893, 2010. [Online]. Available: http://www.opticsexpress.org/abstract.cfm?URI=oe-18-3-2884

[126] P. Kylemark, P. O. Hedekvist, H. Sunnerud, M. Karlsson, and P. A. Andrekson, "Noise characteristics of fiber optical parametric amplifiers," *Journal of Lightwave Technology*, vol. 22, no. 2, pp. 409–416, 2004.

[127] P. L. Voss and P. Kumar, "Raman-noise-induced noise-figure limit for $\chi(3)$ parametric amplifiers," *Opt. Lett.*, vol. 29, no. 5, pp. 445–447, Mar 2004.

[128] R. Tang, P. L. Voss, J. Lasri, P. Devgan, and P. Kumar, "Noise-figure limit of fiber-optical parametric amplifiers and wavelength converters:experimental investigation," *Opt. Lett.*, vol. 29, no. 20, pp. 2372–2374, Oct 2004.

[129] A. Bogris, D. Syvridis, P. Kylemark, and P. A. Andrekson, "Noise characteristics of dual-pump fiber-optic parametric amplifiers," *Journal of Lightwave Technology*, vol. 23, no. 9, pp. 2788–2795, 2005.

[130] A. Durecu-Legrand, C. Simonneau, D. Bayart, A. Mussot, T. Sylvestre, E. Lantz, and H. Maillotte, "Impact of pump OSNR on noise figure for fiber-optical parametric amplifiers," *IEEE Photonics Technology Letters*, vol. 17, no. 6, pp. 1178–1180, 2005.

[131] P. Velanas, A. Bogris, and D. Syvridis, "Impact of dispersion fluctuations on the noise properties of fiber optic parametric amplifiers," *Journal of lightwave technology*, vol. 24, no. 5, pp. 2171–2178, 2006.

[132] X.-x. Liu, X.-j. Xin, J.-h. Yuan, X.-q. Liu, X. Sang, and C.-x. Yu, "Influence of the zero dispersion wavelength fluctuation on the gain and noise performance in dual-pump fiber parametric amplifiers," *Optoelectronics Letters*, vol. 6, no. 5, pp. 367–370, 2010.

[133] Z. Tong, C. Lundstrom, M. Karlsson, and P. A. Andrekson, "Impact of zero-dispersion-wavelength distributions on the noise figure nonreciprocity of a fiber parametric amplifier," *IEEE Photonics Technology Letters*, vol. 23, no. 6, pp. 365–367, 2011.

[134] C. J. McKinstrie, M. Yu, M. G. Raymer, and S. Radic, "Quantum noise properties of parametric processes," *Opt. Express*, vol. 13, no. 13, pp. 4986–5012, Jun 2005. [Online]. Available: http://www.opticsexpress.org/abstract.cfm?URI=oe-13-13-4986

[135] S. L. Olsson, M. Karlsson, and P. A. Andrekson, "Nonlinear phase noise mitigation in phase-sensitive amplified transmission systems," *Optics Express*, vol. 23, no. 9, pp. 11 724–11 740, 2015. [Online]. Available: http://www.opticsexpress.org/abstract.cfm?URI=oe-23-9-11724

[136] K. Croussore, C. Kim, and G. Li, "All-optical regeneration of differential phase-shift keying signals based on phase-sensitive amplification," *Opt. Lett.*, vol. 29, no. 20, pp. 2357–2359, Oct 2004. [Online]. Available: http://ol.osa.org/abstract.cfm?URI=ol-29-20-2357

[137] W. Imajuku and A. Takada, "In-line optical phase-sensitive amplifier with optical-PLL-controlled internal pump light source," in *Optical Amplifiers and Their Applications*. Optical Society of America, 1997, p. FAW23. [Online]. Available: http://www.osapublishing.org/abstract.cfm?URI=OAA-1997-FAW23

[138] A. Bogris and D. Syvridis, "RZ-DPSK signal regeneration based on dual-pump phase-sensitive amplification in fibers," *IEEE Photonics Technology Letters*, vol. 18, no. 20, pp. 2144–2146, 2006.

[139] R. Slavík, F. Parmigiani, J. Kakande, C. Lundström, M. Sjödin, P. A. Andrekson, R. Weerasuriya, S. Sygletos, A. D. Ellis, L. Grüner-Nielsen *et al.*, "All-optical phase and amplitude regenerator for next-generation telecommunications systems," *Nature Photonics*, vol. 4, no. 10, pp. 690–695, 2010.

[140] T. Richter, B. Corcoran, S. L. Olsson, C. Lundström, M. Karlsson, C. Schubert, and P. A. Andrekson, "Experimental characterization of a phase-sensitive four-mode fiber-optic parametric amplifier," in *European Conference and Exhibition on Optical Communication*. Optical Society of America, 2012, p. Th.1.F.1.

[141] C. J. McKinstrie, M. Karlsson, and Z. Tong, "Field-quadrature and photon-number correlations produced by parametric processes," *Optics Express*, vol. 18, no. 19, pp. 19 792–19 823, 2010. [Online]. Available: http://www.opticsexpress.org/abstract.cfm?URI=oe-18-19-19792

[142] Z. Tong, A. Bogris, C. Lundström, C. J. McKinstrie, M. Vasilyev, M. Karlsson, and P. A. Andrekson, "Modeling and measurement of the noise figure of a cascaded non-degenerate phase-sensitive parametric amplifier," *Optics Express*, vol. 18, no. 14, pp. 14 820–14 835, 2010. [Online]. Available: http://www.opticsexpress.org/abstract.cfm?URI=oe-18-14-14820

[143] B. Corcoran, R. Malik, S. L. I. Olsson, C. Lundström, M. Karlsson, and P. A. Andrekson, "Noise beating in hybrid phase-sensitive amplifier systems," *Optics Express*, vol. 22, no. 5, pp. 5762–5771, 2014. [Online]. Available: http://www.opticsexpress.org/abstract.cfm?URI=oe-22-5-5762

[144] S. L. I. Olsson, B. Corcoran, C. Lundström, E. Tipsuwannakul, S. Sygletos, A. D. Ellis, Z. Tong, M. Karlsson, and P. A. Andrekson, "Injection locking-based pump recovery for phase-sensitive amplified links," *Opt. Express*, vol. 21, no. 12, pp. 14 512–14 529, Jun 2013. [Online]. Available: http://www.opticsexpress.org/abstract.cfm?URI=oe-21-12-14512

[145] Z. Liu and R. Slavík, "Optical injection locking: From principle to applications," *Journal of Lightwave Technology*, vol. 38, no. 1, pp. 43–59, 2020.

[146] R. Kakarla, J. Schröder, and P. A. Andrekson, "Optical injection locking at sub nano-watt powers," *Optics Letters*, vol. 43, no. 23, pp. 5769–5772, 2018. [Online]. Available: http://ol.osa.org/abstract.cfm?URI=ol-43-23-5769

[147] B. Corcoran, S. L. I. Olsson, C. Lundström, M. Karlsson, and P. Andrekson, "Phase-sensitive optical pre-amplifier implemented in an 80km DQPSK link," in *OFC/NFOEC*, March 2012, pp. 1–3.

[148] S. L. I. Olsson, M. Karlsson, and P. A. Andrekson, "Long-haul optical transmission of 16-QAM signal with in-line phase-sensitive amplifiers," in *2017 European Conference on Optical Communication (ECOC)*, 2017, pp. 1–3.

[149] M. Wandel, T. Veng, N. T. Quang Le, and L. Gruner-Nielsen, "Dispersion compensating fibre with a high figure of merit," in *European Conference on Optical Communication*, 2001.

[150] L. Grüner-Nielsen, S. N. Knudsen, B. Edvold, T. Veng, D. Magnussen, C. Larsen, and H. Damsgaard, "Dispersion compensating fibers," *Optical Fiber Technology*, vol. 6, no. 2, pp. 164–180, 2000. [Online]. Available: https://www.sciencedirect.com/science/article/pii/S1068520099903243

[151] E. Tipsuwannakul, J. Li, T. A. Eriksson, L. Egnell, F. Sjöström, J. Pejnefors, P. A. Andrekson, and M. Karlsson, "Influence of fiber-Bragg grating-induced group-delay ripple in high-speed transmission systems," *Journal of Optical Communications and Networking*, vol. 4, no. 6, pp. 514–521, 2012. [Online]. Available: http://jocn.osa.org/abstract.cfm?URI=jocn-4-6-514

[152] H. Bülow, F. Buchali, and A. Klekamp, "Electronic dispersion compensation," *Journal of Lightwave Technology*, vol. 26, no. 1, pp. 158–167, 2008. [Online]. Available: http://jlt.osa.org/abstract.cfm?URI=jlt-26-1-158

[153] S. J. Savory, G. Gavioli, R. I. Killey, and P. Bayvel, "Electronic compensation of chromatic dispersion using a digital coherent receiver," *Optics Express*, vol. 15, no. 5, pp. 2120–2126, 2007. [Online]. Available: http://www.opticsexpress.org/abstract.cfm?URI=oe-15-5-2120

[154] E. Agrell, "Nonlinear fiber capacity," in *European Conference on Optical Communication*, 2013.

[155] A. D. Ellis, M. E. McCarthy, M. A. Z. A. Khateeb, M. Sorokina, and N. J. Doran, "Performance limits in optical communications due to fiber nonlinearity," *Adv. Opt. Photon.*, vol. 9, no. 3, pp. 429–503, Sep 2017. [Online]. Available: http://aop.osa.org/abstract.cfm?URI=aop-9-3-429

[156] E. E. Narimanov and P. Mitra, "The channel capacity of a fiber optics communication system: perturbation theory," *Journal of Lightwave Technology*, vol. 20, no. 3, pp. 530–537, 2002.

[157] J. B. Stark, P. Mitra, and A. Sengupta, "Information capacity of nonlinear wavelength division multiplexing fiber optic transmission line," *Optical Fiber Technology*, vol. 7, no. 4, pp. 275–288, 2001. [Online]. Available: https://www.sciencedirect.com/science/article/pii/S1068520000903456

[158] J. P. Gordon and L. F. Mollenauer, "Phase noise in photonic communications systems using linear amplifiers," *Optics Letters*, vol. 15, no. 23, pp. 1351–1353, 1990. [Online]. Available: http://ol.osa.org/abstract.cfm?URI=ol-15-23-1351

[159] P. Minzioni, V. Pusino, I. Cristiani, L. Marazzi, M. Martinelli, and V. Degiorgio, "Study of the Gordon–Mollenauer effect and of the optical-phase-conjugation compensation method in phase-modulated optical communication systems," *IEEE Photonics Journal*, vol. 2, pp. 284–291, 2010.

[160] A. Vannucci, P. Serena, and A. Bononi, "The RP method: a new tool for the iterative solution of the nonlinear schrodinger equation," *Journal of Lightwave Technology*, vol. 20, no. 7, pp. 1102–1112, 2002.

[161] J. K. Fischer, H. Louchet, S. Randel, and K. Petermann, "A simple criterion for the characterization of nonlinear impairments in optical transmission systems," in *Optical Transmission, Switching, and Subsystems III*, R. S. Tucker, D. Chiaroni, W. Gu, and K. ichi Kitayama, Eds., vol. 6021, International Society for Optics and Photonics. SPIE, 2005, pp. 325 – 334. [Online]. Available: https://doi.org/10.1117/12.636888

[162] H. Louchet, A. Hodzic, K. Petermann, A. Robinson, and R. Epworth, "Simple criterion for the characterization of nonlinear impairments in dispersion-managed optical transmission systems," *IEEE Photonics Technology Letters*, vol. 17, no. 10, pp. 2089–2091, 2005.

[163] P. Johannisson and M. Karlsson, "Perturbation analysis of nonlinear propagation in a strongly dispersive optical communication system," *Journal of Lightwave Technology*, vol. 31, no. 8, pp. 1273–1282, 2013.

[164] R. J. Essiambre and P. J. Winzer, "Fibre nonlinearities in electronically pre-distorted transmission," in *2005 31st European Conference on Optical Communication, ECOC 2005*, vol. 2, 2005, pp. 191–192 vol.2.

[165] K. V. Peddanarappagari and M. Brandt-Pearce, "Volterra series transfer function of single-mode fibers," *Journal of Lightwave Technology*, vol. 15, no. 12, pp. 2232–2241, 1997.

[166] R. Dar, M. Feder, A. Mecozzi, and M. Shtaif, "On shaping gain in the nonlinear fiber-optic channel," in *2014 IEEE International Symposium on Information Theory*, 2014, pp. 2794–2798.

[167] G. Saavedra, G. Liga, and P. Bayvel, "Volterra-assisted optical phase conjugation: A hybrid optical-digital scheme for fiber nonlinearity compensation," *Journal of Lightwave Technology*, vol. 37, no. 10, pp. 2467–2479, 2019.

[168] E. Ip, "Nonlinear compensation using backpropagation for polarization-multiplexed transmission," *J. Lightwave Technol.*, vol. 28, no. 6, pp. 939–951, Mar 2010. [Online]. Available: http://jlt.osa.org/abstract.cfm?URI=jlt-28-6-939

[169] L. Beygi, N. V. Irukulapati, E. Agrell, P. Johannisson, M. Karlsson, H. Wymeersch, P. Serena, and A. Bononi, "On nonlinearly-induced noise in single-channel optical links with digital backpropagation," *Opt. Express*, vol. 21, no. 22, pp. 26 376–26 386, Nov 2013. [Online]. Available: http://www.opticsexpress.org/abstract.cfm?URI=oe-21-22-26376

[170] D. Rafique and A. D. Ellis, "Impact of signal-ASE four-wave mixing on the effectiveness of digital back-propagation in 112 Gb/s PM-QPSK systems," *Opt. Express*, vol. 19, no. 4, pp. 3449–3454, Feb 2011.

[Online]. Available: http://www.opticsexpress.org/abstract.cfm?URI=oe-19-4-3449

[171] G. Gao, X. Chen, and W. Shieh, "Influence of PMD on fiber nonlinearity compensation using digital back propagation," *Opt. Express*, vol. 20, no. 13, pp. 14 406–14 418, Jun 2012. [Online]. Available: http://www.opticsexpress.org/abstract.cfm?URI=oe-20-13-14406

[172] G. Liga, T. Xu, A. Alvarado, R. I. Killey, and P. Bayvel, "On the performance of multichannel digital backpropagation in high-capacity long-haul optical transmission," *Opt. Express*, vol. 22, no. 24, pp. 30 053–30 062, Dec 2014. [Online]. Available: http://www.opticsexpress.org/abstract.cfm?URI=oe-22-24-30053

[173] W. Rugh, "Nonlinear system theory: The Volterra / Wiener approach," 1981.

[174] T. K. Biswas and W. F. McGee, "Volterra series analysis of semiconductor laser diode," *IEEE Photonics Technology Letters*, vol. 3, no. 8, pp. 706–708, 1991.

[175] F. P. Guiomar and A. N. Pinto, "Simplified Volterra series nonlinear equalizer for polarization-multiplexed coherent optical systems," *Journal of Lightwave Technology*, vol. 31, no. 23, pp. 3879–3891, 2013.

[176] A. Bakhshali, W. Chan, J. C. Cartledge, M. O'Sullivan, C. Laperle, A. Borowiec, and K. Roberts, "Frequency-domain Volterra-based equalization structures for efficient mitigation of intrachannel Kerr nonlinearities," *Journal of Lightwave Technology*, vol. 34, no. 8, pp. 1770–1777, 2016.

[177] S. Watanabe, T. Chikama, G. Ishikawa, T. Terahara, and H. Kuwahara, "Compensation of pulse shape distortion due to chromatic dispersion and kerr effect by optical phase conjugation," *IEEE Photonics Technology Letters*, vol. 5, no. 10, pp. 1241–1243, 1993.

[178] S. Watanabe and M. Shirasaki, "Exact compensation for both chromatic dispersion and Kerr effect in a transmission fiber using optical phase conjugation," *Journal of Lightwave Technology*, vol. 14, no. 3, pp. 243–248, 1996.

[179] K. Solis-Trapala, T. Inoue, and S. Namiki, "Nearly-ideal optical phase conjugation based nonlinear compensation system," in *OFC 2014*, 2014, pp. 1–3.

[180] R. Jopson, A. Gnauck, and R. Derosier, "10-Gb/s 360-km transmission over normal-dispersion fiber using mid-system spectral inversion," in *Conference on Optical Fiber Communication/International Conference*

on Integrated Optics and Optical Fiber Communication. Optical Society of America, 1993, p. PD3. [Online]. Available: http://www.osapublishing.org/abstract.cfm?URI=OFC-1993-PD3

[181] W. Pieper, "Nonlinearity-insensitive standard-fibre transmission based on optical-phase conjugation in a semiconductor-laser amplifier," *Electronics Letters*, vol. 30, pp. 724–726(2), April 1994. [Online]. Available: https://digital-library.theiet.org/content/journals/10.1049/el_19940494

[182] K. Solis-Trapala, M. Pelusi, H. N. Tan, T. Inoue, S. Suda, and S. Namiki, "Doubled transmission reach for DP-64QAM signal over field-deployed legacy fiber systems enabled by MSSI," in *2015 European Conference on Optical Communication (ECOC)*, 2015, pp. 1–3.

[183] S. Yoshima, Y. Sun, Z. Liu, K. R. H. Bottrill, F. Parmigiani, D. J. Richardson, and P. Petropoulos, "Mitigation of nonlinear effects on WDM QAM signals enabled by optical phase conjugation with efficient bandwidth utilization," *J. Lightwave Technol.*, vol. 35, no. 4, pp. 971–978, Feb 2017. [Online]. Available: http://jlt.osa.org/abstract.cfm?URI=jlt-35-4-971

[184] M. E. McCarthy, M. A. Z. A. Kahteeb, F. M. Ferreira, and A. D. Ellis, "PMD tolerant nonlinear compensation using in-line phase conjugation," *Opt. Express*, vol. 24, no. 4, pp. 3385–3392, Feb 2016. [Online]. Available: http://www.opticsexpress.org/abstract.cfm?URI=oe-24-4-3385

[185] H. Hu, R. M. Jopson, A. H. Gnauck, S. Randel, and S. Chandrasekhar, "Fiber nonlinearity mitigation of WDM-PDM QPSK/16-QAM signals using fiber-optic parametric amplifiers based multiple optical phase conjugations," *Opt. Express*, vol. 25, no. 3, pp. 1618–1628, Feb 2017. [Online]. Available: http://www.opticsexpress.org/abstract.cfm?URI=oe-25-3-1618

[186] K. Solis-Trapala, M. Pelusi, H. N. Tan, T. Inoue, and S. Namiki, "Optimized WDM transmission impairment mitigation by multiple phase conjugations," *J. Lightwave Technol.*, vol. 34, no. 2, pp. 431–440, Jan 2016. [Online]. Available: http://jlt.osa.org/abstract.cfm?URI=jlt-34-2-431

[187] E. Astra, S. L. I. Olsson, H. Eliasson, and P. A. Andrekson, "Dispersion management for nonlinearity mitigation in two-span 28 GBaud QPSK phase-sensitive amplifier links," *Optics Express*, vol. 25, no. 12, pp. 13 163–13 173, Jun 2017. [Online]. Available: http://www.opticsexpress.org/abstract.cfm?URI=oe-25-12-13163

[188] E. Astra, H. Eliasson, T. Ruuben, and P. A. Andrekson, "Improved mitigation of self-phase modulation induced impairments in 28 gbaud phase-sensitive amplified links," *Opt. Express*, vol. 27, no. 4, pp.

4304–4316, Feb 2019. [Online]. Available: http://www.opticsexpress.org/abstract.cfm?URI=oe-27-4-4304

[189] Y. Tian, Y.-K. Huang, S. Zhang, P. R. Prucnal, and T. Wang, "Demonstration of digital phase-sensitive boosting to extend signal reach for long-haul WDM systems using optical phase-conjugated copy," *Optics Express*, vol. 21, no. 4, pp. 5099–5106, 2013. [Online]. Available: http://www.opticsexpress.org/abstract.cfm?URI=oe-21-4-5099

[190] H. Eliasson, P. Johannisson, M. Karlsson, and P. A. Andrekson, "Mitigation of nonlinearities using conjugate data repetition," *Optics Express*, vol. 23, no. 3, pp. 2392–2402, 2015.

[191] X. Liu, S. Chandrasekhar, A. H. Gnauck, P. J. Winzer, S. Randel, S. Corteselli, A. R. Chraplyvy, R. W. Tkach, B. Zhu, T. F. Taunay, and M. Fishteyn, "Digital coherent superposition for performance improvement of spatially multiplexed coherent optical OFDM superchannels," *Opt. Express*, vol. 20, no. 26, pp. B595–B600, Dec 2012. [Online]. Available: http://www.opticsexpress.org/abstract.cfm?URI=oe-20-26-B595

[192] X. Liu, S. Chandrasekhar, P. J. Winzer, R. W. Tkach, and A. R. Chraplyvy, "Fiber-nonlinearity-tolerant superchannel transmission via nonlinear noise squeezing and generalized phase-conjugated twin waves," *Journal of Lightwave Technology*, vol. 32, no. 4, pp. 766–775, 2014.

[193] S. Takasaka, Y. Mimura, M. Takahashi, R. Sugizaki, and H. Ogoshi, "Flat and broad amplification by quasi-phase-matched fiber optical parametric amplifier," in *Optical Fiber Communication Conference*. Optical Society of America, 2012, p. OTh1C.4. [Online]. Available: http://www.osapublishing.org/abstract.cfm?URI=OFC-2012-OTh1C.4

[194] Z. Ye, "Ultralow-loss silicon nitride waveguides for nonlinear optics," *PhD Thesis*, 2021.

[195] R. Kakarla, J. Schröder, and P. A. Andrekson, "One photon-per-bit receiver using near-noiseless phase-sensitive amplification," *Light: Science & Applications*, vol. 9, no. 1, pp. 1–7, 2020.

[196] A. Alvarado, E. Agrell, D. Lavery, R. Maher, and P. Bayvel, "Replacing the soft-decision FEC limit paradigm in the design of optical communication systems," *Journal of Lightwave Technology*, vol. 33, no. 20, pp. 4338–4352, 2015.

[197] J. Cho, L. Schmalen, and P. J. Winzer, "Normalized generalized mutual information as a forward error correction threshold for probabilistically shaped QAM," in *European Conference on Optical Communication (ECOC)*, 2017.

[198] B. Chen, C. Okonkwo, D. Lavery, and A. Alvarado, "Geometrically-shaped 64-point constellations via achievable information rates," in *International Conference on Transparent Optical Networks (ICTON)*, 2018.

[199] S. Zhang and F. Yaman, "Design and comparison of advanced modulation formats based on generalized mutual information," *Journal of Lightwave Technology*, vol. 36, no. 2, pp. 416–423, 2017.

[200] E. Astra, H. Eliasson, and P. A. Andrekson, "Four-span dispersion map optimization for improved nonlinearity mitigation in phase-sensitive amplifier links," in *European Conference on Optical Communication*, 2017.